HAL
open science

Development of a concept of reactive compatibilizer-tracer for studying the evolution of the interfacial reaction and morphology of reactive polymer blends

Wei-Yun Ji

To cite this version:

Wei-Yun Ji. Development of a concept of reactive compatibilizer-tracer for studying the evolution of the interfacial reaction and morphology of reactive polymer blends. Polymers. Université de Lorraine, 2016. English. NNT : 2016LORR0247 . tel-01531354

HAL Id: tel-01531354

https://theses.hal.science/tel-01531354v1

Submitted on 1 Jun 2017

HAL is a multi-disciplinary open access archive for the deposit and dissemination of scientific research documents, whether they are published or not. The documents may come from teaching and research institutions in France or abroad, or from public or private research centers.

L'archive ouverte pluridisciplinaire **HAL**, est destinée au dépôt et à la diffusion de documents scientifiques de niveau recherche, publiés ou non, émanant des établissements d'enseignement et de recherche français ou étrangers, des laboratoires publics ou privés.

UNIVERSITÉ DE LORRAINE

AVERTISSEMENT

Ce document est le fruit d'un long travail approuvé par le jury de soutenance et mis à disposition de l'ensemble de la communauté universitaire élargie.

Il est soumis à la propriété intellectuelle de l'auteur. Ceci implique une obligation de citation et de référencement lors de l'utilisation de ce document.

D'autre part, toute contrefaçon, plagiat, reproduction illicite encourt une poursuite pénale.

Contact : ddoc-theses-contact@univ-lorraine.fr

LIENS

Code de la Propriété Intellectuelle. articles L 122. 4
Code de la Propriété Intellectuelle. articles L 335.2- L 335.10
http://www.cfcopies.com/V2/leg/leg_droi.php
http://www.culture.gouv.fr/culture/infos-pratiques/droits/protection.htm

en co-tutelle avec
l'Université de Zhejiang

Ecole Doctorale :
Ressources Procédés
Produits Environnement
(RP2E)

Ecole Nationale
Supérieure des Industries
Chimiques
(ENSIC)

Laboratoire Réactions
et Génie des Procédés
(LRGP-CNRS)

Développement d'un concept d'agent compatibilisant-traceur réactif visant à étudier l'évolution de la réaction interfaciale et de la morphologie de mélanges de polymères réactifs

T H È S E

Présentée en vue de l'obtention du

DOCTORAT DE L'UNIVERSITE DE LORRAINE
Spécialité : Génie des Procédés et des Produits

par

Wei-Yun JI

Thèse soutenue publiquement le 25 octobre 2016

Composition du Jury :

Rapporteurs :	Christophe SERRA	Professeur (Université de Strasbourg)
	Yong-Jin LI	Professeur (Université Normale de Hangzhou)
Examinateurs:	Guo-Hua HU	Professeur (Université de Lorraine)
	Lian-Fang FENG	Professeur (Université de Zhejiang)
Invités :	Jean-Pierre CORRIOU	Professeur Emérite (Université de Lorraine)
	Cai-Liang ZHANG	Maître des Conférences (Université de Zhejiang)

en co-tutelle avec
l'Université de Zhejiang

Ecole Nationale
Supérieure des Industries
Chimiques
(ENSIC)

Laboratoire Réactions
et Génie des Procédés
(LRGP-CNRS)

Ecole Doctorale :
Ressources Procédés
Produits Environnement
(RP2E)

Development of a concept of reactive compatibilizer-tracer for studying the evolution of the interfacial reaction and morphology of reactive polymer blends

P h D T H E S I S

Requirement for the Diploma of

Doctor of Philosophy

at The University of Lorraine

Specialty: Process and Product Engineering

by

Wei-Yun JI

Defended on October 25th, 2016

Jury:

Reviewers :	Christophe SERRA	Professor (University of Strasbourg)
	Yong-Jin LI	Professor (Hangzhou Normal University)
Advisors:	Guo-Hua HU	Professor (University of Lorraine)
	Lian-Fang FENG	Professor (Zhejiang University)
Invited Members:	Jean-Pierre CORRIOU	Professor Emeritus (University of Lorraine)
	Cai-Liang ZHANG	Associate Professor (Zhejiang University)

Remerciements

I would like to express my deep gratitude to my advisor (In France), Prof. Guo-Hua Hu and my advisor (In China), Prof. Lian-Fang Feng. I feel so lucky to carry out my research under their supervision. I am impressed with their wide knowledge, innovative thinking and rigorous academic attitude.

I am also deeply grateful to Dr. Sandrine HOPPE, Philippe Marchal, Dr. Cai-Liang Zhang, Dr. Xue-Ping Gu and Dr. Jia-Jun WANG for their helps and suggestions.

Great thanks to my mates both in Chinese and French research group: Zhou Tian, Li Wan, Yin Han, Shun-Gang Song, Min Yao, Yi-Wei Yang, Cong Cao, Zi-Zi Li, Yan-Li Wang, Xiao-Lei Jiang, Meng-Jiao Liu, Jia-Nan Wang, Song Zheng, Yao Huang, Yun-Xia Qiu, Shuang Wang, Chun-Yan Ge, Yin Tang, Wen-Kai Cheng, Zu-Yu Jin, Na Li, Lu-Lu Tian, Tao-Tao Wang, Yong-Jun Zhang, Cong Li, Hui-Ru Luo, Xi-Pei Cheng, Peng-Bo Liu, Chao-Zhong Xu, Kun-Hong Wu, Pu-Jie Xia, Di Wang, Jian Chen, Miao-Na Cheng, Si-Wei Zhao, Tian-Qi Liu, Lin-Jiong Zhang, Si-Bo Cheng, Dong-Mei Zhang, Han-Lu Qi, Jun Zhu, Ning Yu, Romain Tessier, Francois BESSON and Binod SHRESTHA for their help. Of all these names, Long Wang deserves a special mention, who helped me in the research work about the twin screw extruder part.

My sincere thanks are given to my parents for their love and understanding. At last, my gratitude goes to my boyfriend Dr. Yi-Peng Wei who encourages me to keep going without fear.

Table of contents

Remerciements ..... **I**

Chapter 1 Introduction **1**

Chapter 2 Literature review **4**

2.1 Introduction 4

2.2 Polymer blending 4

2.2.1 Physical blending 4

2.2.2 Reactive blending 4

2.3 Morphology of polymer blends 5

2.3.1 Morphology development of polymer blends 6

2.4.1 Melting regime 6

2.4.2 Melt flow regime 8

2.4 Interfacial reaction in reactive polymer blends 12

2.4.1 Type of interfacial reaction 12

2.4.2 Measurement of interfacial reaction 13

2.4.3 Follow-up of interfacial reaction in a twin screw extruder 14

2.4.4 Effect of the molecular architecture of reactive compatibilizers 15

2.4.5 Effect of processing parameters 16

2.5 In-line measurement of polymer blending process 17

2.5.1 In-line measurement of properties and chemical composition of polymers 18

2.5.2 In-line measurement of morphology 20

Chapter 3 Effect of molecular architecture of reactive compatibilizer-tracer on the interfacial reaction and morphology in polymer batch blending **22**

3.1 Introduction 22

3.2 Experimental 23

3.2.1 Materials 23

3.2.2 Synthesis of PS-TMI-MAMA 24

3.2.3 Synthesis of Anhy-PS-Anth 25

3.2.4 Blending 27
3.2.5 Fourier transform infrared spectrometer (FTIR) 28
3.2.6 Size exclusion chromatography (SEC) 28
3.2.7 Ultraviolet spectrometer (UV) 28
3.2.8 Morphology of polymer blend 29
3.2.9 Determination of the amount of reacted copolymer 29
3.2.10 Confocal microscopy 30
3.3 Result and discussion 30
3.3.1 Characteristic of PS-TMI-MAMA 31
3.3.2 Characteristic of Anhy-PS-Anth 33
3.3.3 Effect of graft and block reactive compatibilizer-tracer 33
3.3.4 Effect of the molecular architecture of graft reactive compaitbilizer-tracer 37
3.3.5 Mechanism analysis of the sharp increase in the dispersed phase domain size during the latter period of mixing 39
3.4 Conclusion 43
Chapter 4 Effects of mixing and blend composition on reactive polymer blending processes 45
4.1 Introduction 45
4.2 Experimental 45
4.2.1 Material 45
4.2.2 Polymer blending process 45
4.2.3 Rheological measurement 46
4.2.4 SEM 46
4.2.5 Transmission Electron Microscope (TEM) 46
4.3 Result and discussion 46
4.3.1 Effect of mixing speed 46
4.3.2 Effect of annealing time 48
4.3.3 Effect of blend composition 50
4.4 Conclusion 55

Chapter 5 Development of a reactive compatibilizer-tracer for studying reactive polymer blends in a twin-screw extruder 57

5.1 Introduction.....57

5.1 Experimental.....58

5.2.1 Material.....58

5.2.2 In-line fluorescence measuring device.....59

5.2.3 In-line measurement processing 60

5.3 Result and discussion.....61

5.3.1 Establishment of in-line measurement.....61

5.3.2 Assessment of the concept of reactive compatibilizer-tracer - effect of tracer port.....66

5.3.3 Effect of blend composition.....69

5.4 Conclusion 72

Chapter 6 Measurement of the compatibilizing efficiency of reactive comapatibilizers by a fluorescent tracing method 74

6.1 Introduction.....74

6.2 Experimental.....74

6.2.1 Material.....74

6.3 Result and discussion.....75

6.3.1 Effect of molar mass 75

6.3.2 Effect of TMI content 77

6.3.3 Graft reactive compatibilizer-tracer vs. block reactive compatibilizer-tracer 80

6.4 Conclusion 82

Chapter 7 Effect of the degree of fill on the PS/PA6/PS-TMI-MAMA reactive polymer 83

7.1 Introduction.....83

7.2 Experimental.....83

7.2.1 Materials 83

7.2.2 Reactive blending.....83

7.3 Result and discussion 84
7.3.1 Effect of screw speed 84
7.3.2 Effect of throughput 86
7.3.3 Effect of degree of fill 88
7.4 Conclusion 95
Chapter 8 Mixing efficiency of mixing elements in a twin screw extruder 96
8.1 Introduction 96
8.2 Experimental 96
8.2.1 Material 96
8.2.2 Reactive blending 96
8.3 Results and discussion 98
8.3.1 Effect of kneading angle 98
8.3.2 Effect of kneading block width 102
8.3.3 Effect of combined mixing elements 105
8.4 Conclusion 107
Chapter 9 General conclusion and future work 109
9.1 General conclusion 109
9.2 Future work 112
References 114
Résumé 129
Abstract 129

Chapter 1 Introduction

As the society develops, polyethylene (PE), polypropylene (PP) and other single specie could not meet the specific end use requirements. Polymer blending is a common method to obtain new polymer materials by combining existing ones. Figure 1.1 shows the scheme of a typical polymer blending process carried out in a continuous mixer of type twin screw extruder. Polymer pellets are fed to the twin screw extruder. They are melted and mixed to form a polymer blend. The initial size of the polymer pellets is usually on the order of millimeters and the final size of the dispersed phase polymer component is usually on the order of micrometers..

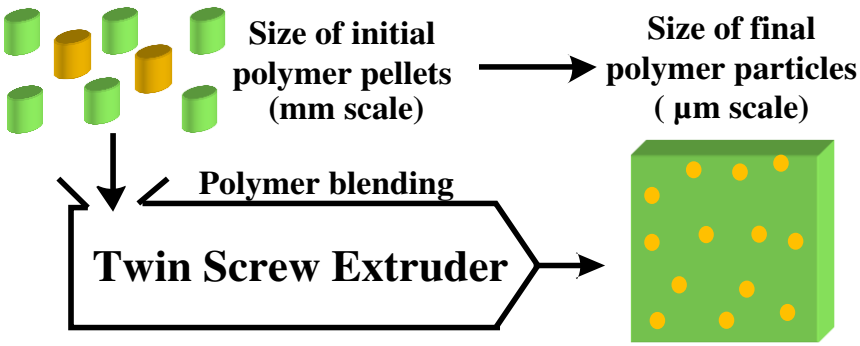

Figure 1.1 Scheme of a typical polymer blending process carried out in a continuous mixer of type twin screw extruder.

However, most polymer pairs are thermodynamically immiscible, leading to the phase separation and sharp decrease in the performance of products. Therefore, a premade block or graft copolymer is added as a compatibilizer to overcome this problem [1-3]. This copolymer is difficult to diffuse to the interface and easy to form micelles in one phase, resulting in low compatbilizing efficiency. Nowadays the popular compatibilizing technology is in-situ compatibilization, reactive compatibilization or reactive polymer blending [4-9], in which a compatibilizer is generated in-situ during the blending process upon reacting two reactive polymers at the interfaces. Reactive polymer components are usually called reactive compatibilizers. In fact they should be called compatibilizer precursors instead as they

are not compatibilizers themselves but become one upon reaction between them. In case one or two of the two polymer components are chemically inert, they are functionalized first. This method has high compatibilizing efficiency as the compatibilizer is formed directly at the interfaces where it is needed. It is therefore mostly practiced in industries.

The key to preparing polymer materials with high performance via a reactive polymer blending process is that the morphology and interfacial reaction can be effectively controlled. However, the interfacial reaction and morphology of reactive polymer blends are highly coupled. How does the morphology and interfacial reaction evolve? What is the effect of mixing on the reactive polymer blending process? What is the relationship between flow field or process parameters, interfacial reaction and morphology? These questions need to be solved.

However it is very challenging to address these questions. One of the challenges lies in the fact that it often requires a large amount to evaluate the compatribilizing efficiency of a reactive compatibilizer in an industrial twin screw extruder. This large amount may not always be available, especially when it comes to a new reactive compatibilizer under development. Another challenge is that it is often difficult to measure the amount of the in-situ formed copolymer.

This thesis aims at developing a concept of reactive compatibilizer-tracer which will allow using small amounts of reactive compatibilizers to evaluate their compatibilizing efficiency in industrial scale twin screw extruders, on the one hand; and to characterize the mixing performance (interfacial reaction and morphology) of a twin screw extruder as a function of process conditions and/or screw profile. The manuscript is composed of 9 chapters including this one.

Chapter 2 provides a literature review on polymer blending.

Chapter 3 describes the synthesis of graft and block reactive compatibilizer-tracers and analysis of the interfacial reaction of reactive polymer blends and the stability of the in-situ formed copolymer.

Chapter 4 discusses the effect of mixing and blend composition on the interfacial reaction and morphology of the reactive polymer blends.

Chapter 5 combines the reactive compatibilizer-tracer and RTD transient experiment to establish the relationship between the interfacial reaction and morphology.

Chapter 6 builds up the emulsification curve of the reactive polymer blends in a twin screw extruder with small amounts of a reactive compatibilizer-tracer to fast and conveniently evaluate its compatibilizing efficiency in a twin screw extruder.

Chapter 7 deals with the effect of the degree of fill on the interfacial reaction and morphology of reactive polymer blends in a twin screw extruder.

Chapter 8 evaluates the distributive and dispersive mixing efficiencies of mixing elements with different geometries in a twin screw extruder

Chapter 9 provides the main conclusions of this thesis and further research directions.

Chapter 2 Literature review

2.1 Introduction

Polymer materials develop fast and find many applications. Blending existing polymers is a convenient method to obtain new polymer materials of high performances [10]. However, most polymer pairs are thermodynamically immiscible, leading to the phase separation and poor properties of products. Therefore, there is a need to improve compatibility and adhesion between polymer pairs.

2.2 Polymer blending

2.2.1 Physical blending

Physical blending is mixing polymer components by diffusion, convection, shear and does not involve chemical reactions. However, it is difficult to well disperse one polymer component in another one because of immiscibility. To overcome this problem, a premade block or graft copolymer is added as a compatibilizer to improve miscibility [4, 11-14]. This is called physical, ex-situ or non-reactive compatibilization. Take a blend of polymer A and polymer B as an example. A premade compatibilizer can be an A-B block or graft copolymer [15-20]. Segments A and B of A-B are miscible with polymers A and B, respectively, leading to a reduction in interfacial tension and an improvement in interfacial adhesion. Moreover, interfaces covered by the copolymer prevent the dispersed phase domains from coalescing and stabilize the morphology of the resulting blend [21-29].

2.2.2 Reactive blending

By reactive blending, it means that fractions of polymers A and B of the blend contain functional groups which can react with each other at the interfaces, leading to the in-situ formation of a block or graft copolymer. It is also called in-situ compatibilization or reactive comaptibilization [30-36]. Take polystyrene

(PS)/polyamide 6 (PA6) as an example. A polystyrene with a terminal anhydride (Anh-PS-Br) synthesized via atom transfer radical polymerization was used as a reactive compatibilizer. The terminal anhydride group of Anh-PS-Br could react with the terminal amine of the PA6 to in-situ form a block copolymer PS-b-PA6 which acted as a compatibilizer [37, 38]. A copolymer of styrene and maleic anhydride SMA could also react with the terminal amine of the PA6 to form a graft copolymer PS-g-PA6 [38].

Compared with a premade copolymer as a compatibilizer, a reactive compatibilizer may have higher compatibilzing efficiency owing to the fact that it may reach the interfaces in a much easier manner and that the copolymer is formed directly at the interfaces where it is needed. Therefore, reactive compatibilization has become a hot research topic in the field of polymer blending [39-54].

2.3 Morphology of polymer blends

Polymer blends can be homogeneous or heterogeneous. If polymer components are thermodynamically miscible, the resulting polymer blend is homogeneous. Otherwise it is heterogeneous, which is often the case. Heterogeneous polymer blends can be divided into two types according to the continuity of the phases: dispersed phase-matrix structure and co-continuous structure.

Consider a blend of polymers A and B which are mutually immiscible. When the volume fraction of polymer A is low enough, the morphology of the blend is a dispersed phase-matrix structure with A being the dispersed phase and B the continuous one. As it increases, the dispersed phase domain size increases and two phases could crisscross as rods to form a co-continuous structure. A further increase in the volume fraction of A will lead to phase inversion, namely, polymer A will become the continuous phase and polymer B the dispersed one.

The morphology of a polymer blend is not only dependent on its composition but also on the characteristics of polymer components such as interfacial tension [55], viscosity [56, 57], interface type [58] and processing conditions. Take viscosity as an example. When the blend composition ratio is 1, the phase whose viscosity is lower

tends to become the continuous phase and the one whose viscosity is higher tends to become the dispersed one.

2.3.1 Morphology development of polymer blends

Most industrial polymer blending processes start with polymers in the form of pellets or powder. Figure 2.1 depicts the morphology development of a polymer blending process starting with pellets [13]. A solid pellet (S) first has to be transformed to the melt (M) before morphology can develop. And then, the initial molten layers (M) stripped from the solid pellet undergo a transient affine deformation to form sheets or threads (T). Being driven by interfacial instability, the latter break up into small particles (P). These small particles may undergo coalescence because of interfacial tension and form larger particles (C). So the polymer-polymer mixing is a result of complex interactions between flow and events occurring at droplet-length scales: deformation, breakup, coalescence and hydrodynamic interactions, as pointed out by Ottino et al. [59]

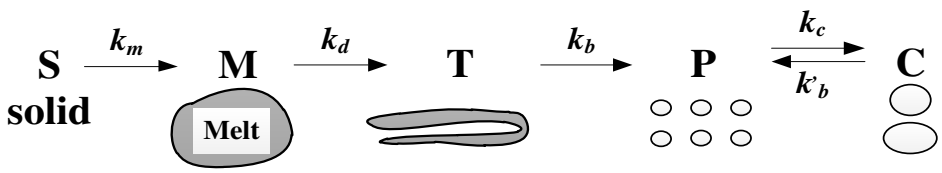

Figure 2.1 Different steps involved in the process of the morphology development of an immiscible polymer blend starting from solid pellets: transformation of solid pellets (S) to the corresponding polymer melt (M); stretching/deformation of the molten polymer to slender threads (T); breakup of slender threads to small particles (P); and coalescence of small particles forming larger ones (C).

2.4.1 Melting regime

In the melting regime, solid pellets of polymers are melting or softening, and are then transformed to the polymer melts. The rotor torque applied to the material in the melting regime reaches a maximum. The viscosity and the velocity gradients in the material are highest. Therefore, flow stresses applied to the deformation of the material and breakage of domains to smaller size are greatest, leading to a dramatic reduction in the dispersed phase domain size [60]. For instance, Scott et al [61]

investigated polymer blends in a batch mixer and found that the dispersed phase domain size decreased from mm scale to μm scale in 2 min of mixing. The characteristics of the melting regime in terms of morphology development and melting time are mainly controlled by material properties such as viscosity, molar mass, melting temperature/glass transition temperature, mixing devices and mixing conditions [13, 62].

Scott and Macosko [61] proposed a mechanism of morphology development during a mixing melting process, as shown in Figure 2.2. This mechanism involves the formation of sheets or ribbons of the dispersed phase in the matrix[63-65], which are drawn out of a large mass of the dispersed phase. These formed sheets are unstable and holes begin to form in them because of the effects of flow and interfacial tension. These holes are filled with the matrix, which surrounds the sheets on either side. When those holes in the sheet or ribbon attain a sufficient size and concentration, a fragile lace structure is formed and then begins to break apart due to flow and interfacial forces into irregularly shaped pieces. These pieces are of approximately the diameter of the particles that are generated on the blend at long mixing times. These irregular pieces continue to break down until all of the particles become nearly spherical. They also found that the direct formation of strands or formation of strands from break-up of the sheets occurred in the process.

The addition of compatibilizer has a great effect on the morphology development of polymer blend. It can accelerate the morphology evolution of the polymer blend. Hu et al [13] showed that for the polypropylene (PP) and PA6 blend, the melting time of PA6 is 6.1 min at 20 rpm and 230°C. The addition of the graft copolymer of PP and PA6 reduce the melting time of PA6 to 5.1 min. The melting order during polymer blending is PP, PP-g-PA6 and PA6. PP-g-PA6 at the interface could transfer the heat to the PA6 pellet more quickly.

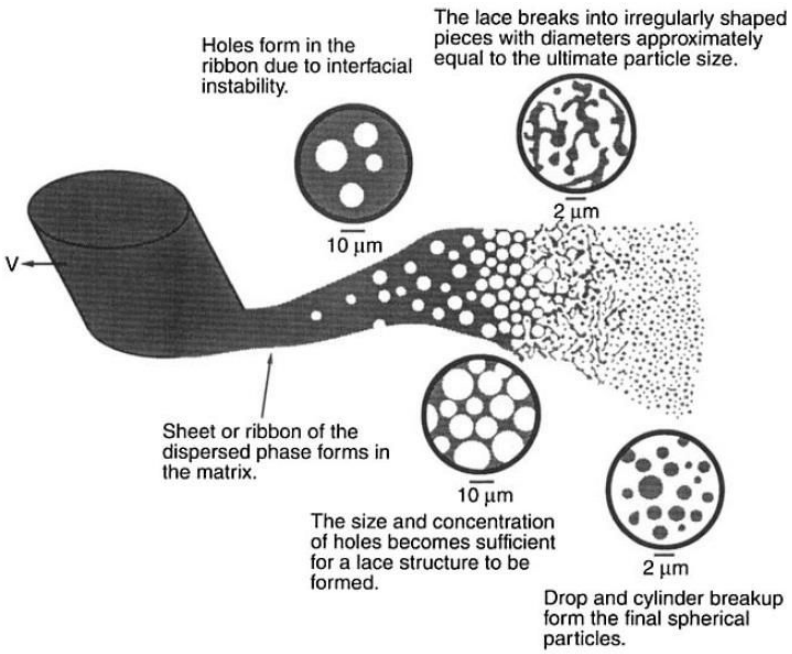

Figure 2.2 Proposed mechanism for initial morphology development in the process of the polymer-polymer mixing.

2.4.2 Melt flow regime

2.3.1.1 Breakup and coalescence of dispersed phase

It is well-known that a real polymer blending process is often carried out in a batch mixer or a screw extruder which creates a flow field. This flow field can increase the deformation of the dispersed phase domains and can then break them into smaller domains. In the same time, it can also promote the collision between domains, which may lead to the coalescence of the dispersed phase domains. Thus, the morphology evolution of the dispersed phase domains is controlled by the competition between break-up and coalescence of the dispersed phase domains[66]. Whether or not a dispersed phase domain breaks up depends on the capillary number, *Ca*, which is the ratio of deforming viscous stress to resisting interfacial stress (equation 1-1):

$$Ca = \frac{Deforming\ viscous\ stress}{Resisting\ interfacial\ stress} = \frac{\eta_m \dot{\gamma}}{2\sigma/D} \tag{1-1}$$

On the one hand, for break-up of a dispersed phase domain to occur, the capillary number must exceed a critical value (Ca_{crit}). Thus, this critical value of capillary number gives the maximum value of the dispersed phase domain size that can survive

in a given flow in the absence of coalescence. When two immiscible polymers are being mixed, the maximum diameter of the dispersed phase domain, denoted as D_{max}, can be expressed by the following equation:

$$D_{max} = \frac{2\sigma}{\eta_m \dot{\gamma}} Ca_{crit} \tag{1-2}$$

Take the values of σ, η_m, $\dot{\gamma}$ and Ca_{crit} as 1×10^{-2} N/m, 100 Pa·s, 100 s^{-1} and 1, respectively. The corresponding value of D_{max} is equal to 2 μm. This implies that under such typical processing conditions, the diameter of the dispersed phase domains bigger than 2 μm cannot be stable and will be broken up to smaller ones. Those whose diameters are smaller than 2 μm will be stable, if no coalescence occurs [67].

On the other hand, the flow stress deforms and breaks the dispersed phase domains and the interfacial tension resists the deformation. When the flow stress and interfacial tension reaches an equilibrium, the diameter of the dispersed phase domain can be calculated using equation (1-3) proposed by Taylor [68, 69]:

$$D = \frac{4\sigma(\eta_r+1)}{\dot{\gamma}\eta_m[(19/4)\eta_r+4]} \qquad (\eta_r < 2.5) \tag{1-3}$$

where η_r is the viscosity ratio of the dispersed phase and the matrix, which is an important dimensionless number. When this viscosity ratio is close to unity, the dispersed phase domain breaks up easily. However, when it is above 5, the breakup of droplets could not occur regardless of how high the capillary number is.

It should be noticed that the Taylor equation is based on the assumption that the dispersed phase domains are dispersed in infinitely dilute Newtonian systems as spheres. However, most polymer melts are viscoelastic, which is different from Newtonian fluids. Under a shear force, the elasticity of the dispersed phase can resist its deformation. Therefore it hinders break up. Based on a blend composed of PA6 and poly(ethylene-ran-propylene) rubber, Wu et al [70] modified the Taylor equation to an empirical one as follows:

$$D = \frac{4\sigma\eta_r^{\pm 0.84}}{\dot{\gamma}\eta_m} \tag{1-4}$$

where the plus sign is used for η_r greater than 1 and minus sign for η_r less than 1. However, it neglects the influence of blend composition on the morphology. As a

matter of fact, there are several empirical equations based on different blend systems and they have different limitations.

Coalescence of dispersed phase domains could be divided into three steps: contact of dispersed phase droplets, rupture of the matrix film between adjacent dispersed phase droplets and drain of the matrix film, as shown in Figure 2.3[71, 72]. The contact time of two dispersed phase droplets is very short. Thus the drain rate of the matrix film must be very fast. Otherwise coalescence hardly happens. Coalescence is controlled by the interface mobility. As the matrix viscosity increases, it is more difficult for the interface between two phases to move and the time for the drain of the film increases too [73]. Elmendorp [74] found that the coalescence probability is very high when the interface has high mobility.

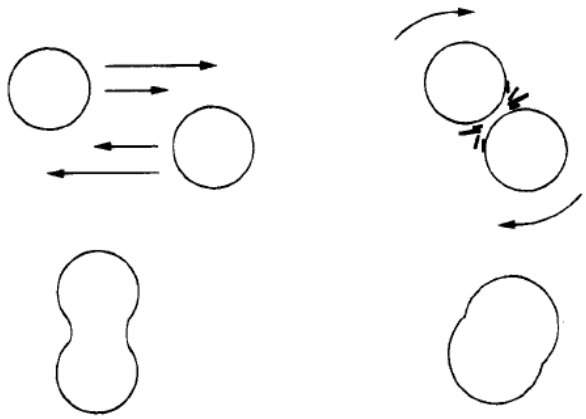

Figure 2.3 Scheme of coalescence of the dispersed phase.

2.3.1.2 Effect of compatibilizer

The above discussion is based on uncompatibilized polymer blends. Addition of a compatibilizer can have a significant influence on the morphology development, especially in the melt flow regime. Normally, the copolymer at the interface can reduce the dispersed phase domain size [75-77]. Early researchers attributed this reduction to a lower interfacial tension [78-82]. However, Lyu [83] found that the reduction in interfacial tension was not sufficient to explain the decrease of the dispersed phase domain size. The suppression of coalescence may be one of the important reasons.

There are two mechanisms for the suppression of coalescence, as shown in Figure 2.4. One was proposed by Milner and Xi [84]. According to their mechanism, suppression of coalescence is caused by Marangoni force which is induced by a gradient of copolymer concentration at interfaces. As shown in Figure 2.4a, when two droplets approach each other, the matrix escaping from the gap between them sets up a recirculating fountain flow which carries the copolymer at the interface out from the gap, forming a concentration gradient.

The other mechanism was proposed by Sundararaj and Macosko [73]. In this mechanism, suppression of coalescence is due to steric interaction between droplets that results from the compression between the block copolymer layers that are attached to the interfaces. Usually, the interface is surrounded by a layer or multi-layers of copolymers. When two droplets approach each other, the copolymer at the interface hinders these two droplets to meet and collide, as shown in Figure 2.4b. Only when the copolymer has moved out of the interface, these two droplets could meet each other. However, it is very difficult to move the copolymer out of the interface, leading to the suppression of coalescence of the dispersed phase domains.

Actually, both mechanisms may operate in compatibilized polymer blends. Which one dominates is dependent on the interfacial coverage of compatibilizer. When the interfacial coverage of copolymer is high, steric interaction between droplets dominates. When the interfacial coverage is low, Marangoni force dominates. In general, the interfacial coverage of the copolymer in compatibilized polymer blends is relatively high. Therefore the steric stabilization is believed to be the main mechanism of suppression of coalescence right now[73, 85, 86].

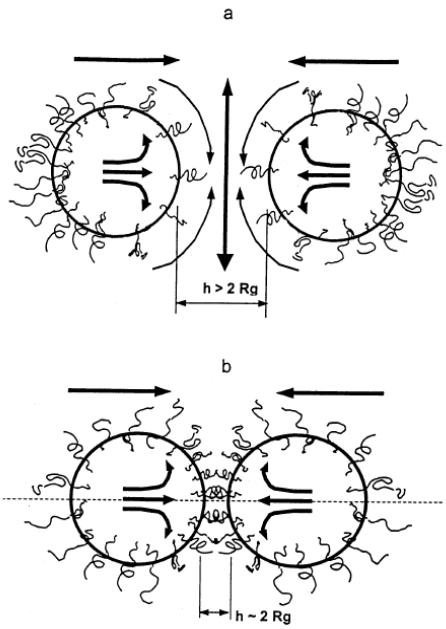

Figure 2.4 Two mechanisms proposed for the suppression of coalescence by copolymers: (a) surface tension gradient (Marangoni) force and (b) steric repulsion.

2.4 Interfacial reaction in reactive polymer blends

The key to a reactive compatibilization process is to control the interfacial reaction between reactive polymer components so as to control the rate of formation, amount and molecular architecture of the resulting copolymer which dictate the morphology development of the blend [87].

2.4.1 Type of interfacial reaction

A typical processing time is within one or two minutes if the polymer blending process is carried out in a twin screw extruder. Therefore, the interfacial reaction must go sufficiently fast. Otherwise the interfaces could not be covered by a sufficient amount of the in-situ formed copolymer to compatibilize the polymer blend [88].

Figure 2.5 shows common interfacial reactions between functional groups used for reactive compatibilization of polymer blends. The most common reactive pair is amine/anhydride which has frequently been used in commercial reactively compatibilized polymer blends

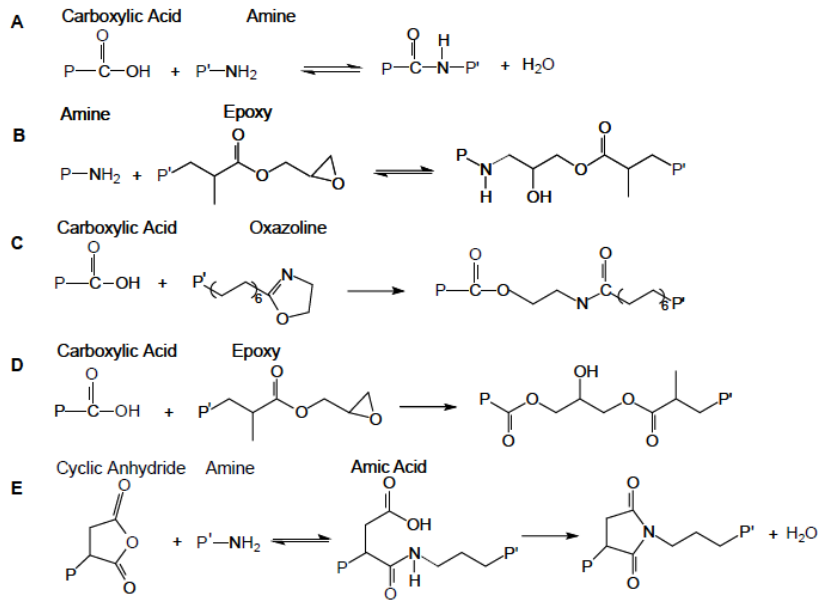

Figure 2.5 Chemical reactions between functional groups: (A) acid/amine reaction to form an amide; (B) amine/epoxy reactions; (C) carboxylic acid/oxazoline; (D) carboxylic acid/epoxy; (E) two-step reaction to form an imide from amines and cyclic anhydrides.

Orr et al [89] measured homogeneous reaction kinetics at 180°C using a number of polystyrene (PS) with different terminal groups. The reactivity of the functional group is in the following order: amine/isocyanate > amine/anhydride > carboxylic/anhydride > acid/epoxy > acid/oxazoline > amine/epoxy. The reaction between amine and isocyanate is fastest and conversion reaches 99% in 2 min.

2.4.2 Measurement of interfacial reaction

It is often very difficult to measure the amount of an in-situ formed copolymer by an interfacial reaction because its concentration is often too low to be detected by standard techniques like nuclear magnetic resonance (NMR) and infrared (IR) spectroscopy [90-92]. Moreover, it is difficult to separate the in-situ formed copolymer from the polymer blend. Some researchers separated in-situ formed copolymers from polymer blends by solvent extraction and then measured their contents. An extraction procedure was carried out to remove the PA6 phase and the remaining SMA was analyzed by FTIR to measure the amount of the reacted functional group. Similar FTIR experiments were performed by Tan et al. [90] who investigated the interfacial reinforcement of reactive PS/PA6 blends. Dedecker et al. [64] investigated the

interfacial graft copolymer formation during reactive melt blending of PA6 and SMA. Jeon et al. studied the effect of the reaction rate on the morphology of the reactive blend using PS-mCOOH/PMMA with PMMA-GMA as a reactive compatibilizer [92]. A mixture of solvents (cyclohexane and toluene) was used to separate the in-situ formed PMMA-g-PS from the blend. Unfortunately, that extraction method led to high errorr due to the incomplete removal of the unreacted polymer. In general, it is not always possible to find an appropriate solvent to separate in-situ formed copolymers from polymer blends. To overcome this difficulty, fluorescent groups are incorporated in reactive compatibilizers, allowing accurate detection of very small amounts of in-situ formed copolymers.

Macosko [93, 94] synthesised anhydride-terminal PMMA (PMMA-eAn) and amine-terminal PS (PS-NH_2) to compatibilize PS/PMMA blends. A fluorescent group was incorporated into the PMMA-eAn to allow detecting the interfacial reaction via a size exclusion chromatography (SEC) with a UV detector. The results showed that the interfacial reaction between aliphatic amine/anhydride was very fast and final conversions were reached in 10 min for all polymer blends.

2.4.3 Follow-up of interfacial reaction in a twin screw extruder

Yquel et al. [95] developed a sampling device to near-real-time investigate the interfacial reaction occurring inside a laboratory twin-screw extruder. It is shown in Figure 2.6. It allows sampling about 2 g of material from the circular aperture in a barrel wall (1) which takes about 3-5 s. The sample flow is controlled by a cylindrical valve (2), containing two cavities (3) and (4). When the valve is positioned as shown in Figure 2.6, there is no flow out of the extruder. The valve is rotated to expose hole (1) to the cavity to collect the sample. The residual MA content in SMA was measured by FTIR. The results showed that from the feeder of the extruder to the first kneading zone (t=38s) the MA content of SMA was decreased from 23.9 to 17.6 mol%. The MA conversion only slightly decreased from location B to location D (53 s-145 s). The results indicated that the imidation mainly occurred in the melting zone.

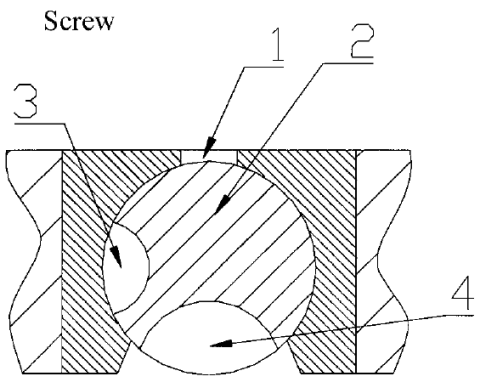

Figure 2.6 Scheme of a sampling device.

2.4.4 Effect of the molecular architecture of reactive compatibilizers

The molecular architecture of a reactive compatibilizer may have a significant effect on the interfacial reaction (rate of formation, molecular architecture and amount of the in-situ formed copolymer) and consequently on its compatibilizing efficiency [96-104]. In general, a reactive compatibilizer with a smaller molar mass would diffuse to the interface faster and a decrease in the dispersed phase domain size would occur earlier [105-110]. However, when the molar mass of the reactive compatibilizer is smaller than a critical value, the molecular architecture of the resulting graft or block copolymer would be asymmetrical that it would tend to leave the interfaces and lose its compatibilizing efficiency. For instance, in case of a hydroxyl terminated PS/PMMA blend, when the molar mass of the in-situ formed block copolymer PS-b-PMMA was small enough, many micelles were formed in the dispersed PMMA phase PMMA and the compatibilizing efficiency was low [111].

The content of the reactive group of a reactive compatibilizer could affect the interfacial reaction and the molecular architecture of the in-situ formed copolymer [112-114]. When the reactive group of the reactive compatibilizer increases from one to multiple per chain, the in-situ formed graft copolymer changes from a Y shaped structure to a comb-shaped structure. The change in the molecular architecture of the copolymer would influence the comaptibilizing efficiency [115]. Dedecker [91] investigated the effect of MA content of a SMA on the PA6/SMA blend. As the MA content of the SMA increased, the amount of the copolymer increased and the

dispersed phase domain size decreased. However, when the content of the reactive group of a reactive compatibilizer exceeds a critical value, the in-situ formed copolymer could leave the interface due to its thermodynamic instability at the interface, losing its compatibilizing efficiency. For example, Zhang et al. [116] investigated the PS/PA6/PS-TMI reactive polymer blend and found that the compatibilizing efficiency of PS-TMI with 8 wt% TMI was much lower than that of PS-TMI with 4 wt% TMI.

2.4.5 Effect of processing parameters

Mixing is one of the most important effects on reactive compatibilization processes [117]. Intense mixing could improve the dispersion and generate large interface area, leading to an increase in the interfacial reaction rate. For example, Hu and Kadri [118] studied the effect of the mixing speed on the hydroxyl terminated PS (PS-OH) and the methyl methacrylate and 3-isopropenyl-α, α'-dimethylbenzene isocyanate copolymer (PMMA-TMI). As the mixing speed increased, more interfaces were generated, leading to more interfacial reaction. Marechal et al. [119] found similar results in a PA6/ethylene-propylene rubber reactive blend. When the mixing time was fixed at 2 min, the interfacial reaction rate increased with increasing mixing speed.

Temperature may also affect the interfacial reaction of a reactive compatibilization process. Hu and Kadri[118] found when the molar mass of PS-OH (56400 g/mol) was higher than the entanglement molar mass M_e (13000 g/mol), the interfacial reaction rates at 175 and 205°C were almost the same. When the molar mass of PS-OH was decreased to 8500 g/mol which was lower than M_e, the interfacial reaction rate increased with increasing temperature. This indicates that when molar mass of PS-OH was high, the interfacial reaction rate was not sensitive to temperature; when the molar mass of PS-OH was low, the interfacial reaction rate was sensitive to it. The difference could be explained as follows: the interfacial reaction was controlled by diffusion when the molar mass of PS-OH was high and it was controlled by reaction kinetics when the molar mass of PS-OH was low. The activation energy of diffusion (5-10 kcal/mol) is much lower than that of chemical reaction (15-25

kcal/mol). The reaction rate is more sensitive to temperature when the activation energy increases.

2.5 In-line measurement of polymer blending process

It is very difficult to investigate mixing and interfacial reaction of a reactive compatibilization process in a twin screw extruder because of complex thermomechanical conditions. The use of process analysis technology (PAT) [120, 121] could measure the temperature, pressure, viscosity, morphology and reaction in real time [122], which helps control and optimize the process and product quality. Moreover, PAT help deep understanding of the process by providing data necessary for process simulation [123].

PAT could be divided into off-line, on-line and in-line measurements. Off-line methods are simple but often lead to large delays between the occurrence of defects or process instabilities and their detection. On-line techniques require a sampling stream to be diverted from the process flow line and transferred to the measurement device. Thus, it is isolated from the main stream which simplifies maintenance work. In-line measurements are implemented directly within the processing line, resulting in very short (or even non-existent) delays for sampling. However, in-line sensors may interfere with the process and sensors can be influenced by temperature or pressure. In-line methods could reflect real polymer blending conditions and thus attract much attention. Traditional PAT in chemical engineering processes is based on temperature and pressure measurements. However, it could not necessarily guarantee the stability of the manufacturing process and the performance of the product, especially for complex processes such as polymer blending processes. Therefore, researchers attempted to develop specific in-line measurement methods for polymer blending processes, as shown in Figure 2.7 [123].

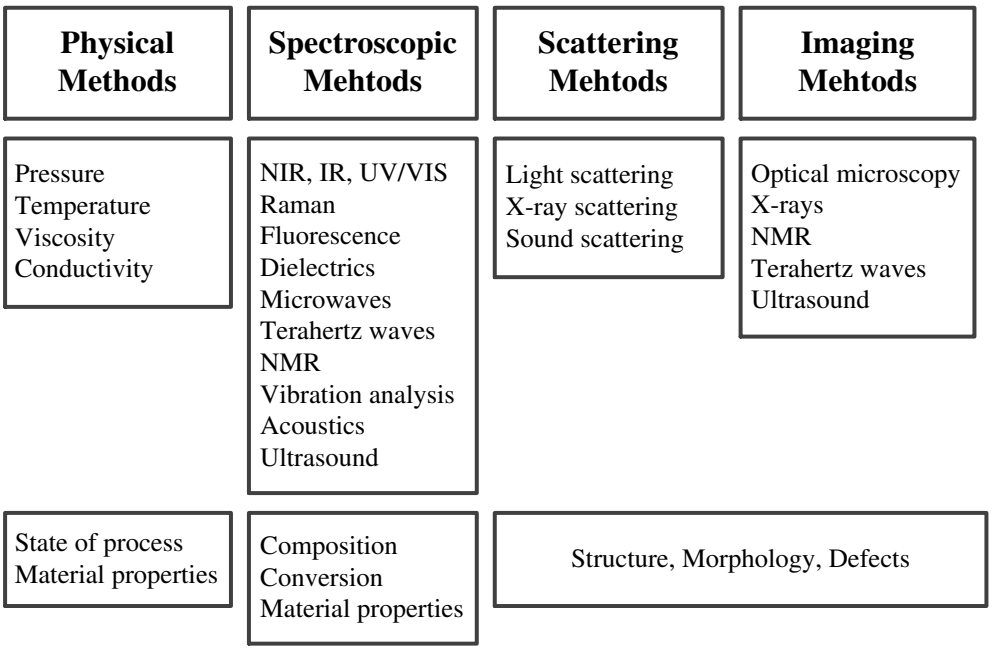

Figure 2.7 Methods for in-line monitoring of polymer blending processes.

2.5.1 In-line measurement of properties and chemical composition of polymers

Since an ultrasound spectroscopy probe could stand high-pressure, it has been applied to polymer processing including polymer foaming, polymer blending and thermoset processing [121, 124-128] from 1980s to in-line measure the melting behaviour and blend compositions during processing.

In-line measurement of electrical conductivity is another PAT. Dielectric relaxation spectroscopy (DRS) is usually used to in-line measure the conductivity to probe the content of conductive fillers (carbon or carbon nanotube) during a polymer blending process. For example, Alig et al. [129, 130] installed insulated electrodes of the plate-capacitor in the die exit of a twin screw extruder (Figure 2.8) to in-line measure the conductivity of polycarbonate (PC) melt containing multi-walled carbon nanotubes (MWCNT).

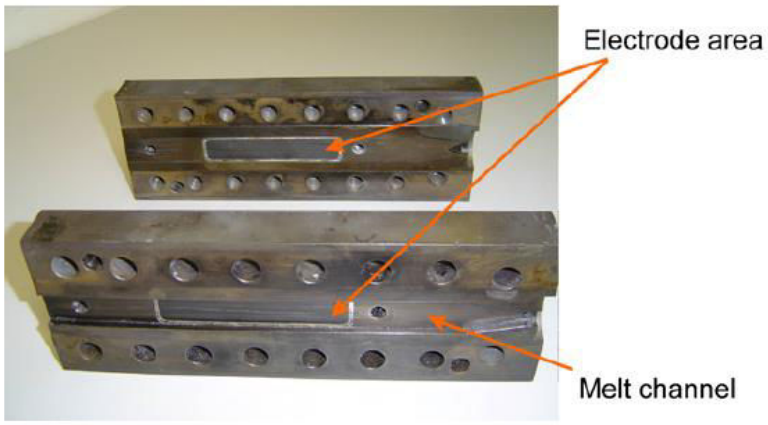

Figure 2.8 Configuration of the die of the extruder.

Optical spectroscopic techniques are used to measure the chemical structure of polymers in a screw extruder. Fourier-transform infrared spectroscopy (FTIR) was the first optical spectroscopic method that was applied for polymer processing. Fisher et al. [123] mounted a ZnSe-attenuated total reflection (ATR) probe in the crotch region between the screws of a twin screw extruder to in-line monitor the copolymerization of the styrene-maleic-anhydride system. Later, near infrared spectroscopy (NIR) [131-134], Raman spectroscopy [135, 136], ultraviolet spectroscopy (UV) [137-139] and fluorescent spectroscopy [140-142] were applied to polymer blending processes. Alig et al. [143] combined NIR, Roman and ultrasound spectroscopy to in-line measure polymer blend compositions in a twin screw extruder, as shown in Figure 2.9.

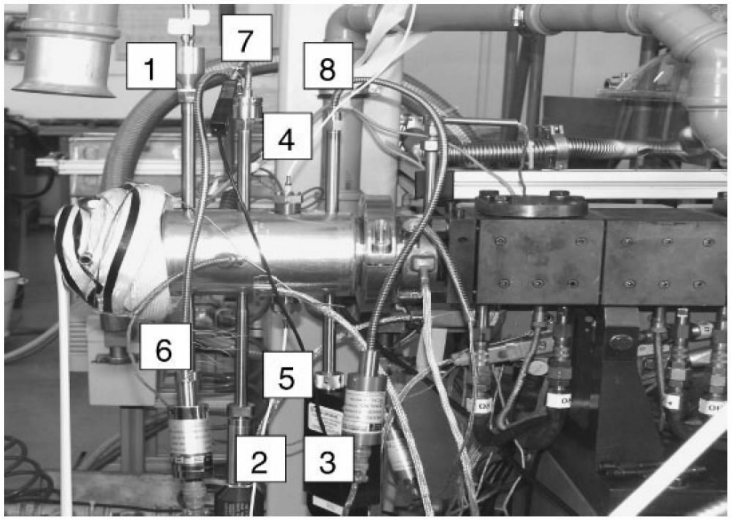

Figure 2.9 Picture of a slit die of a twin-screw extruder: NIR reflectance probe (1), Raman probes

(2, 3), ultrasonic transducer (4, 5), temperature (6) and pressure sensor (7, 8).

2.5.2 In-line measurement of morphology

The morphology of polymer blends directly influences their final performances. Therefore, it is important to in-line monitor the morphology during polymer processing. The dispersed phase domain size for immiscible polymer blends to exhibit optimum mechanical properties such as impact strength usually ranges from around 0.2 to 1 μm, which could be measured via small-angle light scattering. Figure 2.10 is the scheme of a small-angle light scattering setup for morphology monitoring during extrusion [123]. The sapphire windows were mounted face to face at the melt channel so that the melt could be detected by a laser beam. The incident laser light is scattered by the dispersed phase domains and the scattering cone was captured by a diffusive screen. The scattering pattern was projected onto the chip of a CCD camera to obtain the morphology of the polymer blend. Figure 2.11 compares the light scattering pattern (left column) and SEM images at different positions within the extruded strand of a polypropylene (PP)/ polyolefin elastomer (POE) blend. The morphology at different positions was different because of the boundary effect. At a throughput of 2.5 kg/h, the scattering pattern and SEM exhibited superposition of fibers and spheres. Increasing the throughput to 20 kg/h, the needle structure was not stable and became spheres.

The ultrasound spectroscopy could be used to in-line measure the morphology of polymer blends in complement with small-angle light scattering. Alig et al. [123] used the pulse transmission setup (thickness of the melt channel 4 mm) to in-line ultrasound measure the dispersion of PP/chalk composites. The contribution of the polymer matrix to ultrasonic absorption could be neglected and, therefore, the sound attenuation in the PP/chalk melts was dominated by scattering of the ultrasonic waves on the filler particles. The nanoparticle size could be obtained by theoretical calculation. Besides, the ultrasonic in-line measurements are not limited to optical transparent samples.

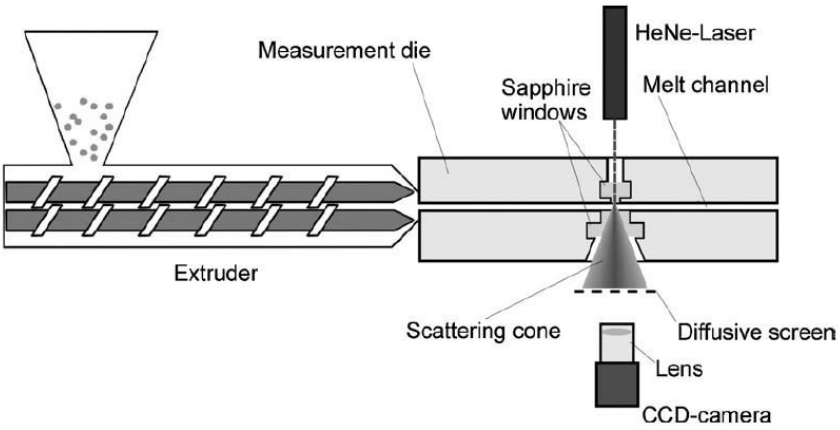

Figure 2.10 Scheme of a small-angle light scattering setup for morphology monitoring during extrusion.

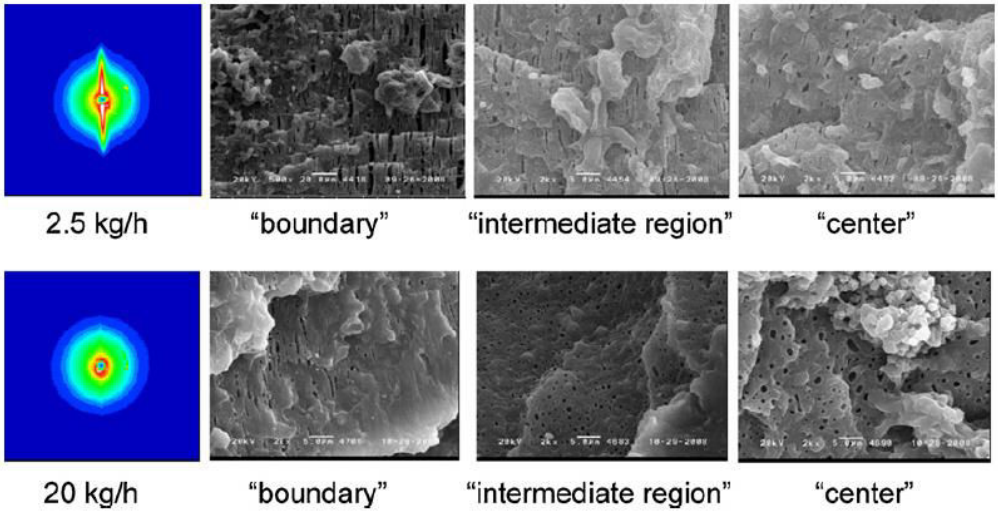

Figure 2.11 Light scattering pattern (left column) and SEM images at different positions within the extruded strand of a PP/POE blend. "Boundary" represents the position near the screw wall; "center" represents the axis; "intermediate region" represents for the position between the axis and screw wall.

Chapter 3 Effect of molecular architecture of reactive compatibilizer-tracer on the interfacial reaction and morphology in polymer batch blending

3.1 Introduction

During reactive polymer blending, the evolution of morphology and interfacial reaction are highly coupled. Moreover, the amount of the in-situ formed copolymer is often too small to measure. In order to take this challenge, fluorescent groups are incorporated into a reactive compatbilizer to form a reactive compatibilizer-tracer. The latter acts both as a reactive compatibilizer to reduce the dispersed phase domain size and a tracer allowing for accurate detection of small amounts of the in-situ formed copolymer.

This chapter is based on the polymer blending system of polystyrene (PS) and polyamide 6 (PA6). Two reactive compatibilizer-tracers are synthesized: (1) 9-(methylaminomethyl)anthracene (MAMA) containing fluorescent group is introduced into the styrene (St) and 3-isopropenyl-α, α'-dimethylbenzene isocyanate (TMI) copolymer (PS-TMI) to form a multifunctional reactive compatibilizer-tracer PS-TMI-MAMA; (2) 9-Anthracenecarboxylic acid containing fluorescent group is introduced into the anhydride-terminated polystyrene (Anhy-PS-Br) to form a chain-end functional reactive compatibilizer-tracer Anhy-PS-Anth.

PS-TMI-MAMA and Anhy-PS-Anth are chosen as the reactive compatibilizer-tracers for two reasons. Firstly, the isocyanate (NCO) groups in PS-TMI-MAMA and anhydride group in Anhy-PS-Anth could react with the terminal amine group of PA6 to in-situ form graft copolymer PS-g-PA6-MAMA and block copolymer PS-b-PA6-Anth, respectively. Secondly and most importantly, the anthracene groups in PS-g-PA6-MAMA and PS-b-PA6-Anth have fluorescent properties which allow detecting the amount of the reaction via size exclusion chromatography (SEC) with an ultraviolet (UV) detector.

3.2 Experimental

3.2.1 Materials

Table 3.1 shows the information of chemicals used in this chapter. Styrene (St) was purified under vacuum distillation to remove the polymerization inhibitor Toluene was purified by distillation. Benzoyl peroxide (BPO) as the initiator was purified by dissolution in chloroform, precipitation in methanol, and vacuum-drying at room temperature. Other chemicals were used as received. Selected characteristics of PS and PA6 used in this work are shown in Table 3.2.

Table 3.1 Selected information on chemicals

Chemicals	Standard	Supplier
Styrene (St)	AR	Sinopharm Chemicals
Toluene	AR	Sinopharm Chemicals
Benzoyl peroxide (BPO)	AR	Sinopharm Chemicals
3-isopropenyl-α, α'-dimethylbenzene isocyanate (TMI)	AR	Sigma Aldrich
Methanol	AR	Sinopharm Chemicals
9-(methylaminomethyl)anthracene (MAMA)	AR	Sigma Aldrich
Tetrahydrofuran (THF)	AR	Sinopharm Chemicals
Formic acid	AR	Sinopharm Chemicals
4-methylphthalic anhydride	AR	ACROS
N-bromosuccimide (NBS)	AR	ACROS
CuCl	AR	Aladdin
2,2-bipyridyl (dpy)	AR	Sinopharm Chemicals
9- anthracene carboxylic acid (Anth)	AR	J & K
K_2CO_3	AR	Sinopharm Chemicals
N, N-dimethyl formamidine (DMF)	AR	Sinopharm Chemicals

Table 3.2 Characteristics of PS and PA6 used in this study.

Materials	M_w[a] (kg/mol)	M_n[a] (kg/mol)	Content of terminal amine (μmol/g)[b]	Supplier
PS	228.8	101.3	-	Yangzi-BASF Styrenics Co. Nanjing, China
PA6	49.4	19.4	60.3	UBE Nylon Ltd., Thailand

[a] Molar masses measured by SEC using PS standards for the calibration and tetrahydrofuran (THF) as the eluent. PA6 was first N-trifluoroaeetylated before the SEC measurement.
[b] The content of terminal amine in PA6 was titrated by hydrochloric acid solution.

3.2.2 Synthesis of PS-TMI-MAMA

3.2.2.1 Synthesis of PS-TMI

The copolymer PS-TMI of St and TMI was synthesized via free radical solution polymerization, which is shown in Figure 3.1. The polymerization was prepared in a 1-L glass reactor equipped with mechanical stirrer under the protection of N_2. Toluene, St and TMI were charged to the reactor firstly followed by the addition of BPO when the reactor reached at the setting temperature controlled by the circulating water. The polymerization lasted for 12h. The product was precipitated in the icy methanol twice and dried in vacuum oven at 80°C for 12h. More details of synthesis are provided elsewhere. [144-148] The compositions of St/TMI/BPO/toluene and polymerization temperature are shown in Table 3.3.

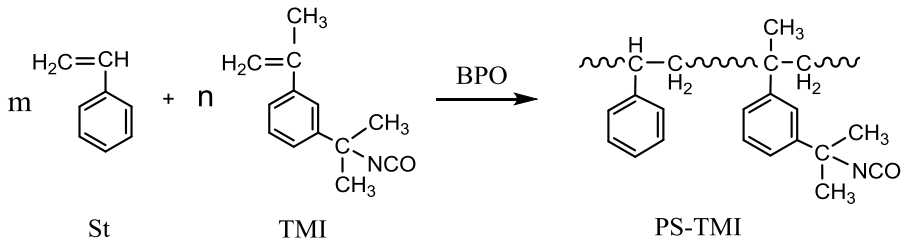

Figure 3.1 Scheme of PS-TMI synthesis.

Table 3.3 Compositions of St/TMI/BPO/toluene and polymerization temperature used for the synthesis of PS-TMI

PS-TMI	St/TMI/BPO/Toluene	Temperature (^{o}C)
PS-TMI1	60 ml/4.8 ml/0.35 g/40 ml	80
PS-TMI2	40 ml/3.2 ml/0.021 g/60 ml	70

3.2.2.2 Synthesis of PS-TMI-MAMA

Scheme of PS-TMI-MAMA synthesis is shown in Figure 3.2. PS-TMI-MAMA was prepared by coupling PS-TMI and MAMA in the THF at 40°C for 4 h. The resulting product was predicated in the icy methanol twice and dried in vacuum oven at 80°C for 12h. The composition of PS-TMI/MAMA/THF is shown in Table 3.4. During the reaction, only a fraction of isocyanate group in PS-TMI reacted with MAMA so that there were a large amount of isocyanate groups in PS-TMI-MAMA.

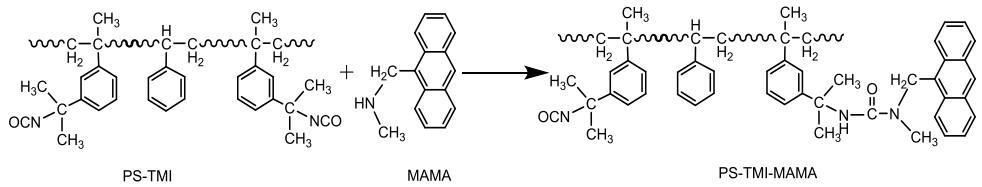

Figure 3.2 Scheme of PS-TMI-MAMA synthesis.

Table 3.4 Compositions of PS-TMI/MAMA/THF for the synthesis of PS-TMI-MAMA.

PS-TMI-MAMA	PS-TMI/MAMA/THF	PS-TMI
PS-TMI-MAMA1	10 g/0.05 g/50 ml	PS-TMI1
PS-TMI-MAMA2	10 g/0.72 g/50 ml	PS-TMI2
PS-TMI-MAMA3	10 g/0.20 g/50 ml	PS-TMI2

3.2.3 Synthesis of Anhy-PS-Anth

3.2.3.1 Synthesis of 4-bromomethylphthalic anhydride

The scheme of 4-bromomethylphthalic anhydride synthesis is shown in Figure 3.3. 4-methylphthalic anhydride (5.0 g) was dissolved in carbon tetrachloride (CCl_4; 50 mL). NBS (5.5 g) and BPO (0.31 g) were added later. After the reaction mixture was refluxed at 90°C for 2 h, the mixture was cooled in an ice bath and then the succinimide was filtered off. Lastly, the organic phase was evaporated under vacuum

to remove CCl_4 yielding yellowish oil. The resulting product was 4-bromomethylphthalic anhydride, which was subsequently used as the ATRP initiator.

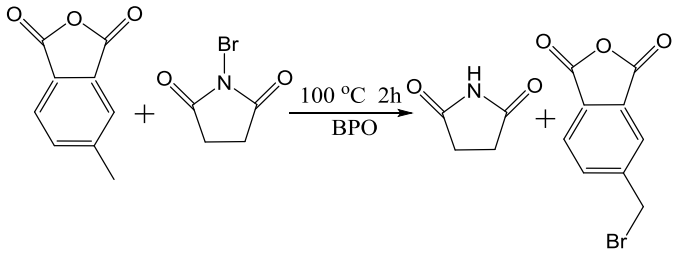

Figure 3.3 Scheme of 4-bromomethylphthalic anhydride synthesis.

3.2.3.2 Synthesis of Anhy-PS-Br

Anhy-PS-Br was synthesized via atom transfer radical polymerization (ATRP) which is shown in Figure 3.4. 4-bromomethylphthalic anhydride was used to initiate the polymerization of styrene with the catalyst system of CuCl/Cu/bpy.

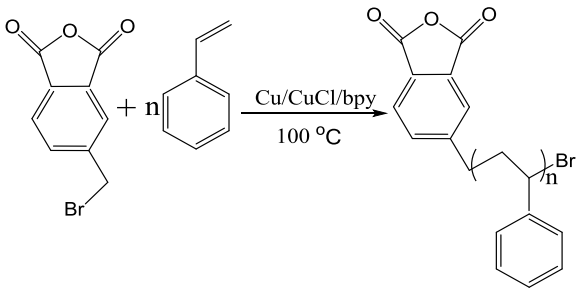

Figure 3.4 Scheme of Anhy-PS-Br synthesis.

CuCl (0.079 g), Cu (0.051 g), bpy (0.373 g), 4-bromomethylphthalic anhydride (0.236 g) were dissolved in 33.1 ml of styrene and the solution was then transferred to a 50 ml flask and degassed by three freeze-pump-thaw cycles. The flask was placed in an oil bath at 80°C to initiate the polymerization. The reaction lasted for 12 h and the mixture was dissolved in THF, followed by passing through a cation exchange resin column to remove the catalyst. Most of THF was distilled under reduced pressure and then the solution was precipitated in cold methane. The product was dried under vacuum at 80°C.

3.2.3.3 Synthesis of Anhy-PS-Anth

Anhy-PS-Anth was obtained by a nucleophilic substitution reaction which is illustrated in Figure 3.5.

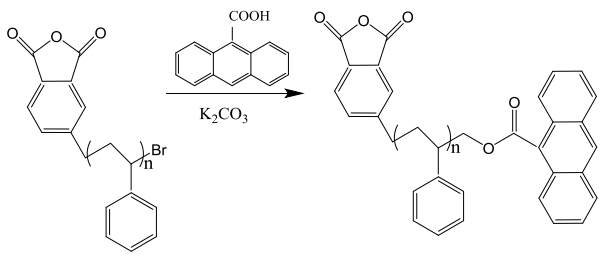

Figure 3.5 Scheme of Anhy-PS-Anth synthesis

Anhy-PS-Br, 9-Anthroic acid and K_2CO_3 with a molar ratio of 1/1.5/1.5 were dissolved in 60 ml DMF in a 100 ml flask. The reaction was carried out under N_2 atmosphere at 70°C for 12 h. The yellow solution was precipitated in cold water and the yellow product was washed by cold methane for three times and dried under vacuum at 80°C.

3.2.4 Blending

PS/PA6/PS-TMI-MAMA blends were processed in a batch mixer of type Brabender torque rheometer with a mixing chamber of 50 ml in capacity, which is shown in Figure 3.6. The two rotors located in the mixing chamber ensure the mixing. The PS-TMI-MAMA content in the blends was always 1.5 wt% of the total mass of the PS and PA6. The mixing of the blending systems was ensured by the rotation of two rotors of the mixing chamber. Two mixing modes were adopted, as show below:

1) Continuous mixing: after mixing at several minutes (1, 2, 3, 4, 5, 8 or 10 min), the samples are taken out to the liquid nitrogen to freeze the morphology.
2) Stepwise mixing: after mixing at 2 min, the rotors stopped rotating, and the blending system was annealed under the quiescent condition for a period of time (3 min, 5 min or 8 min) and then the mixing was resumed at 100 rpm.

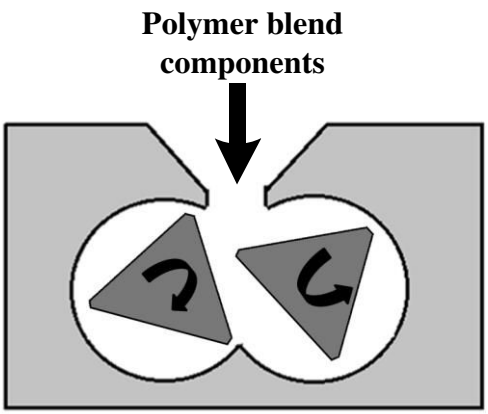

Figure 3.6 Scheme of a batch mixer.

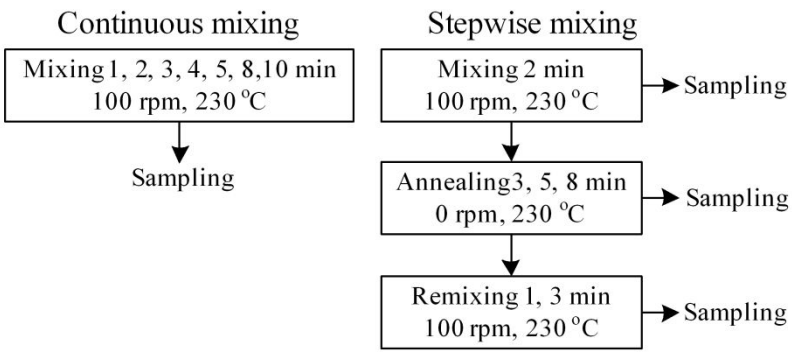

Figure 3.7 Mixing modes used for polymer blending.

3.2.5 Fourier transform infrared spectrometer (FTIR)

FTIR (Nicolet 5700) was used to characterize the polymer products. FTIR spectra were then recorded on those films with 32 scans and a resolution of 4 cm^{-1}. The polymer was dissolved in THF with the concentration of 0.03 g/ml and the polymer solution was cast to thin films on a KBr disc.

3.2.6 Size exclusion chromatography (SEC)

The polymer products were dissolved in THF with a concentration of 3 mg/ml. After filtration, the solution was injected into the SEC apparatus (Waters 1525/2414; injection volume: 50 μl) with a refractometer and a UV-detector (UV 254nm and UV 367 nm).

3.2.7 Ultraviolet spectrometer (UV)

The polymer products were dissolved in THF and measured by UV (UV3802) between 200-400 nm.

3.2.8 Morphology of polymer blend

The size of the PA6 domains in the PS matrix was characterized by scanning electron microscopy (SEM) of type ZEISS ULTRA55. Before the SEM observation, samples were fractured in liquid nitrogen, and immersed in formic acid at room temperature for 12 h to remove the dispersed phase domains (PA6) from the fractured surface, and finally dried in a vacuum oven at 80°C for 12 h. The dried samples were sputtered with gold and analyzed by SEM at 5 kV. A semi-automatic image analysis was used to determine the diameter of the dispersed phase domains. It was characterized by the volume average particle diameter, dv, defined as follows:：

$$d_v = \frac{\sum n_i d_i^4}{\sum n_i d_i^3} \quad (3\text{-}1)$$

For each blend, at least 500 particles were counted for statistically meaningful values of d_v. In this work, the number average diameter followed the same trend as d_v.

3.2.9 Determination of the amount of reacted copolymer

Before the SEC measurement, the reacted copolymer and the intact (non-reacted) one were separated from the blends in the following manner. Take PS-TMI-MAMA as an example. About 1 g of the blend was introduced to a centrifuge tube filled with 50 ml (THF) at room temperature. The tube was then placed in a shaker to promote the dissolution of the PS and the intact PS-TMI-MAMA. After 48 h of dissolution, the solution was centrifuged at 9000 rpm for 20 min. The supernatant solution was thrown away and THF was added to the tube. The solution in the tube was shaken for another 48 h. That process was repeated three times in order to thoroughly remove the PS and the intact PS-TMI-MAMA. The final insoluble products were mixtures of the non-reacted PA6 and PS-g-PA6-MAMA graft copolymer formed by the interfacial reaction between the PS-TMI-MAMA and PA6.

The PA6 and PS-g-PA6-MAMA became soluble in THF after they had reacted with N-trifluoroacetic anhydride (TFAA). [149] Before the N-trifluoroacetylation, the

mixture of the PA6 and PS-g-PA6-MAMA was dried in a vacuum oven at 80°C for 12 h to remove moisture. About 0.03 g of the dried mixture was added to a flask followed by 4 ml CH_2Cl_2, 2 ml TFAA and 6 ml $CHCl_3$ in a sequential manner. After 24 h of reaction, the TFAA modified mixture was isolated by rotary evaporation at 30°C, and then dissolved in THF to prepare SEC solution with a concentration of 3 mg/ml. After the filtration, 50 μl of the solution was injected into a SEC apparatus equipped with a refractometer and a UV detector. Caution: the solution should be measured by SEC within a few hours after it was prepared. Otherwise it would form gel.

The fluorescent labels of the PS-TMI-MAMA and Anhy-PS-Anth allowed determining the amount of the PS-TMI-MAMA and Anhy-PS-Anth that had reacted during the reactive blending process via SEC with a UV detector. MAMA and Anth had very strong UV-absorption at 367 nm while the PA6 and PS did not have any absorption there. It should be noted that the extent of the interfacial reaction was defined as the percentage of the amount of the reacted reactive compatibilizer-tracer with respect to that of the PS/PA6 blend. PS-TMI-MAMA has multiple NCO groups per chain. Once one NCO group in PS-TMI-MAMA reacted with PA6, this PS-TMI-MAMA chain was counted into the content of reacted PS-TMI-MAMA

3.2.10 Confocal microscopy

The formation and size of PS-g-PA6-MAMA graft copolymer micelles in the PS/PA6 blends were examined by confocal microscopy. Polymer blends were cut to specimens of 1 to 2 mm thick and 1 cm x 1 cm large. Fluorescent microscopy measurements were performed on an improved Leica Microsystems apparatus.[22] The fluorescence signal for anthracene was collected in the reflected light channel. All image acquisition procedures were performed at an excitation wavelength of 800 nm, with the pinhole fully opened (8.41 AU). A band-pass filter enabled to select the detection spectral range (400/25 nm center wavelength/bandwidth) for anthracene and to reject the infrared excitation beam.

3.3 Result and discussion

3.3.1 Characteristic of PS-TMI-MAMA

3.3.1.1 FTIR of PS-TMI

The FTIR spectrums of PS and PS-TMI1 are shown in Figure 3.8. It can be seen that PS and PS-TMI have peaks at 1601 $cm^{-1}$and 1492 cm^{-1} which indicate the benzene ring and overtone peaks between 1667 cm^{-1} and 2000 cm^{-1} which indicate the benzene derivatives. Besides, PS-TMI-1 also has a peak at 2254 cm^{-1} which indicates the -N=C=O. These results show that the polymer product has benzene ring and TMI. Because the TMI monomer could not polymerization itself, indicating that the polymer product is PS-TMI.

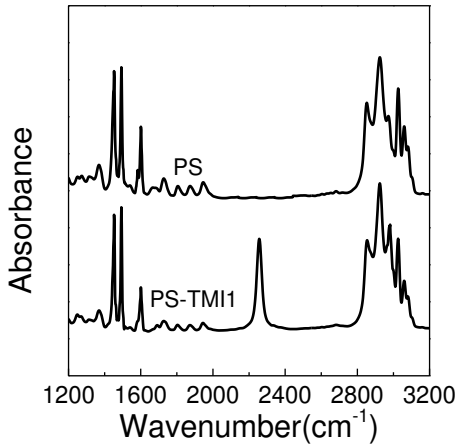

Figure 3.8 FTIR spectrums of PS and PS-TMI1.

3.3.1.2 Content of TMI

PS-TMI reacted with excess MAMA so that all the NCO groups in PS-TMI were resumed. The polymer product was precipitated in the icy methanol twice to wash the excess MAMA away. Then the molar content of MAMA in PS-MAMA is equal to that of TMI in PS-TMI.

The ultraviolet absorption spectrum of MAMA and polymer product PS-MAMA1 of the reaction of PS-TMI1 and excess MAMA in THF solution are shown in Figure 3.9. It can be seen that in the wavelength range between 300 nm and 420 nm, these two polymers have the same maximum wavelength at 367 nm and their UV absorption spectrum almost superimposes, which indicates that the introduction

of St and TMI has no influence on the UV absorption of MAMA. Hence, the MAMA content in PS-MAMA1 could be calculated based on the linear relationship between MAMA concentration and UV intensity at 367nm (Figure 3.10).

The characteristics of PS-TMI-MAMA are shown in Table 3.5.

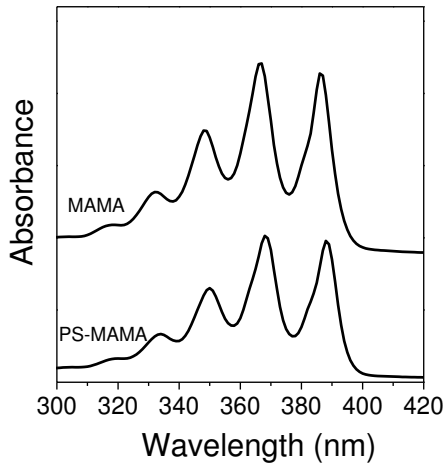

Figure 3.9 Ultraviolet absorption spectrum of MAMA and PS-MAMA1.

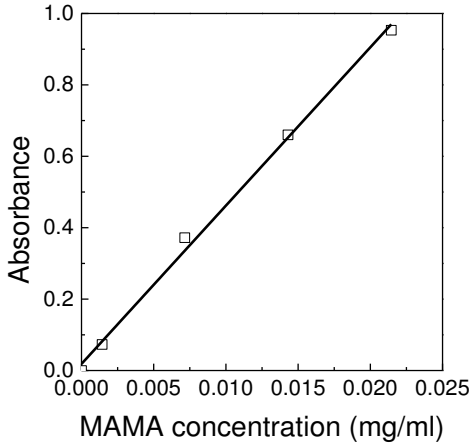

Figure 3.10 Linear relationships between the intensity of UV absorption of MAMA and its concentration in THF under 367 nm.

Table 3.5 Charateristics of PS-TMI-MAMA.

PS-TMI-MAMA	M_n (kg/mol)	TMI (wt%)	MAMA (wt%)	Number of TMI per chain	Number of St between TMI
PS-TMI-MAMA1	37.6	7.1	0.5	13.3	23.0
PS-TMI-MAMA2	118	2.4	7.2	14.1	68.0
PS-TMI-MAMA3	118	7.7	1.9	45.2	22.4

3.3.2 Characteristic of Anhy-PS-Anth

The FTIR spectrum of Anhy-PS-Br and Anhy-PS-Anth is shown in Figure 3.11. It can be seen that Anhy-PS-Br and Anhy-PS-Anth have absorption peaks at 1258 cm^{-1}, 1782 cm^{-1} and 1850 cm^{-1} which indicate the anhydride group and absorption peaks at 1601 cm^{-1} and 1492 cm^{-1} which indicate the benzene ring and overtone peaks of benzene ring between 1667 cm^{-1} and 2000 cm^{-1}. The results show 4-bromomethylphthalic anhydride initiate the polymerization of St monomer to produce Anhy-PS-Br. Besides, Anhy-PS-Anth has peak absorption of carbonyl group at 1679 cm^{-1}, indicating the product of the reaction between Anhy-PS-Br and 9-anthracene carboxylic acid is Anhy-PS-Anth. The number-average molar mass of Anhy-PS-Anth is 32.9 kg/mol.

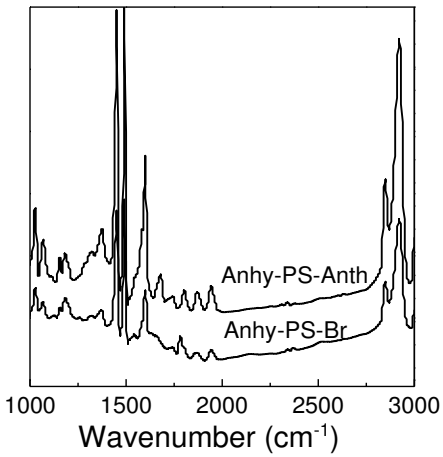

Figure 3.11 FTIR spectrums of Anhy-PS-Br and Anhy-PS-Anth.

3.3.3 Effect of graft and block reactive compatibilizer-tracer

During the reactive polymer blending, the PS-TMI-MAMA and Anhy-PS-Anth would migrate to the interface of PS and PA6 and react with the terminal amine group of PA6 to in-situ form the graft copolymer PS-g-PA6-MAMA and block copolymer PS-b-PA6-Anth respectively, as shown in Figure 3.12 and Figure 3.13.

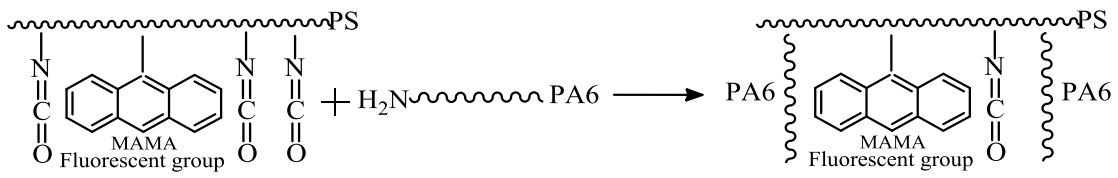

Figure 3.12 The scheme of formation of PS-g-PA6-MAMA of PS/PA6/PS-TMI-MAMA system.

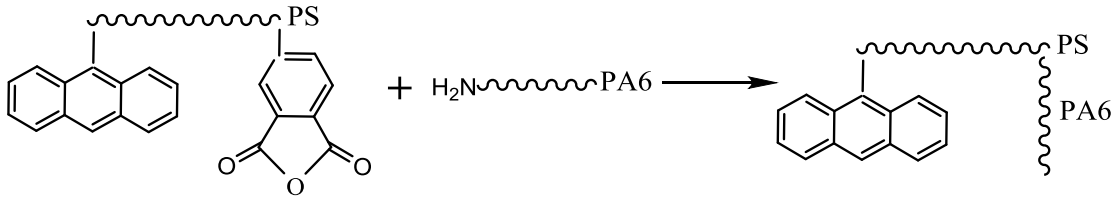

Figure 3.13 formation of PS-b-PA6-Anth by in-situ comnpatibilization of PS/PA6/Anhy-PS-Anth blend system.

Figure 3.14 shows the evolution of the content of reacted copolymer (a), dispersed phase domain size (b) as a function of time and the evolution of the dispersed phase domain size as a function of the content of the reacted copolymer (c) of the PS/PA6 (80/20) blend with PS-TMI-MAMA1 as the graft reactive compatibilizer-tracer and Anth-PS-Anth as the block reactive compatibilizer-tracer. It can be seen that during the short blending time (< 4 min), the content of the reacted Anhy-PS-Anth and PS-TMI-MAMA1 are almost the same. However, the dispersed phase domain size of the polymer blend system with PS-TMI-MAMA1 as the reactive compatibilizer-tracer is smaller than that of the polymer blend system with Anhy-PS-Anth as the reactive compatibilizer-tracer. For example, in terms of the polymer blend system with PS-TMI-MAMA1, the dispersed phase domains size is about 0.5 μm in less than 1 min of mixing, and reaches the minimum value at 0.45 μm for another 1 min of mixing. In terms of the polymer blend system with Anhy-PS-Anth, the dispersed phase domains size reaches about 1.5 μm in less than 1 min of mixing, and reaches the minimum value at 1.0 μm for another 3 min of mixing. It indicates that the compatibiliizng efficiency of Anhy-PS-Anth is lower than that of PS-TMI-MAMA1 during the initial period of mixing. The number-average molar mass of PS-TMI-MAMA1 (M_n=37.8 kg/mol) is very close to that of Anhy-PS-Anth (M_n=32.9 kg/mol). However, PS-TMI-MAMA1 has 13.3 NCO groups per chain and Anhy-PS-Anth just has one terminal anhydride group. Thus, the compatibilizing

efficiency of PS-TMI-MAMA1 is higher here.

When the mixing time increases to 5 min, the in-situ formed graft copolymer or block copolymer both increase slightly. The dispersed phase domain size of the polymer blending system with Anhy-PS-Anth remains unchanged, indicating that the in-situ formed block copolymer reaches a critical concentration. However, the dispersed phase domain size of PS-TMI-MAMA1 system increases sharply. It can also be seen from Figure 3.14c and 3.15 that for both compositions PS/PA6 (80/20) and (95/5), the dispersed phase domain size starts to drastically increase when the content of the reacted PS-TMI-MAMA1 reaches a critical value.

For a normal reactive polymer blending process, the dispersed phase domain size is expected to decrease with mixing time first and then level off, such as the PS/PA6/Anhy-PS-Anth (80/20/1.5) blend. However, in the case of the PS/PA6/PS-TMI-MAMA1 (80/20/1.5) and (95/5/1.5) blending systems, a strange phenomenon occurs, which may be related to the molecular architecture of the in-situ formed copolymer. In the later period of mixing, the number of PA6 grafts in the in-situ formed PS-g-PA6-MAMA increases. Then PS-g-PA6-MAMA with multiple grafts could not be stable at the interface and would be pulled out of the interface, resulting in the sharp increase in the dispersed phase domain size. However, for the Anhy-PS-Anth blending system, the molecular architecture of the in-situ formed block copolymer remains unchanged with mixing time. The block copolymer would be stable at the interface and prevent the dispersed phase domains from coalescence.

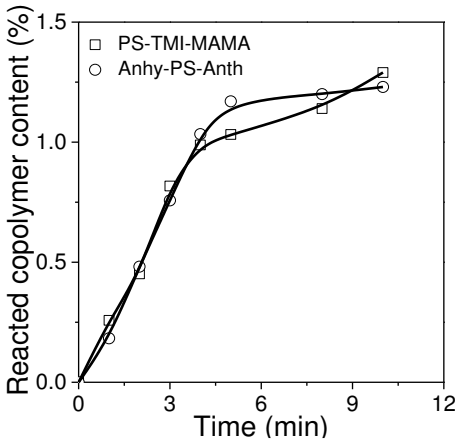

（a）

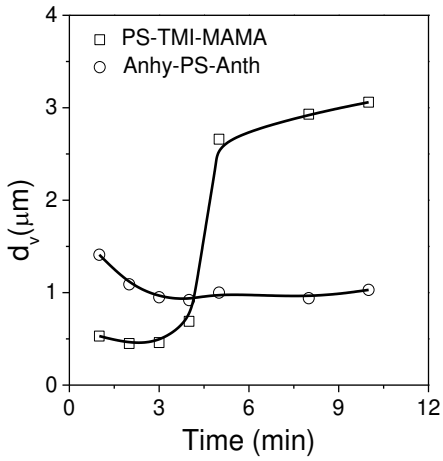

（b）

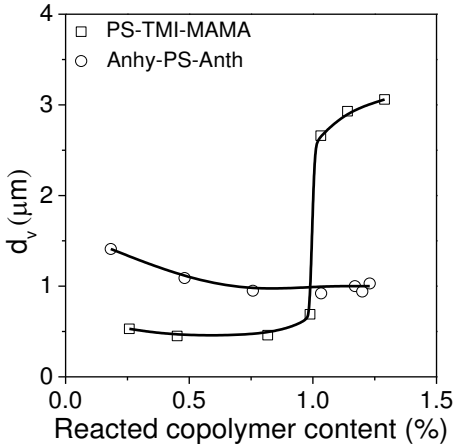

（c）

Figure 3.14 Evolution of the content of the reacted copolymer (a)，dispersed phase domain size (b) as a function of time and the evolution of the dispersed phase domain size as a function of the content of the reacted copolymer (c) of the PS/PA6 (80/20) blend with PS-TMI-MAMA1 as the graft reactive compatibilizer-tracer and Anth-PS-Anth as the block reactive compatibilizer-tracer.

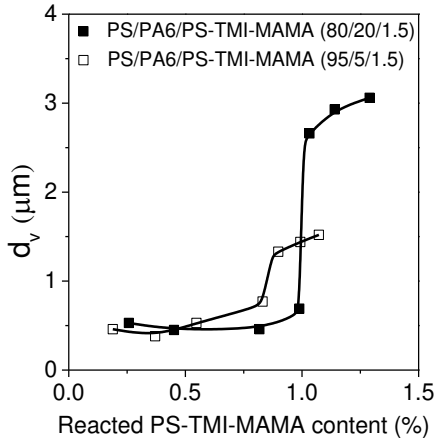

Figure 3.15 Evolution of the dispersed phase domain size (PA6) of the PS/PA6/PS-TMI-MAMA1 (80/20/1.5) and (95/5/1.5) reactive blending system as a function of the content of the reacted PS-TMI-MAMA.

3.3.4 Effect of the molecular architecture of graft reactive compaitbilizer-tracer

In order to confirm that the increase in the dispersed phase domain size during the later period of mixing is related to the molecular architecture of the compatibilizer, three graft reactive compatibilizer-tracers with different molecular architectures (Figure 3.16) are used to investigate the effect of the molecular architecture on the PS/PA6 (80/20) blend.

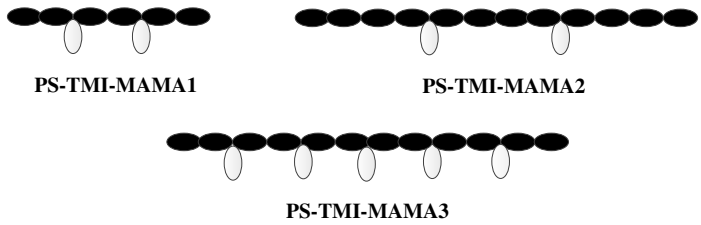

Figure 3.16 Three different kinds of reactive compatibilizer-tracers PS-TMI-MAMA.

PS-TMI-MAMA1 and PS-TMI-MAMA2 have the same number of TMI per chain, but the molar mass of the latter is about twice that of the former. It indicates that the PA6 graft density in the PS-TMI-MAMA1 blend system is twice that of the PS-TMI-MAMA2 blend system after complete reaction with the PA6. Hence, compared to the PS-TMI-MAMA1 system, the repulsion force between the PS backbone of PS-g-PA6-MAMA and the dispersed phase PA6 is much larger than the

PS-TMI-MAMA2 system. The PS-g-PA6-MAMA of the PS-TMI-MAMA2 system needs to overcome much higher energetic barriers to migrate to the PA6.

Figure 3.17 is the evolution of the content of the reacted PS-TMI-MAMA (a) and the dispersed phase domain size (b) as a function of time using PS-TMI-MAMA1 and PS-TMI-MAMA2 as the reactive compatibilizer-tracers for the PS/PA6 (80/20) blend. It can be seen that during the later period of mixing, in the case of PS-TMI-MAMA2 whose molar mass is higher than that of PS-TMI-MAMA1, the amount of the in-situ formed graft copolymer is smaller than that of PS-TMI-MAMA1 but the degree of the increase in the dispersed phase domain size is less serious than that of PS-TMI-MAMA1. It confirms that PS-g-PA6-MAMA with more spaced PA6 grafts would be more stable at the interface and more difficult to be pulled out of the interface, resulting in a more moderate increase in the dispersed phase domain size.

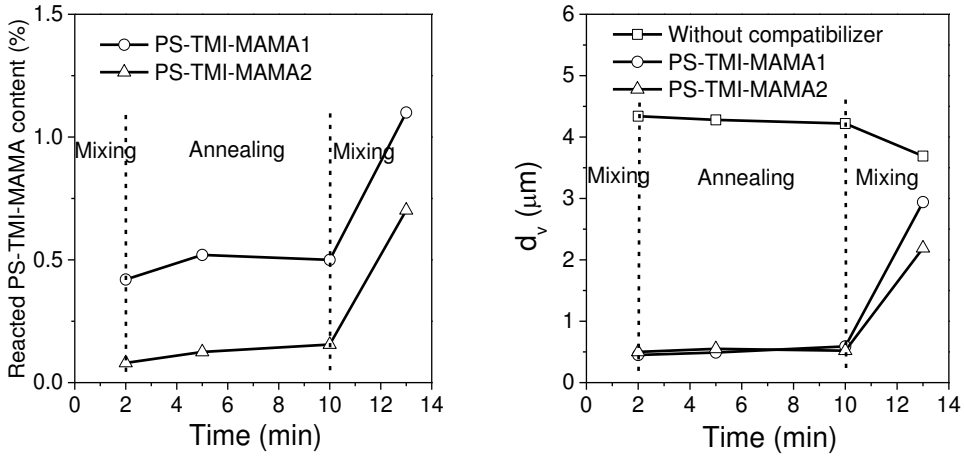

(a) (b)

Figure 3.17 Evolution of the content of reacted PS-TMI-MAMA (a) and the dispersed phase domain size (b) as a function of time using PS-TMI-MAMA1 and PS-TMI-MAMA2 as the reactive compatibilizer-tracers for the PS/PA6 (80/20) blend.

PS-TMI-MAMA1 and PS-TMI-MAMA3 are used to investigate the effect of molar mass for a given TMI density. Figure 3.18 is the evolution of the content of the reacted PS-TMI-MAMA (a) and he dispersed phase domain size (b) as a function of time using PS-TMI-MAMA1 and PS-TMI-MAMA3 as the reactive compatibilizer-tracer for the PS/PA6 (80/20) blend. It can be seen that the contents of the reacted PS-TMI-MAMA are almost the same for both reactive

compatibilizer-tracer. Moreover, the evolution of the dispersed phase domain size is almost the same. These results indicate that when the TMI density is fixed, the molar mass of PS-TMI-MAMA has no influence on the dispersed phase domain size within the molar mass range studied. In other words, it is the PA6 graft density and not the molar mass that dictates the sharp increase in the dispersed phase domain size during the latter period of mixing.

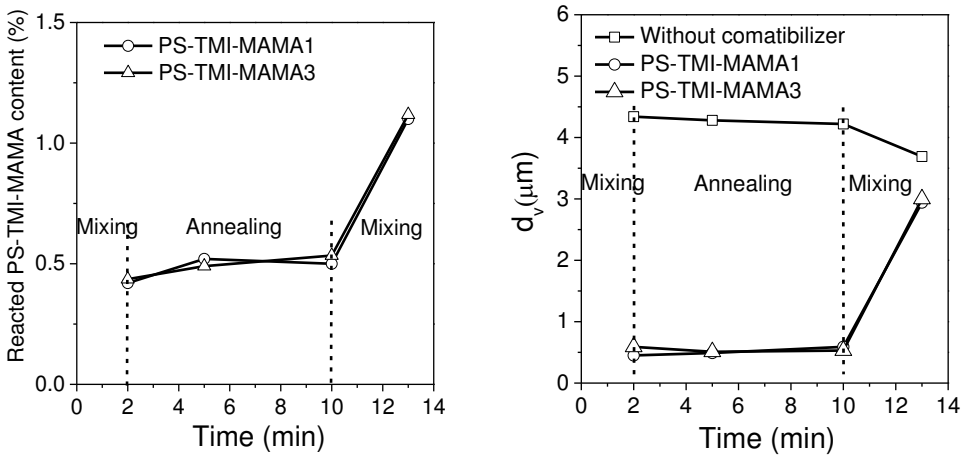

（a） (b)

Figure 3.18 Evolution of the content of the reacted PS-TMI-MAMA (a) and the dispersed phase domain size (b) as a function of time using PS-TMI-MAMA1 and PS-TMI-MAMA3 as the reactive compatibilizer-tracers for the PS/PA6 (80/20) blend. These two reactive compatibilizer-tracers have the same TMI density but different molar masses.

3.3.5 Mechanism analysis of the sharp increase in the dispersed phase domain size during the latter period of mixing

Let us consider the evolution of the interfacial coverage of the copolymer Σ during the reactive blending. Σ is defined as the number of copolymer chain per interfacial area and can be estimated by：

$$\Sigma = \frac{w_{cr} N_a \rho_{PA6} d_v}{6\phi_{PA6} M_n} \tag{3-2}$$

where w_{cr} is the percentage of the reacted PS-TMI-MAMA, N_a is Avogardro's number, ρ_{PA6} is the density of PA6 (1.14g/cm^3), d_v is the volume average dispersed phase domain size and M_n is the number average molar mass of the compatibilizer. The maximum interfacial coverage, $\sum_{max}$ can be estimated by assuming a dense monolayer

of copolymers at the interface. Russell et al[151] came up with the following empirical equation for a block copolymer:

$$\Sigma_{max} = 2.06N^{-0.39} \quad (3\text{-}3)$$

N is the polymerization degree. However, this equation is not applicable for the graft copolymer. Kim et al [39] found that a PS-g-PI graft copolymer has an interfacial area about 1.7 times that of a block analogue. Hence the maximum interfacial coverage of PS-g-PA6-MAMA could be calculated based on the equation: $\Sigma_{max} = 2.06N^{-0.39}/1.7$.

Figure 3.19 shows the dispersed phase domain size as a function of $\sum/\sum_{max}$ for the PS/PA6/PS-TMI-MAMA blend with two compositions. For both compositions, the dispersed phase domain size is very small when $\sum/\sum_{max}$ is below 0.6. It seems to decrease with increasing $\sum/\sum_{max}$ till the latter is about 0.6. Nevertheless, this trend is not obvious, due to the narrow range of the data points. When $\sum/\sum_{max}$ is above 0.6 or so, the dispersed phase domain size starts to increase with increasing $\sum/\sum_{max}$ and this trend continues even when $\sum/\sum_{max}$ exceeds 1. A value of $\sum/\sum_{max}$ higher than 1 indicates that the amount of the copolymer is in excess compared with what is necessary to saturate the interfaces with a monolayer of the copolymer. The copolymer in excess is expected to form micelles. This is shown by the images of the confocal spectroscopy of the PS/PA6/PS-TMI-MAMA (80/20/3) blend after 2 min (Figure 3.20a) and 10 min of continuous mixing (Figure 3.20b). It is seen that there are much more micelles (corresponding to turquoise dots) in the blend with 10 min of mixing than in the one with 2 min of mixing. This supports the above statement that the pull out of the in-situ formed PS-g-PA6-MAMA graft copolymer from the interfaces is responsible for the loss of its compatibilizing efficiency.

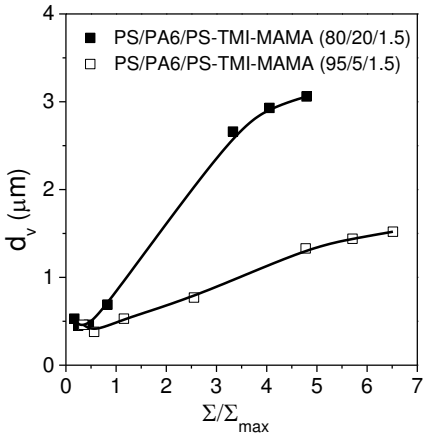

Figure 3.19 Diameter of the dispersed phase domains as a function of the relative interfacial coverage of the copolymer Σ/Σ_{max} for PS/PA6/PS-TMI-MAMA1 reactive blends.

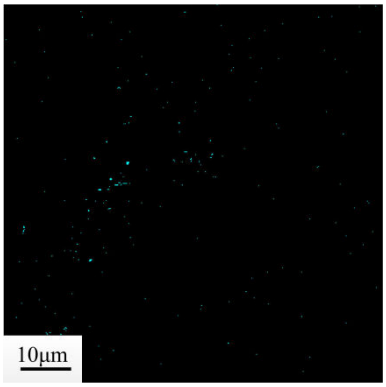

(a)

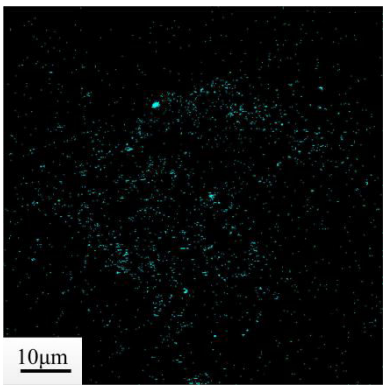

(b)

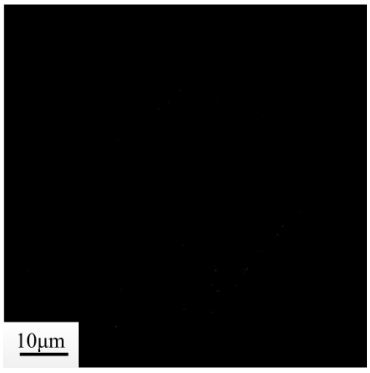

（c）

Figure 3.20 Images of the confocal spectroscopy of the PS/PA6/PS-TMI-MAMA1 (80/20/3) blend after 2 min (a) and 10 min of continuous mixing (b). (c) Confocal spectroscopy image of the PS/PS-TMI-MAMA1 (80/3) control system after 10 min of continuous mixing. Turquoise dots correspond to the PS-g-PA6-MAMA graft copolymer micelles whose d_n and d_v are about 200 and 300 nm, respectively.

Therefore the mechanism of the sharp increase in the dispersed phase domain size of the PS/PA6/PS-TMI-MAMA (80/20/1.5) after a certain time of mixing could be depicted in Figure 3.21. At the beginning of the reactive blending process, one PA6 chain is attached to the PS-TMI-MAMA (Figure 3.21a), forming a Y-shape copolymer at the interface. As the interfacial reaction proceeds further, more PA6 grafts may be attached to the PS-TMI-MAMA backbone and the resulting graft copolymer may become comb-like (Figure 3.21b). Once it is highly asymmetrical (for example, the number of PA6 grafts is high enough), it may become less attracted to the interface, causing its detachment from interfaces and forming micelles in one of the polymer component phases (Figure 3.21c). Mixing aggravates this detachment by literally pulling the copolymer off the interfaces.[152] Once the copolymer is no longer located at the interfaces, it losses completely its compatibilzing efficiency (Figure 3.21d).

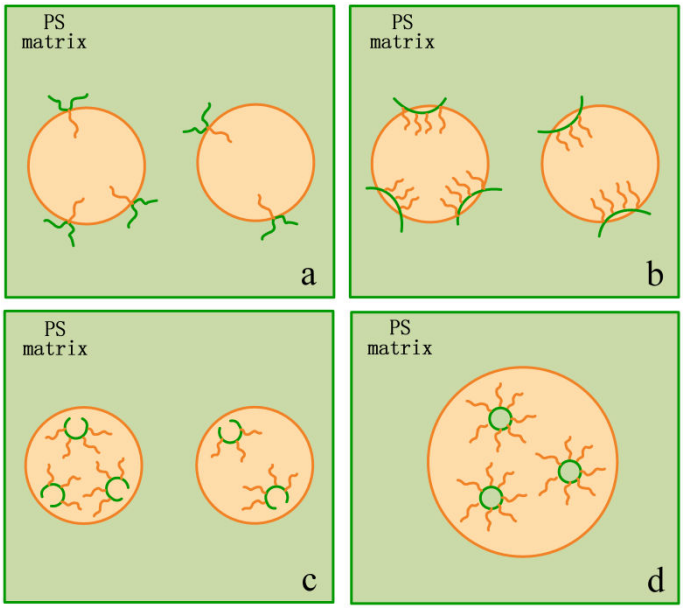

Figure 3.21 A sketch of the morphology evolution of the PS/PA6/PS-TMI-MAMA (80/20/1.5) system. (a) Y-shape copolymer, (b) comb-like copolymer, (c) pull-out of the copolymer from the interface (d) formation of micelles and coalescence of the dispersed phase domains due to the copolymer pull-out from the interface.

3.4 Conclusion

This chapter has reported on the design and synthesis of a graft reactive compatibilizer-tracer PS-TMI-MAMA and a block reactive compatibilizer-tracer. Both act as reactive compatibilizers and tracers. On the one hand, the NCO group of PS-TMI-MAMA and anhydride group of Anhy-PS-Anth could react with the terminal amine group of the PA6 to in-situ form a graft copolymer PS-g-PA6-MAMA and a block copolymer PS-b-PA6-MAMA which act as compatibilizers to prevent the dispersed phase domains from coalescence. On the other hand, the anthracene group of PS-TMI-MAMA and Anhy-PS-Anth is sensitive to fluorescent emission that the concentrations of the in-situ formed graft and block copolymers can be measured by SEC with a UV detector.

In the short blending time (<4 min), the content of the reacted PS-TMI-MAMA1 and Anhy-PS-Anth is almost the same and the dispersed phase domain size of PS-TMI-MAMA1 blend system is smaller than that of Anhy-PS-Anth, indicating that the compatibilizing efficiency of PS-TMI-MAMA1 is higher than Anhy-PS-Anth. In

the later period of mixing, the dispersed phase domain size of the Anhy-PS-Anth blend system remains unchanged with mixing time. However, the dispersed phase domain size of PS-TMI-MAMA1 system increases sharply and almost reaches that of the blend without compatibilizer. This is because the number of PA6 grafts of PS-g-PA6-MAMA increases during the later period of mixing. PS-g-PA6-MAMA with a larger number of PA6 grafts could be pulled out of the interface to the PA6 phase, leading to a sharp increase in the dispersed phase domain size. This phenomenon is related to the PA6 graft density of PS-g-PA6-MAMA. The PA6 graft density of PS-g-PA6-MAMA increases with increasing TMI density of PS-TMI-MAMA. PS-g-PA6-MAMA with a larger PA6 graft density is more unstable at the interface and is easier to be pulled out of the interface, resulting in a more severe increase in the dispersed phase domain size.

Chapter 4 Effects of mixing and blend composition on reactive polymer blending processes

4.1 Introduction

Mixing and blend composition may have effects on the interfacial reaction and morphology of reactive polymer blends. Generally speaking, increasing mixing intensity improves the interfacial reaction and the dispersion of the dispersed phase domains in the matrix, leading to a decrease in the dispersed phase domain size. When the dispersed phase and matrix are inversed, the viscosity ratio changes and the morphology will be different. According to Chapter 3, in the case of the PS/PA6/PS-TMI-MAMA1 (80/20/1.5) blend system, the in-situ formed graft copolymer PS-g-PA6-MAMA could be pulled out of the interface to the PA6 phase in the later period of mixing, resulting in a sharp increase in the dispersed phase domain size. This chapter reports on the effects of mixing and blend composition on the interfacial reaction kinetics and morphology development of PS/PA6/ PS-TMI-MAMA1 blending systems.

4.2 Experimental

4.2.1 Material

The characteristics of PS and PA6 are shown in Table 3.2. The number-average molar mass of PS-TMI-MAMA1 is 37.8 kg/mol, the TMI content is 7.1 wt% and the MAMA content is 0.5 wt%.

4.2.2 Polymer blending process

PS, PA6 and PS-TMI-MAMA1 were charged into the Brabender mixer. The PS-TMI-MAMA1 content in the blends was always 1.5 wt% of the total mass of the PS and PA6. The mixing mode could be either continuous or stepwise mixing, as described in 3.2.4.

4.2.3 Rheological measurement

The rheological behaviors of PS and PA6 were measured by a parallel plate rheometer (HAAKE RS6000，German). Before measurement, the sample was mold to the disks of 20 mm in diameter and about 1 mm in thickness. A dynamic mode was used to measure the complex viscosity as a function of frequency. The strain amplitude was set 10%, which is in the range of the linear viscoelastic shear oscillation. The test was performed within the frequency range from 0.01-100 Hz.

4.2.4 SEM

SEM (ZEISS ULTRA55) was used to measure the morphology of the polymer blend. For PS/PA6 (80/20) blend, the measurement method is expressed in 3.2.8. For PS/PA6 (20/80) blend, the samples were first fractured in liquid nitrogen. The fractured surfaces were then immersed in THF to remove the dispersed phase PS at room temperature for 12 h. They were dried for 12 h in the vacuum oven at 80 ºC and then gold sputtered for measurement.

4.2.5 Transmission Electron Microscope (TEM)

The morphology PS/PA6/PS-TMI-MAMA can also be characterized by transmission electron microscopy (TEM) of type JEOL JEM1230. Prior to the TEM analysis, specimens were stained in the following manner. They were microtomed into films of less than 100 nm thick. They were then placed on a drop of 2% phosphotungstic acid solution for 30 min at 50 °C using a specimen grid. Thereafter they were rinsed three times with distilled water.

4.3 Result and discussion

4.3.1 Effect of mixing speed

At first, the mixing speed was set at 100 rpm for 2 min and was changed to 50 rpm, 100 rpm and 150 rpm subsequently for several minutes. Figure 4.1(a) compares the evolution of the content of the reacted PS-TMI-MAMA for PS/PA6/PS-TMI-MAMA1 (80/20/1.5) blend system as a function of mixing time at

different mixing speed. It can be seen that the content of the reacted PS-TMI-MAMA increases with increasing mixing time and mixing speed, indicating that a higher mixing speed improved the interfacial reaction between PS-TMI-MAMA and PA6. On the other hand, the evolution of the dispersed phase domain size as a function of time at different mixing speeds is shown in Figure 4.1b. In the case of 50 rpm, the dispersed phase domain size starts to increase after 4 min of mixing and it is increased from 0.5 to 2.8 μm between 4 and 10 min. In the case of 100 rpm, the dispersed phase domain size increases sharply from 0.7 to 2.7 μm between 4 and 5 min. In the case of 150 rpm, the dispersed phase domain size increases sharply from 0.5 to 2.9 μm between 2 and 4 min. This indicates that a higher mixing speed advances the time at which the dispersed phase domain size starts increasing.

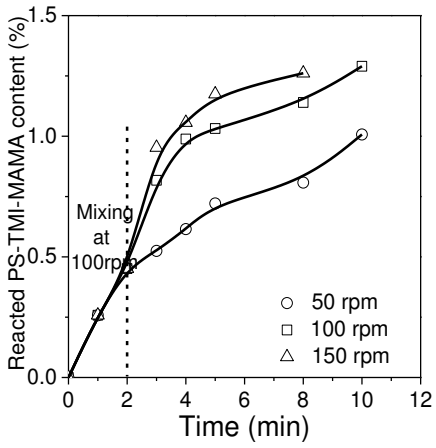

（a）

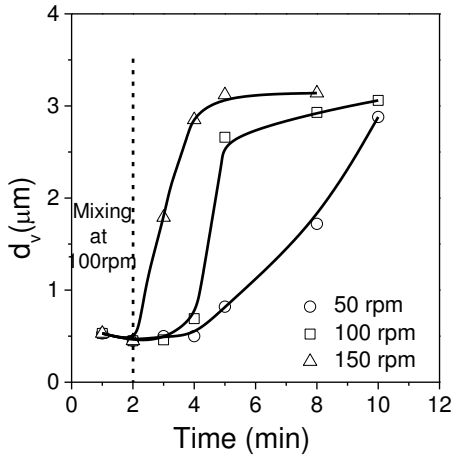

(b)

Figure 4.1 Effects of mixing speed on the evolution of the content of the reacted PS-TMI-MAMA (a) and dispersed phase domain size (b).

Mixing has a dual effect on the PS/PA6/PS-TMI-MAMA1 (80/20/1.5) blend system. Increasing mixing speed could promote the interfacial reaction between NCO groups of PS-TMI-MAMA and the terminal amine group of PA6 and that between the NCO groups of the PS-g-PA6-MAMA and the terminal amine group of PA6, on the one hand, and could aggravate the pull out of the PS-g-PA6-MAMA from the interfaces, on the other hand. A further reaction of the NCO groups of the PS-g-PA6-MAMA with the terminal amine group of PA6 increases the PA6 graft density of the PS-g-PA6-MAMA and consequently its thermodynamic instability at the interfaces. A thermodynamically less stable PS-g-PA6-MAMA at the interfaces together with a stronger mixing as a result of an increase in mixing speed shortens the time at which the dispersed phase domain size starts to increase, as shown in Figure 4.1b. The question is which of these two factors is dominating. To answer this question, the reactive polymer blend is processed by stepwise mixing.

4.3.2 Effect of annealing time

The stepwise mixing procedure is the following: after 2 min of mixing at 100 rpm, the rotors stopped rotating, and the blending system was annealed under the quiescent condition for a given period of time and then the mixing was resumed at 100 rpm.

Figure 4.2a is the evolution of the content of the reacted PS-TMI-MAMA as a function of time. It can be seen that the content of the reacted PS-TMI-MAMA remains almost the same during the annealing, indicating that no additional PS-TMI-MAMA has participated in the interfacial reaction. On the other hand, the evolution of the dispersed phase domain size as a function of time is shown in Figure 4.2b. It can be seen that after a short annealing time (1 min and 3 min) and 1 min of remixing, the dispersed phase domain size increases slightly from 0.5 to 0.6 μm which is close to that after 3 min of continuous mixing. After 5 min of annealing and 1 min of remixing, the dispersed phase domain size increases more seriously from 0.5 to 1.0 μm. After 8 min of annealing and 1 min of remixing, the dispersed phase domain size

increases sharply from 0.5 to 2.6 μm. This implies that when the whole mixing time is set at 3 min, the degree of increase in the dispersed phase domain size increases with longer annealing time. After 3 min of remixing, the dispersed phase domain size is almost the same regardless of the annealing time.

Even though no additional PS-TMI-MAMA participates in the interfacial reaction during the annealing, the NCO groups of the PS-g-PA6-MAMA could continue to react with the PA6 at the interfaces, which increases the number of PA6 grafts per PS-g-PA6-MAMA. The PS-g-PA6-MAMA with a higher number of PA6 grafts is dynamically more unstable at the interface and could be more prone to be pulled out of the interface when mixing is resumed. Therefore, it is the content of the reacted NCO group of the PS-g-PA6-MAMA which amounts to the number of the PA6 grafts per PS-g-PA6-MAMA and not the content of the reacted PS-TMI-MAMA that controls the sharp increase in the dispersed phase domain size. It is in agreement with the results reported in Chapter 3.

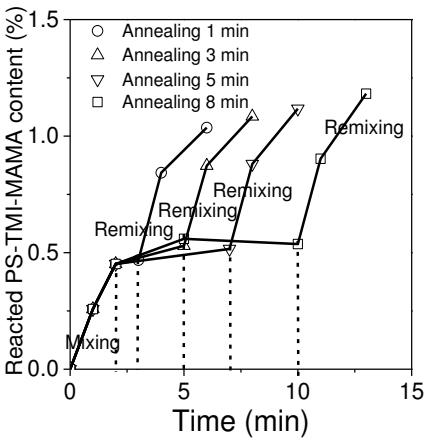

（a）

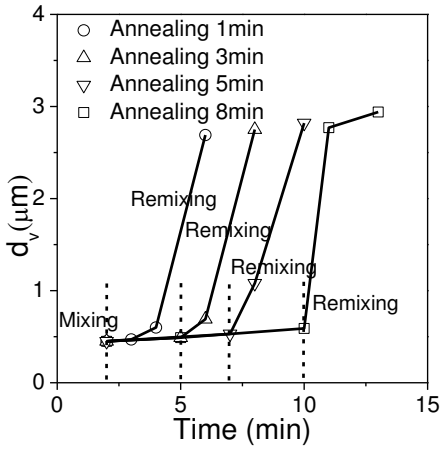

（b）

Figure 4.2 Effect of annealing time on the evolution of the content of the reacted PS-TMI-MAMA (a) and dispersed phase domain size (b).

4.3.3 Effect of blend composition

4.3.3.1 Rheological results

The complex viscosity of the PS and PA6 as a function of frequency is shown in Figure 4.3. The complex viscosity of the PA6 is lower than that of the PS in the whole frequency range.

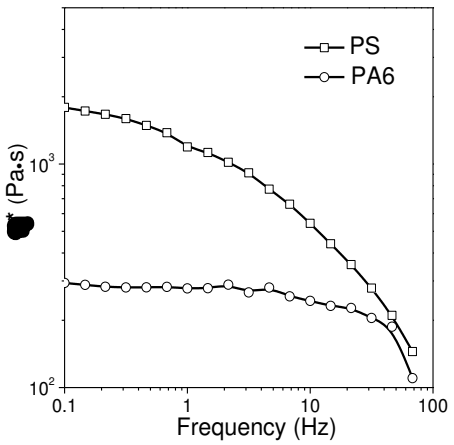

Figure 4.3 Complex viscosity vs frequency of PS and PA6 at 230°C.

4.3.3.2 Evolution of the morphology of the PS/PA6/PS-TMI-MAMA1（80/20/1.5）and（20/80/1.5）blends

In the case of the PS/PA6/PS-TMI-MAMA1 (80/20/1.5) blend system, the PS is the matrix and the PA6 is the dispersed phase. It is shown that PS-TMI-MAMA1 has high compatibilizing efficiency at the very beginning of mixing and loses its

efficiency in the later period of mixing. If the PS is the dispersed phase and PA6 is matrix, will the dispersed phase domain size still increase in the later period of mixing?

The dispersed phase domain size as a function of time for the PS/PA6/PS-TMI-MAMA1 (80/20/1.5) and PS/PA6/PS-TMI-MAMA1 (20/80/1.5) reactive blends is shown in Figure 4.4 and Table 4.1. For the polymer blend without compatibilizer, the dispersed phase domain size of the PS/PA6 (20/80) is larger than that of the PS/PA6 (80/20). As shown in Figure 4.3, the viscosity of the PA6 is larger than the PS. The dispersed phase domain size decreases with increasing viscosity of the matrix. Therefore the dispersed phase domain size of the PS/PA6 (20/80) is larger than that of the PS/PA6 (20/80). In the case of PS/PA6/PS-TMI-MAMA1 (20/80/1.5), the dispersed phase domain diameter reaches 1.7 μm after 2 min of mixing, which is much smaller than that of the blend without compatibilizer. It reaches a minimum of 1.2 μm after 4 min of mixing, which is much larger than that of the PS/PA6/PS-TMI-MAMA1 (80/20/1.5) system. This indicates that in the initial period of mixing, the compatibilizing efficiency of PS-TMI-MAMA1 is higher for the PS/PA6 (80/20) system than that for the PS/PA6 (20/80) system.

After 4 min of mixing, the dispersed phase domain size of the PS/PA6/PS-TMI-MAMA1 (20/80/1.5) blend remains unchanged with a further increase in mixing time. This trend is very different from that of the PS/PA6/PS-TMI-MAMA1 (80/20/1.5) system. This difference may be related to the location of the PS-g-PA6-MAMA micelles. As mentioned before, the in-situ formed PS-g-PA6-MAMA graft copolymer could be pulled out from the interface to the PA6 phase in the later period of mixing. For the PS/PA6/PS-TMI-MAMA1(20/80/1.5) system, the PA6 phase is not the dispersed phase but the matrix. The PS-g-PA6-MAMA micelles in the PA6 matrix could prevent the PS dispersed phase domains from coalescence. In other words, micelles play a role in compatibilizing the blend.

Figure 4.5 shows the TEM micrographs of the PS/PA6/PS-TMI-MAMA1 (80/20/1.5) and PS/PA6/PS-TMI-MAMA1 (20/80/1.5) blends. There are particles of

nanometers in size in the PS/PA6/PS-TMI-MAMA1 (20/80/1.5) blend. They should be the PS-g-PA6-MAMA micelles in the PA6 matrix (Figure 4.5 A and 4.5 B), indicating that the in-situ formed PS-g-PA6-MAMA was pulled out of the interface to the PA6 matrix. Theses micelles may hinder the dispersed phase droplets from contacting each other and consequently from coalescing, which is in agreement with the hypothesis of pull out of the in-situ formed copolymer discussed earlier. Besides, Figure 4.5 C and 4.5 D show that there are no micelles in the PS matrix of the PS/PA6/PS-TMI-MAMA1 (80/20/1.5) blend, further confirming that micelles are located in the PA6 phase. It is not possible to observe micelles in the PA6 phase from Figure 4.5 C and 4.5 D. This is because both the PA6 and the PA6 grafts of the PS-g-PA6-MAMA are stained. PS-g-PA6-MAMA micelles could not be distinguished from the PA6 phase.

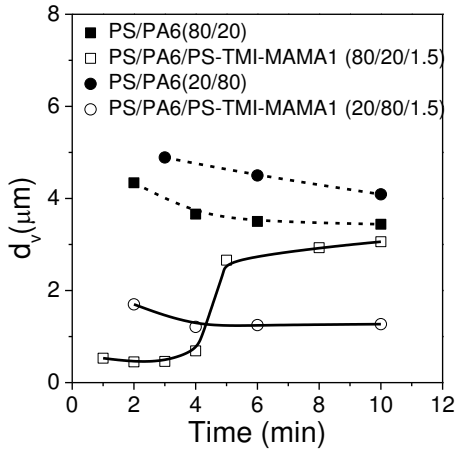

Figure 4.4 Evolution of the dispersed phase domain size as a function of time under the continuous mixing for the PS/PA6/PS-TMI-MAMA1 (80/20/1.5) and PS/PA6/PS-TMI-MAMA1 (20/80/1.5) reactive blend.

Table 4.1 Dispersed phase domain size of the PS/PA6/PS-TMI-MAMA1 blends.

	Mixing Time (min)	$(d_v)_{PA6}$ (μm)	$(d_v)_{PS}$ (μm)
Without compatibilizer	6	3.5	4.5
	10	3.4	4.1
PS-TMI-MAMA	2	0.45	1.7
	4	0.69	1.2
	10	3.1	1.3

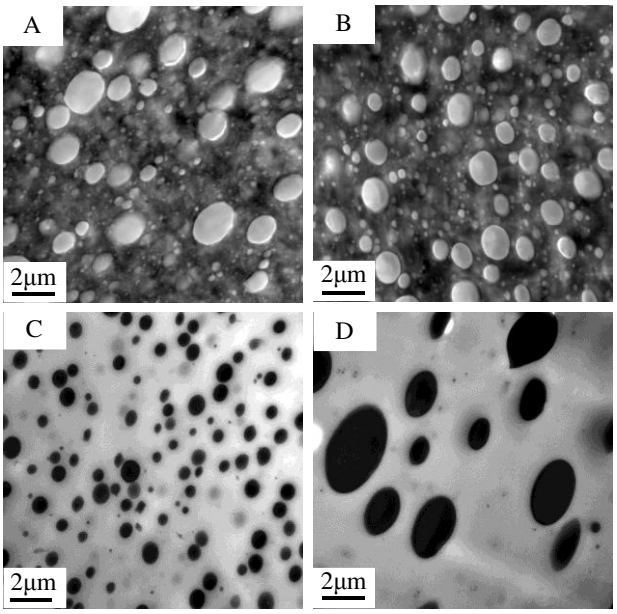

Figure 4.5 TEM micrographs of the PS/PA6/PS-TMI-MAMA1 (20/80/1.5) blend: (A) 2min; (B): 10min; TEM micrographs of the PS/PA6/PS-TMI-MAMA1 (80/20/1.5) blend: (C): 2min; (D): 10 min.

In order to confirm the role of the PS-g-PA6-MAMA micelles, the PA6 and PS-TMI-MAMA1 were mixed in the Brabender mixer for 10 min at 100 rpm and 230°C. During the 10 min of mixing, the PA6 had enough time to react with the PS-TMI-MAMA to form PS-g-PA6-MAMA copolymer micelles dispersed in the PA6 phase. This mixture is denoted as A. Then A was mixed with the PS (PS/A = 80/21.5) and PS/PA6 (PS/PA/A = 20/60/21.5) in the Brabender mixer for given time intervals. The composition of the PS/A (80/21.5) is the same as that of the PS/PA6/PS-TMI-MAMA (80/20/1.5) and that of the PS/PA6/A (20/60/21.5) is the same as that of the PS/PA6/PS-TMI-MAMA (20/80/1.5).

Figure 4.6 shows the evolution of the dispersed phase domain size of the PS/A (80/21.5) and PS/PA6/A (20/60/21.5) systems as a function of mixing time. The dispersed phase domain size of the PS/A (80/21.5) system is close to that of the PS/PA6 (80/20) system without compatibilizer. Because PS-g-PA6-MAMA copolymer micelles are in the PA6 dispersed phase, they do not have any compatibilizing efficiency. However, the dispersed phase domain size of the in terms of PS/PA6/A (20/60/21.5) system is 2 μm after 10 min, which is much smaller than that of the PS/PA6 (20/80) system without compatibilizer. This indicates that the

PS-g-PA6-MAMA micelles in the PA6 matrix hinder PS dispersed phase domains from coalescing.

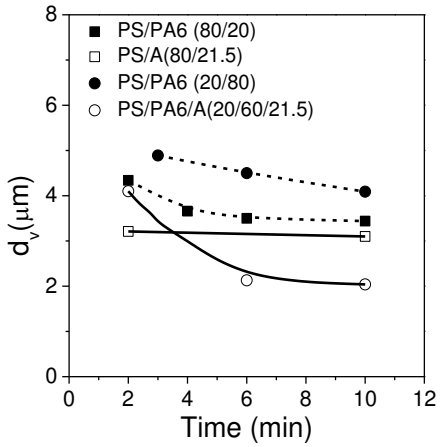

Figure 4.6 Evolution of the dispersed phase domain size of the PS/A (80/21.5) and PS/PA6/A (20/60/21.5) systems as a function of mixing time. "A" stands for the PS-TMI-MAMA/PA6 (7.5/100) blend obtained after 10 min of mixing.

Figure 4.7 depicts the morphology development of the PS/PA6/PS-TMI-MAMA1 (20/80/1.5) reactive blend during melt blending. In the initial period of mixing, PS-TMI-MAMA migrates to the PS/PA6 interface and reacts with the PA6 to form an inversed Y-shaped PS-g-PA6-MAMA graft copolymer to hinder the dispersed phase domains from coalescing and reduce their size. As mixing proceeds, the remaining NCO groups of the inversed Y-shaped PS-g-PA6-MAMA graft copolymer would continue to react with the PA6 to form an inversed comb-shaped graft copolymer. The latter is thermodynamically unstable at the interface and would be prone to pull out of the interface to form micelles in the matrix. Theses micelles may hinder the dispersed phase domains from contacting each other and coalescing. Therefore, compared to the PS/PA6/PS-TMI-MAMA1 (80/20/1.5) blend, the dispersed phase domain size of the PS/PA6/PS-TMI-MAMA1 (20/80/1.5) blend would not increase in the later period of mixing.

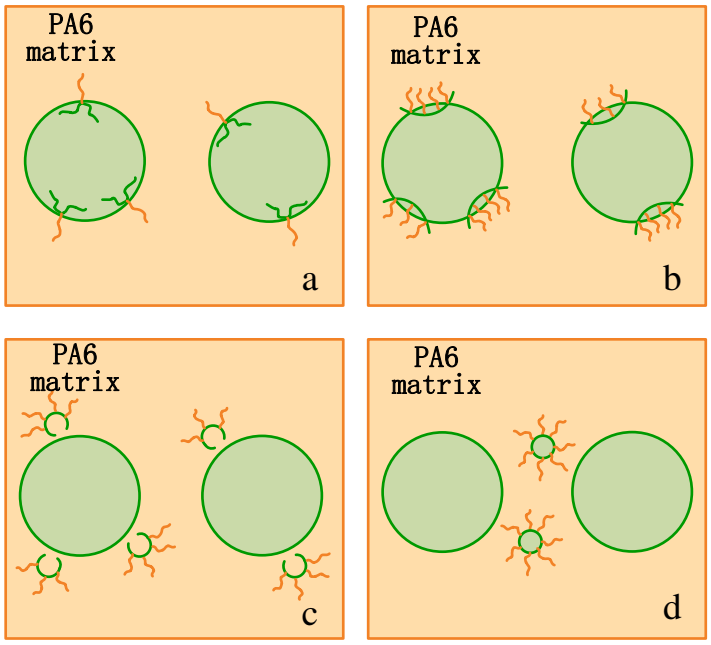

Figure 4.7 Morphology development of the PS/PA6/PS-TMI-MAMA (20/80/1.5) reactive blend during melt blending.

4.4 Conclusion

This chapter mainly investigates the effects of mixing and blend composition on the reactive polymer blending in a batch mixer.

Mixing has a dual effect on the PS/PA6/PS-TMI-MAMA1 (80/20/1.5) blend system. On the one hand, increasing mixing speed could improve the interfacial reaction between the PS-TMI-MAMA and PA6. On the other hand, it promotes the reaction between the NCO groups of the PS-g-PA6-MAMA and PA6, leading to an increase in the number of PA6 grafts per PS-g-PA6-MAMA, and mechanically aggravates the pull out of the PS-g-PA6-MAMA from the interface. The last two phenomena shorten the time at which the dispersed phase domain size starts to increase when increasing mixing speed.

Even though no additional PS-TMI-MAMA participates in the interfacial reaction during annealing, NCO groups of the PS-g-PA6-MAMA could continue to react with the PA6, increasing the number of PA6 grafts of the PS-g-PA6-MAMA and reducing its thermodynamic stability at the PS/PA6 interfaces. As a result, PS-g-PA6-MAMA would be more easily to be pulled out of the interfaces when

mixing is resumed.

The compatibilizing efficiency of PS-TMI-MAMA1 depends on the composition of the PS/PA6 blend. In the initial period of mixing, the compatibilizing efficiency of PS-TMI-MAMA1 is higher for the PS/PA6 (80/20) blend than for the PS/PA6 (20/80) blend. In the later period of mixing, its compatibilizing efficiency is lost for the PS/PA6 (80/20) blend and remains high for the PS/PA6 (20/80) blend. For both blends, when PS-g-PA6-MAMA is pulled out of the interface, it forms micelles in the PA6 phase. When the PA6 phase is the matrix, the micelles there play a role of compatibilization by hindering the PS dispersed phase domains from coalescing.

Chapter 5 Development of a reactive compatibilizer-tracer for studying reactive polymer blends in a twin-screw extruder

5.1 Introduction

A so-called emulsification curve, which essentially follows the evolution of the dispersed phase domain size of a (reactive) polymer blend as a function of a (reactive) compatibilizer concentration, is successfully used to evaluate the interfacial behavior and efficiency of the (reactive) compatibilizer.[2-8] When a batch mixer is used, the emulsification curve can be built up in the following manner. Given compositions of the polymer components of the blend as well as the (reactive) compatibilizer are charged to the mixer. After a certain elapse of time (usually 5 to 10 min), the process reaches a steady state and samples are taken from the mixer. The size of the dispersed phase domains of the blend is measured. This makes up a point on the emulsification curve. The above process is repeated upon varying the (reactive) compatibilizer concentration. An emulsification curve is then build-up for the said composition of the blend. In the case of a screw extruder, the so-called steady-state experiments can also be carried out. They are similar to those in a batch mixer. Given compositions of the polymer components of the blend as well as the (reactive) compatibilizer are charged to the hopper of the extruder. After a certain elapse of time (usually more than 10 times the average residence time), the process reaches a steady state and samples are taken from the die exit for measurement.

Studies reported in the literature concerning emulsification curves often use batch mixers and not screw extruders. The main reason is that batch mixers are often more accessible in a laboratory than twin-screw extruders and that they are much easier to operate too. More importantly, the amount of the (reactive) compatibilizer required for building up an emulsification curve in a batch mixer is often much smaller than in a twin-screw extruder. This is especially true for a pilot or industrial-scale screw extruder of which the production rate can reach from a few dozens of kilograms per

hour to a few tones per hour. In such a case, the amount of the (reactive) compatibilizer required may be too large to build up an emulsification curve.

This work aims at developing a so-called reactive compatibilizer-tracer concept for polymer blending processes in order that a very small amount of a reactive compatibilizer still allows building up an emulsification curve in a pilot or industrial-scale screw extruder. The idea is based on transient experiments for measuring residence time distributions.[8-12] Unlike a steady-state experiment in which given compositions of the polymer components of the blend and the reactive compatibilizer are charged to the hopper of the extruder altogether, in a transient experiment the polymer components are first fed to the hopper of the extruder. When the process reaches its steady state, a given and small amount of the copolymer is introduced to the hopper of the extruder as a pulse. Samples are taken at the die exit as a function of time. Both the evolution of the reactive compatibilizer concentration (RCC) and that of the morphology as a function of time can be obtained. The former provides the reactive compatibilizer concentration distribution (RCCD) and the latter the dispersed phase domain diameter distribution (DDD) for dispersed type polymer blends. From both distributions, the emulsification curve should easily be deduced.

The usefulness of the reactive compatibilizer-tracer concept for building emulsification curves under real reactive polymer blending conditions and with a small amount of reactive compatibilizer-tracer is shown using PS/PA6/PS-TMI-MAMA reactive blends.

5.1 Experimental

5.2.1 Material

The characteristics of the PS and PA6 are shown in Table 3.2. The number-average molar mass, TMI content and MAMA content of PS-TMI-MAMA were 38.9 kg/mol, 5.1 wt% and 0.5 wt%, respectively.

5.2.2 In-line fluorescence measuring device

An in-line fluorescence measuring device was developed to detect the concentration of reactive compatibilizer-tracer. As shown in Figure 5.1, it was mainly composed of the following three parts: fluorescent light generation, in-line fluorescent light detection device, and signal processing. The source of the fluorescent light was ultraviolet high-pressure mercury lamp (125w) and was divided into two beams. Each of them successively passed through its own coupler and bifurcated optical fiber before it irradiated the anthracene tracer containing polymer flow stream in a screw extruder. The light with a specific wavelength emitted from the provocative tracer was subsequently transmitted to a fluorescent detector (a photomultiplier) through the bifurcated optical fiber probe and was then amplified through an amplifier. Finally, the amplified optical signals coming from the two fluorescent detectors reached the signal processing unit. The latter converted them to two analogs. They were then collected by a computer system and were displayed in real time on the screen.

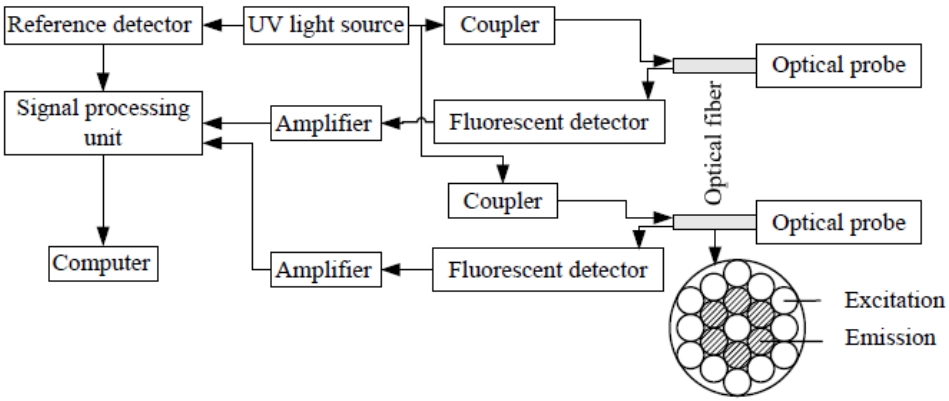

Figure 5.1 Diagram of the in-line fluorescent measuring system.

Figure 5.2 shows a picture and schematic diagram of optical probe. The front end of probe was a quartz window which could withstand high-temperature and high-pressure. The light filter was to let the monochromatic light (420 nm fluorescent light) through and excluded the unnecessary part of light. The sensitivity of the device could be regulated to adapt to different tracers. The signal was collected every second.

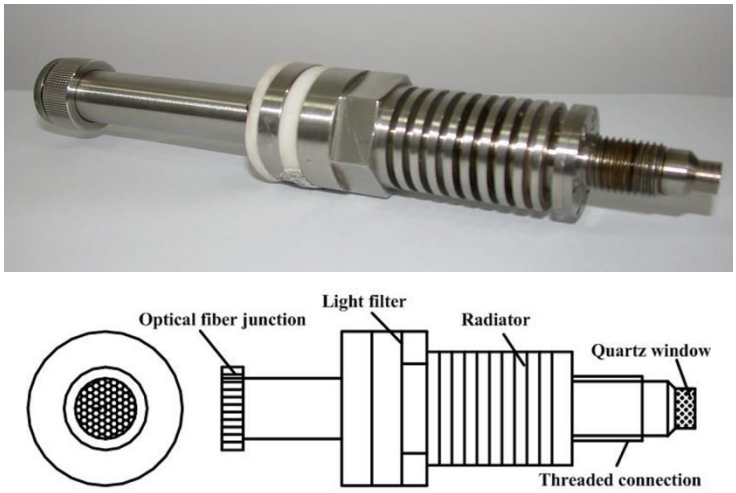

Figure 5.2 A picture and schematic diagram of optical probe.

The die exit was designed to allow installing the probe and allow the probe to detect the fluorescent signal. The die exit was a cuboid and there was a hole in the side. The probe was installed in the hole to allow touching the polymer material. When the reactive compatibilizer-tracer was extruded from the die exit, the in-line measurement could detect the fluorescent signal. The residence time distribution between the tracer port and the die exit could be obtained.

5.2.3 In-line measurement processing

An intermeshing co-rotating twin-screw extruder of type TSE-35A (Nanjing Ruiya twin-screw extruder cooperation) was used to carry out polymer blending processes. Its diameter and length-to-diameter ratio were 35 mm and 48, respectively. The screw elements in this study could be divided into transporting elements and kneading discs, as shown in Figure 5.3. The last part of the screw configuration was a kneading zone composed of 11 kneading blocks. Every kneading block was composed of 7 kneading discs of 32 mm in total length and the angle between two adjacent kneading discs was 30°, unless specified otherwise.

The reactive compatibilizer-tracer was introduced as a pulse either at tracer port 1 or tracer port 2. Tracer port 1 is near the die exit and tracer port 2 is far from the die exit.

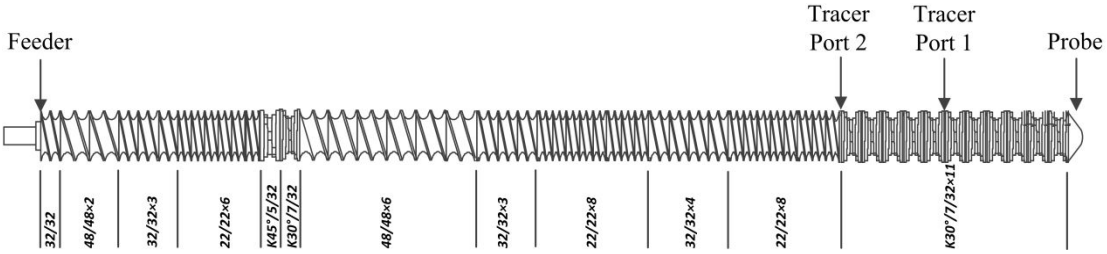

Figure 5.3 Screw configuration of the twin-screw extruder.

The barrel temperature and screw speed were set at 230 ^{o}C and 100 rpm, respectively. The feed rate of the PS/PA6 blend was 13 kg/h. Its composition was either 80/20 or 95/5 by mass.

A typical blending process was carried out in the following manner: pellets of the PS and PA6 were charged to the TSE from the feeder. When the extrusion process reached a steady state, the reactive compatibilizer-tracer was introduced as a pulse either at port 1 or 2 in order to study the effect of the kneading zone length on the reactive blending process. Meanwhile, an in-line fluorescent device began to record the signal of its fluorescent emission at the die exit. Samples were taken from the die exit every 5 seconds and were quenched in liquid nitrogen to freeze-in interfacial reactions and morphologies for subsequent analyses.

Based on the linear relationship between the reactive compatibilizer-tracer concentration and the analog fluorescent signal in voltage, the normalized reactive Compatibilizer-tracer Concentration Distribution (CCD) could be calculated according to the following expression:

$$E(t_i) = \frac{V(t_i)}{\sum_{i=1}^{n} V(t_i)(t_i - t_{i-1})} \quad (5\text{-}1)$$

where V_i is the voltage at time t_i (i = 1, 2, …, n).

5.3 Result and discussion

5.3.1 Establishment of in-line measurement

When the reactive compatibilizer-tracer is introduced to the TSE at port 1 as a pulse (3.2 g), the fluorescent signal intensity as a function of residence time via in-line measuring device is shown in Figure 5.4. Because the reactive compatibilizer-tracer

concentration is linear to the analog fluorescent signal in voltage, the normalized reactive Compatibilizer-tracer Concentration Distribution (CCD) (Figure 5.5a) could be obtained based on the equation (5-1). Actually, the CCD is also its residence time distribution (RTD) in the TSE. During the experiment, the samples are taken from the die exit and measured by SEM to obtain the dispersed phased domain size. The corresponding dispersed phase (PA6) Domain Diameter Distribution (DDD) is shown in Figure 5.5b. The DDD curves match the CCD ones in the sense that the higher the reactive compatibilizer-tracer concentration, the smaller the diameter of the dispersed PA6 domains. The content of reacted PS-TMI-MAMA could be measured based on the method explained in Chapter 3, The Reacted reactive Compatibilizer-tracer (PS-TMI-MAMA) Content Distribution (RCCD) could be obtained, as shown in Figure 5.5c. It follows more or less the trends of the CCD and DDD curves. When the reactive compatibilizer-tracer concentration increases, the content of the reacted PS-TMI-MAMA increases and then the dispersed phase domain size decreases.

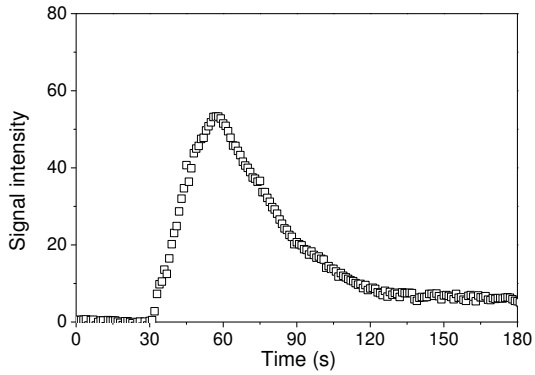

Figure 5.4 The fluorescent signal intensity as a function of residence time.

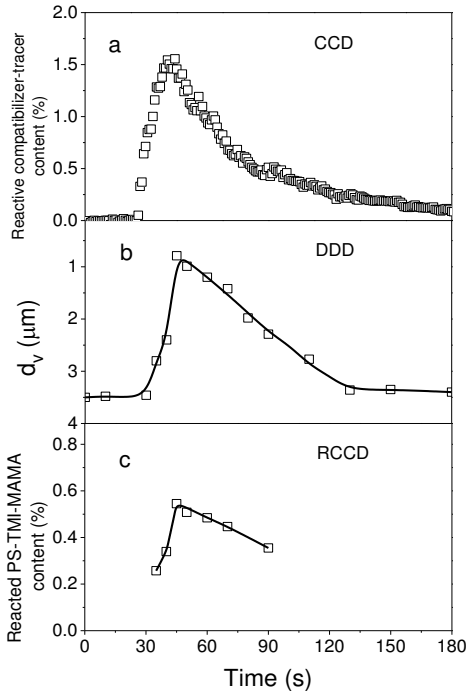

Figure 5.5 CCD (a), DDD (b) and RCCD (c) of the PS/PA6 (80/20) blend in the TSE with PS-TMI-MAMA as a reactive compatibilizer-tracer which is injected at port 1. Feed rate: 13 kg/h; screw speed: 100 rpm.

The CCD and DDD curves of Figure 5.5 can be converted to a so-called emulsification curve, namely, the evolution of the dispersed domain size as a function of the reactive compatibilizer-tracer content. As it is well known, the typical emulsification curve should follow the trend that the dispersed phase domain size decrease and then level off with the compatibilizer concentration. However, as shown in Figure 5.6, it is a loop instead of a single curve. It is obtained in the following manner. The CCD curve is divided into a short time domain and a long time domain which are demarcated by its maximum which physically corresponds to the highest reactive compatibilizer-tracer concentration. As a result, the evolution of the dispersed phase domain size as a function of the reacted reactive compatibilizer concentration in the short time domain yields the upper part of the loop and that in the long time domain corresponds to its lower part. This indicates that under the specified conditions, the compatibilizing efficiency of the reactive compatibilizer-tracer is more efficient in the long time domain than in the short time domain.

One may expect that compared to the short time domain, reactive

compatibilizer-tracer molecules in the long time domain spend a longer residence time in the TSE from port 1 to the die exit and thus may react more with the PA6, resulting in a higher reacted reactive compatibilizer-tracer content or a higher amount of the in-situ formed PS-g-PA6-MAMA graft copolymer. If it is true, the reactive compatibilizer-tracer molecules in the long time domain are expected to be more compatibilization efficient than those in the short time domain. This is confirmed by Figure 5.7 which plots the reacted reactive compatibilizer-tracer content (RCC) as a function of the reactive compatibilizer-tracer content (CC) (data from Figure 5.5). The RCC in the long time domain is indeed higher than that in the short time domain. As for d_v as a function of CC, a loop is also obtained the RCC as a function of CC.

According to the results of PS/PA6/PS-TMI-MAMA (80/20/1.5) blend in Chapter 3 and Chapter 4, the in-situ formed graft copolymer PS-g-PA6-MAMA could be pulled out of the interface during the latter period of mixing in the batch mixer, leading to the sharp increase in the dispersed phase domain size. It can be seen from Figure 5.5a that the residence time of the reactive compatibilizer-tracer in the TSE is very short about 1.5 min (throughput: 13 kg/h; screw speed: 100 rpm; tracer port:1). Besides, in the earlier stage the reaction between PS-TMI-MAMA and PA6 is very fast and the graft copolymer PS-g-PA6-MAMA is formed at the interface. However, the reaction between the NCO group of PS-g-PA6-MAMA and PA6 would become slower because of the steric effect. Therefore, the graft copolymer could be stable at the interface even in the long time domain in TSE and the dispersed phase domain size will not increase. TSE provides a tool to investigate the evolution of interfacial reaction and morphology of the reactive polymer blending in the short time.

Figure 5.8 shows the effective emulsification curve of the PS/PA6 (80/20) blend, namely, the dispersed phase domain size as a function of the RCC. It is seen that the curves corresponding to the short and long time domains superimpose now. This implies that under the specified conditions, it is the reacted PS-TMI-MAMA content in the blend and not the PS-TMI-MAMA content that dictates the dispersed domain size.

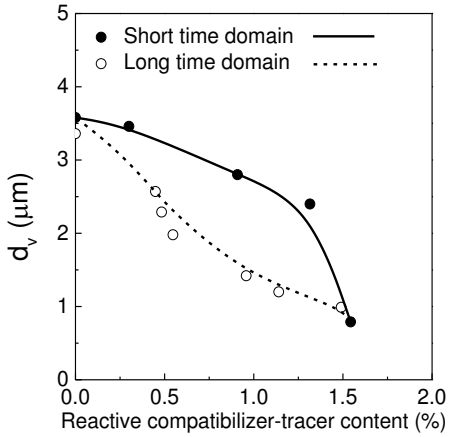

Figure 5.6 Emulsification curve of the PS/PA6 (80/20) blend using PS-TMI-MAMA as the reactive compatibilizer-tracer (data from Figure 5.5).

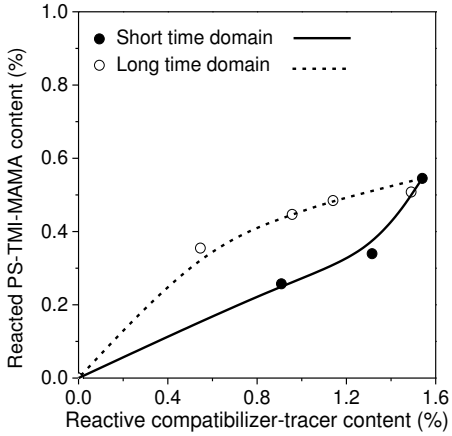

Figure 5.7 RCC-CC: reacted reactive compatibilizer-tracer content as a function of the reactive compatibilizer-tracer content in the PS/PA6 (80/20) blend (data from Figure 5.5).

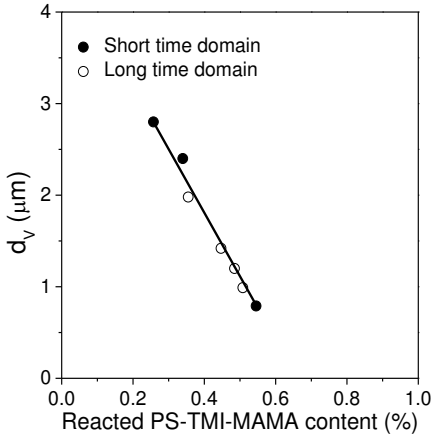

Figure 5.8 Effective emulsification curve of the PS/PA6 (80/20) blend using PS-TMI-MAMA as the reactive compatibilizer-tracer (data from Figure 5.5).

The above results show that the use of PS-TMI-MAMA as a reactive compatibilizer-tracer together with transit experiments allows evaluating its compatibilizing efficiency on a large TSE with small amounts of reactive compatibilizer-tracer. It also provides information on the CCD, DDD, RCCD, emulsification curve, RCC- CC curve, and effective emulsification curve. All these pieces of information are very useful for in-depth understanding and optimization of reactive polymer blending processes in screw extruders, especially industrial scale ones.

5.3.2 Assessment of the concept of reactive compatibilizer-tracer - effect of tracer port

The reactive compatibilizer-tracer (PS-TMI-MAMA) is injected as a pulse either at port 1 or 2. Figure 5.9 compares these two cases in terms of the CCD, DDD and RCCD for the PS/PA6 (80/20) blend. The CCD of the short time domain for port 1 precedes that for port 2. This is expected as port 1 is closer to the die exit than port 2.。

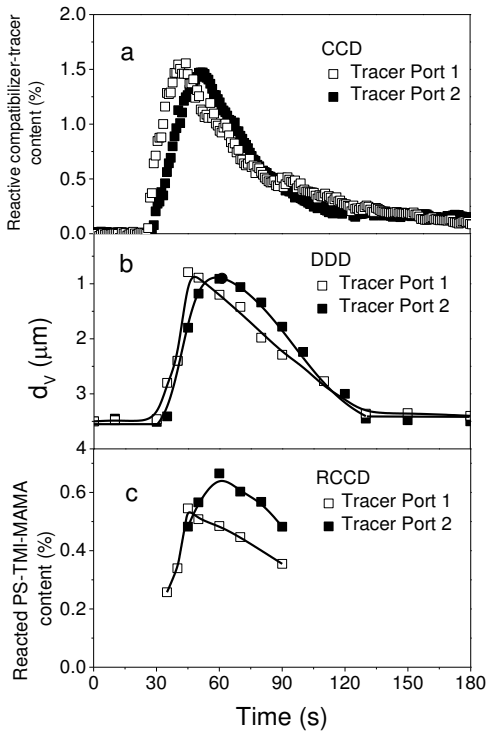

Figure 5.9 Effect of the reactive compatibilizer-tracer location on the CCD (a), DDD (b) and RCCD (c) for the PS/PA6 (80/20) blend. Feed rate: 13 kg/h; screw speed: 100 rpm; amount of reactive compatibilizer-tracer: 3.2g.

Figure 5.10 shows their emulsification curves (a), RCC-CC curves (b), and effective emulsification curves (c). When the reactive compatibilizer-tracer is injected at port 2, the emulsification curves of the short and long time domains almost superimpose, indicating that the mixing performance the short time domain provides is similar to what the long time domain does. However, when it is injected at port 1, they do not superimpose anymore and the one of the short time domain is significantly above that of the long time domain, indicating that in the case of port 1, the time in the short time domain is not long enough to provide the reactive compatibilizer-tracer with sufficient mixing with the PS/PA6 blend. As a result, the reacted PS-TMI-MAMA content is expected to be lower too. This is indeed the case, as shown in Figure 5.10(b). In the case of port 1, the reacted PS-TMI-MAMA content in the short time domain is much lower than that in the long time domain. The above results are further corroborated by the effective emulsification curves shown in Figure 5.10(c). It is seen that for both reactive compatibilizer-tracer injection ports, the short and long time domain data all superimpose on a single line within experimental errors. This indicates that in these cases, it is the reacted PS-TMI-MAMA content that dictates the state of the dispersion of the PA6 phase in the PS.

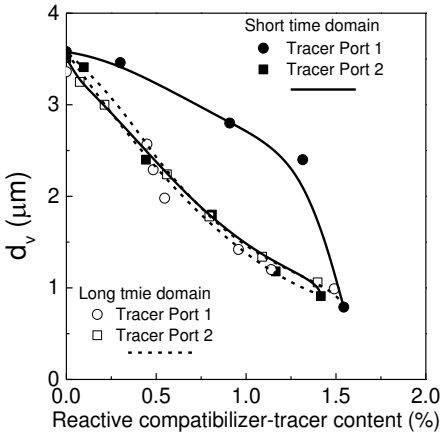

(a)

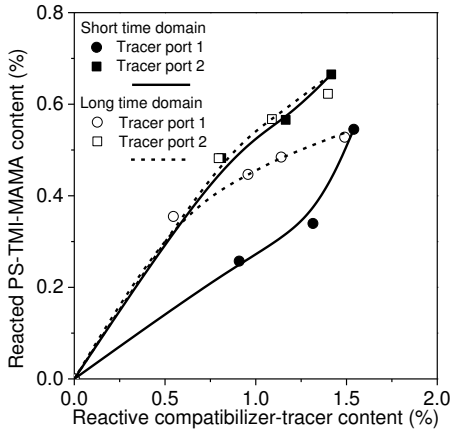

(b)

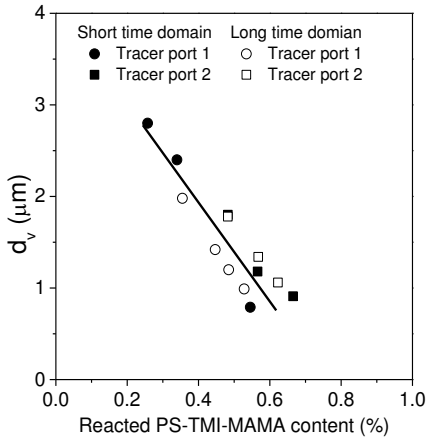

(c)

Figure 5.10 Effect of the feed location of the reactive compatibilizer-tracer on the emulsification curve (a), the RCC-CC curve (b) and the effective emulsification curve (c) of PS/PA6 (80/20) system. Feed rate: 13 kg/h; screw speed: 100 rpm; amount of tracer-compatibilizer: 3.2 g.

5.3.3 Effect of blend composition

Figure 5.11 compares their emulsification curves (a1 & a2), the RCC-CC curves (b1 & b2), and the effective emulsification curves (c1 & c2). From the emulsification curves (Figure 5.11 a1 & a2), when there is no reactive compatibilizer-tracer, the dispersed phase domain size of the 95/5 is smaller than that of the 80/20, as expected. However, when the reactive compatibilizer-tracer is added, it may be larger than that of the 80/20 at the high reactive compatibilizer-tracer content. This is true for both blend compositions and both reactive compatiblizer-tracer injection locations, especially port 1. This is surprising at the first glance.

During the reactive blending process, the reactive compatibilizer-tracer (PS-TMI-MAMA) molecules have to meet the PA6 molecules in order to react with each other. When the PA6 volume fraction in the PS/PA6 blend is very low, the probability of collisions between the reactive compatibilizer-tracer and the PA6 is low, resulting in a low reacted reactive compatibilizer-tracer concentration (or graft copolymer concentration). Therefore, the dispersed phase domain size of the PS/PA6 (95/5) blend can be even larger than that of the PS/PA6 (80/20) blend. Figures 5.11 (b1 & b2) show that the reacted PS-TMI-MAMA content of the 95/5 is indeed significantly lower than that of the 80/20. This validates the above hypothesis that the interfacial reaction between the reactive compatibilizer-tracer and PA6 in the 95/5 proceeds more slowly than in the 80/20 because of the lower PA6 volume fraction.

The effective emulsification curves (Figures 5.11 c1 & c2) show that as the reacted PS-TMI-MAMA content in the PS/PA6 blends increases, the difference in the dispersed phase domain size between the 95/5 and 80/20 narrows, indicating that for both reactive compatiblizer-tracer injection locations, the effect of the blend composition on the state of the dispersion of the dispersed phase decreases as the amount of the in-situ formed graft copolymer increases, due to reduced interfacial tension as well as reduced coalescence.

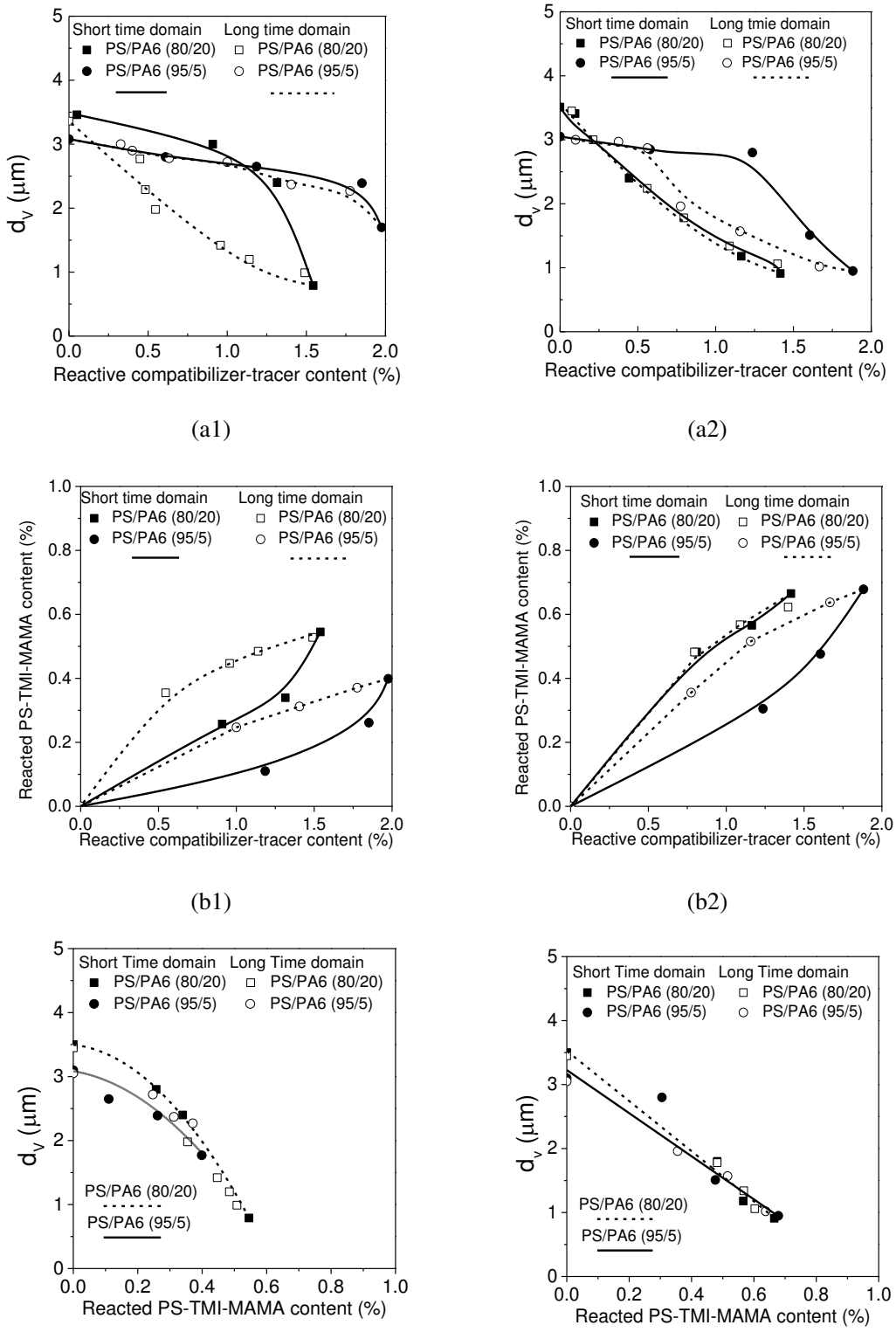

Port 1 Port 2

Figure 5.11 Effect of composition of the PS/PA6 blend on the emulsification curve (a), RCC-CC curve (b) and the effective emulsification curve. Feed rate: 13 kg/h; screw speed: 100 rpm.

Figure 5.12 depicts a simplified scheme of the development of the interfacial

interaction and morphology of the PS/PA6 (80/20) and PS/PA6 (95/5) blends using a reactive-compatibilizer-tracer such as PS-TMI-MAMA. Statistically speaking, when the PA6 volume fraction is lower, the distance between the PA6 domains and the reactive compatibilizer-tracer is longer, requiring a longer mixing time (or a stronger mixing intensity) for them to collide and react with each other to form the graft copolymer. Therefore, it is possible that the PA6 domain size of the PS/PA6 blend containing a lower PA6 content be temporally even larger than that of the PS/PA6 blend containing a large PA6 content. In other words, a polymer blend with a lower dispersed polymer content may require more mixing (a longer mixing time, a longer screw length and/or higher mixing intensity) than one with a higher dispersed polymer content.

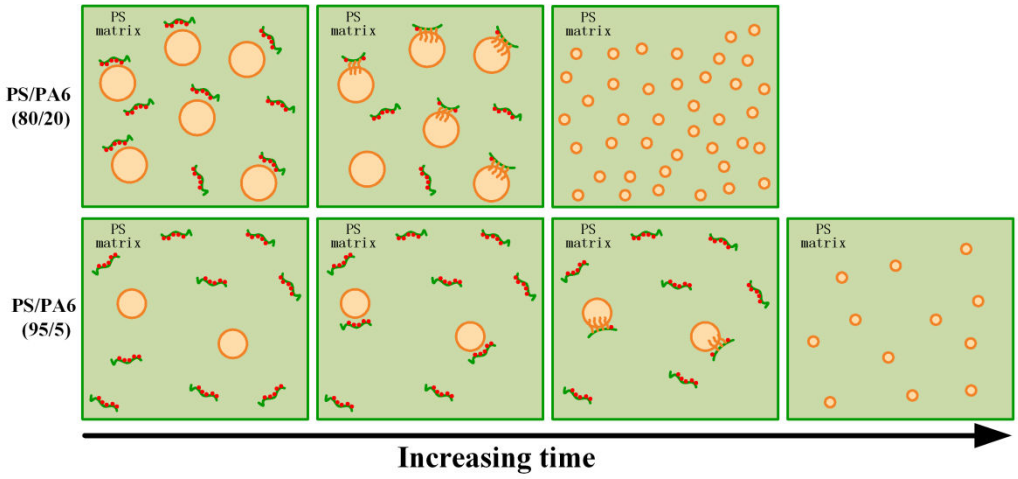

Figure 5.12 A simplified vision of the development of the interfacial interaction and morphology of the PS/PA6 (80/20) and PS/PA6 (95/5) using a reactive-compatibilizer-tracer PS-TMI-MAMA.

The above scheme could help exploit further the data in Figure 5.11 in order to shade more light on processing parameters that dictate the relationship between mixing, interfacial reaction and morphology development in the reactive blending processes. For example, in the case of the PS/PA6 (80/20) blend, the area of the loop of dispersed phase domain size versus reactive compatibilizer-tracer content narrows considerably when the reactive compatibilizer-tracer injection location is shifted from port 1 to port 2 (Figure 5.11 a1 and a2). This narrowing results from the fact that when the reactive compatibilizer-tracer injection location is shifted from port 1 to port 2, the dispersed phase domain size of the long time domain is not much affected by

the shift because in both cases the mixing time is long enough. However, that of the short domain is significantly decreased due to an increased mixing time in the short time domain. On the other hand, in the case of the PS/PA6 (95/5) blend the area of the loop of the dispersed phase domain size versus reactive compatibilizer-tracer content enlarges considerably when the reactive compatibilizer-tracer is shifted from port 1 to port 2 (Figure 5.11 a1 and a2). This is mainly because whatever the reactive compatibilizer-tracer injection location (port 2 or 1), when the PA6 content is low, the short time domain is too short for the reactive compatibilizer-tracer and the PA6 to have sufficient collisions to react with each other. The value of dispersed phase domain size remains large. However, the effect of the long time domain on the dispersed phase domain size becomes significant when the reactive compatibilizer-tracer injection location is shifted from port 1 to 2.

5.4 Conclusion

The use of small amounts of a reactive compatibilizer-tracer together with transient experiments is a new and powerful approach to studying reactive polymer blending processes in a twin-screw extruder. It allows one to assess the evolutions of the reactive compatibilizer-tracer content, the dispersed phase domain size and the amount of the in situ formed graft copolymer, respectively, as a function of the residence time in a twin-screw extruder. Based on that, the emulsification curve, the RCC-CC curve (the content of the in situ formed graft copolymer as a function of compatibilizer-tracer concentration) and effective emulsification curve (the dispersed phase domain size as a function of the content of the in situ formed graft copolymer) could also be obtained. These data are very precious and crucial for understanding and optimizing reactive polymer blending processes in terms of the molecular architecture of reactive compatibilizers, screw profile, and process conditions.

For example, this approach helps one to understand that it is not necessarily easier to obtain a finer dispersion with a reactive polymer blend whose dispersed phase content is low as compared to one whose dispersed phase content is high. This is because when the dispersed phase content is low, the probability of collision

between the reactive compatibilizer and the dispersed phase is low, resulting in a low amount of the in situ formed graft copolymer.

Chapter 6 Measurement of the compatibilizing efficiency of reactive comapatibilizers by a fluorescent tracing method

6.1 Introduction

Chapter 5 has used the reactive compatibilizer-tracer PS-TMI-MAMA together with RTD transient experiment to investigate the dynamic evolution of interfacial reaction and morphology of the reactive polymer blend in the TSE. As we known, the molecular architecture of the reactive compatibilizer-tracer has significant effect on the interfacial reaction and morphology of the reactive polymer blend which needs to be investigated. In chapter 3 the molecular architecture of reactive compatibilizer on the stability of the graft copolymer at interface for long time mixing has been investigated. However, the structure of reactive compatibilizer-tracer PS-TMI-MAMA on the compatibilizing efficiency in the short time remains unclear. This chapter mainly studies the molar mass, reactive group content and copolymer type on the compatibilizing efficiency in the TSE during short time mixing (<1.5 min) based on the reactive compatibilizer-tracer and RTD transient experiment

6.2 Experimental

6.2.1 Material

The characteristics of PS and PA6 are shown in Table 3.2. Table 6.1 shows the characteristics of PS-TMI-MAMA with different molecular architecture. The molar mass of the block reactive compatibilizer-tracer Anhy-PS-Anth with a terminal anhydride group was 32.9 kg/mol.

Table 6.1 Characteristics of PS-TMI-MAMA.

PS-TMI-MAMA	M_n (kg/mol)	TMI (wt%)	MAMA (wt%)	Number of TMI per chain	Number of St between TMI
PS-TMI-MAMA1	37.6	7.1	0.5	13.3	23.0
PS-TMI-MAMA4	64.6	5.1	0.5	16.4	33.9
PS-TMI-MAMA5	38.9	5.1	0.5	9.90	32.6
PS-TMI-MAMA6	17.0	5.0	0.5	4.23	29.7
PS-TMI-MAMA7	38.4	2.0	0.5	3.80	75.4

6.3 Result and discussion

6.3.1 Effect of molar mass

The effect of the molar mass of the reactive compatibilizer-tracer on the RTD is shown in Figure 6.1. It can be seen that the RTD curves of PS-TMI-MAMA4, PS-TMI-MAMA5 and PS-TMI-MAMA6 almost superimpose, indicating that the molar mass of PS-TMI-MAMA has no effect on the RTD in the range of 17.0-64.6 kg/mol.

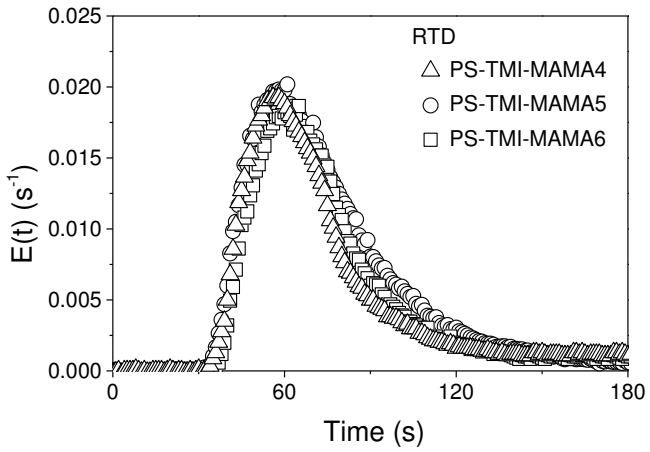

Figure 6.1 Effect of the molar mass of the reactive compatibilizer-tracer on the RTD curve for the PS/PA6 (95/5) blend. Feed rate: 13 kg/h; screw speed: 100 rpm; amount of reactive compatibilizer-tracer: 3.2g; reactive compatibilizer-tracer injection location: port 2.

The effect of molar mass of PS-TMI-MAMA on the emulsification curve (a), RCC-CC curve (b) and effective emulsification curve (c) is shown in Figure 6.2. The

emulsification curve of PS-TMI-MAMA4 with the largest molar mass (64.6 kg/mol) is at the top, indicating that the dispersed phase domain size of PS-TMI-MAMA4 is the largest. When the molar mass of PS-TMI-MAMA is decreased to 38.9 kg/mol, the emulsification curve of PS-TMI-MAMA5 moves down, indicating that the dispersed phase domain size decreases significantly. When the molar mass is further decreased to 17.0 kg/mol, the emulsification curve of PS-TMI-MAMA4 does not further move down. These imply that the dispersed phase domain size decreases with the molar mass of the reactive compatibilizer-tracer and levels off. Koning [153] found similar results based on the SMA/polyphenylene oxide (PPO) blend system with the amino terminated PS (PS-NH_2) as the reactive compatibilizer.

During the reactive polymer blending process, the reactive compatibilizer-tracer PS-TMI-MAMA needs to diffuse to the PS/PA6 interface to react with PA6 to form the PS-g-PA6-MAMA graft copolymer which acts as a compatibilizer to decrease the dispersed phase domain size. The reactive compatibilizer with a higher molar mass diffuses to the interface in a slower pace [105-110]. In other words, when the molar mass of PS-TMI-MAMA is 64.6 kg/mol, the interfacial reaction rate is slow and the amount of in-situ formed PS-g-PA6-MAMA is low. However, in the case of PS-TMI-MAMA5 (38.9 kg/mol) and PS-TMI-MAMA6 (17.0 kg/mol), they diffuse to the interface faster resulting in an increase in the amount of in-situ formed PS-g-PA6-MAMA. This could be confirmed by Figure 6.2(b) that the content of the reacted PS-TMI-MAMA4 with the largest molar mass is much lower than that of PS-TMI-MAMA5 and PS-TMI-MAMA6. Therefore, decreasing the molar mass is favorable for the interfacial reaction and morphology of the reactive polymer blending process. Figure 6.2 (c) shows that the effective emulsification curves of PS-TMI-MAMA4, PS-TMI-MAMA5 and PS-TMI-MAMA6 almost superimpose, indicating that when the amount of in-situ formed graft copolymer is fixed, the molar mass of the reactive compatibilizer-tracer has no significant influence on the dispersed phase domain size.

In general, the molar mass of the reactive compatibilizer-tracer is one of the most important factors on the reactive polymer blending process. When the content of the

reactive group TMI is fixed, the reactive compatibilizer-tracer with a higher molar mass diffuses to the interface in a slower pace and the amount of the in-situ formed graft copolymer is less, resulting in a larger dispersed phase domain size. However, when the amount of the in-situ formed graft copolymer is enough, the dispersed phase domain size of the system with different molar masses of PS-TMI-MAMA is the same. The molar mass of the reactive compatibilizer-tracer influences the reaction rate and then the dispersed phase domain size. However, it has no effect on the effective compatibilizing efficiency.

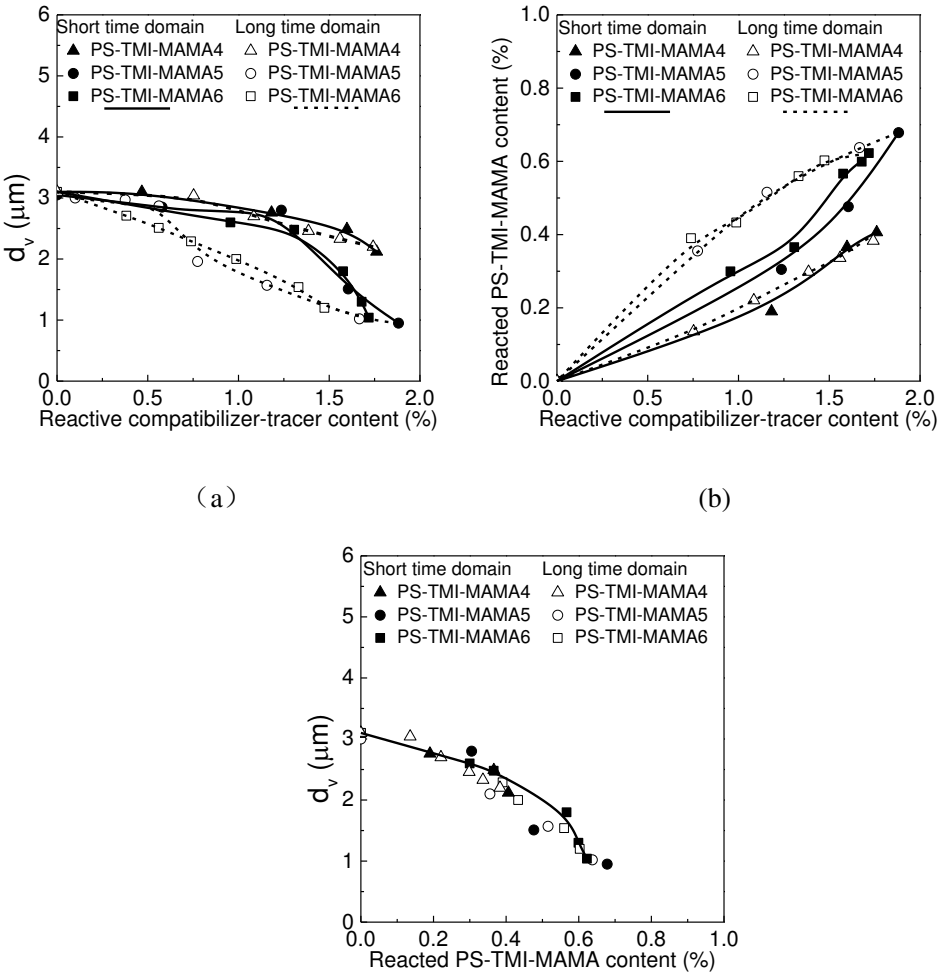

（a） (b)

（c）

Figure 6.2 Effect of the molar mass of the reactive compatibilizer-tracer on the emulsification curve (a), RCC-CC curve (b) and the effective emulsification curve (c) of PS/PA6 (95/5) system. Feed rate: 13 kg/h; screw speed: 100 rpm; amount of tracer-compatibilizer: 3.2 g；reactive compatibilizer-tracer injection location: port 2.

6.3.2 Effect of TMI content

The effect of the TMI content of the PS-TMI-MAMA on the RTD curves is shown in Figure 6.3. It can be seen that the RTD curves of PS-TMI-MAMA1, PS-TMI-MAMA5 and PS-TMI-MAMA7 almost superimposes, indicating that TMI content (2 wt%-7.1 wt%) has no influence on the residence time.

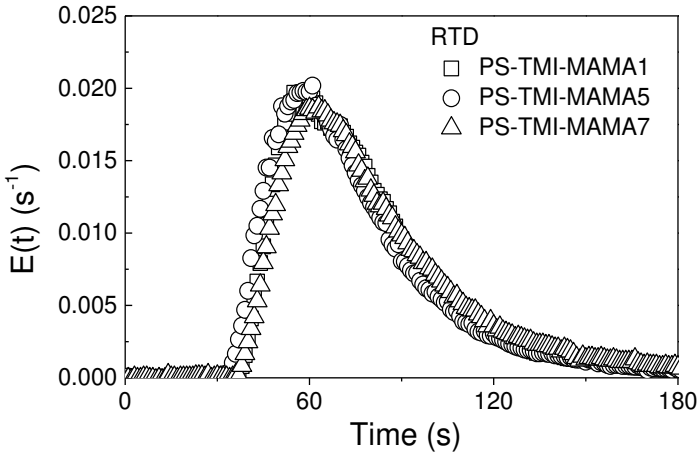

Figure 6.3 Effect of the TMI content of the reactive compatibilizer-tracer on the RTD curve for the PS/PA6 (95/5) blend. Feed rate: 13 kg/h; screw speed: 100 rpm; amount of reactive compatibilizer-tracer: 3.2g; reactive compatibilizer-tracer injection location: port 2.

Figure 6.4 shows the effect of TMI content on the emulsification curve (a), RCC-CC curve (b) and effective emulsification curve (c). It can be seen from Figure 6.4 (a) that as the TMI content increases, the emulsification curve moves down. This indicates that the dispersed phase domain size decreases with increasing TMI content. It can be seen from Figure 6.4 (b) that the RCC-CC curves of PS-TMI-MAMA1, PS-TMI-MAMA5 and PS-TMI-MAMA7 almost superimpose, indicating that TMI content has only a small influence on the RCC. In other words, the difference in the dispersed phase domain size of the three systems with different PS-TMI-MAMA is caused by the molecular architecture of the in-situ formed PS-g-PA6-MAMA and not by its amount. This is confirmed by Figure 6.4 (c). When the content of the reacted PS-TMI-MAMA is fixed, the dispersed phase domain size decreases with increasing TMI content. Therefore, when the molar mass of PS-TMI-MAMA is fixed, the TMI content does not influence much the interfacial reaction but affects significantly the compatibilizing efficiency. As the TMI content increases, the number of PA6 grafts of PS-g-PA6-MAMA increases. Its compatibilizing efficiency increases and the

dispersed phase domain size decreases. De Roover [154] investigated the MA content of PP-g-MA on the PP/PA6 blend and found similar results that the dispersed phase domain size decreases and levels off with increasing MA content.

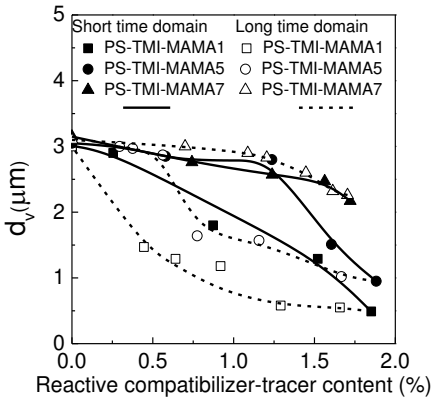

（a）

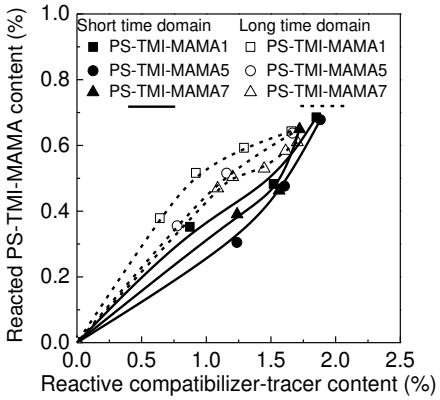

（b）

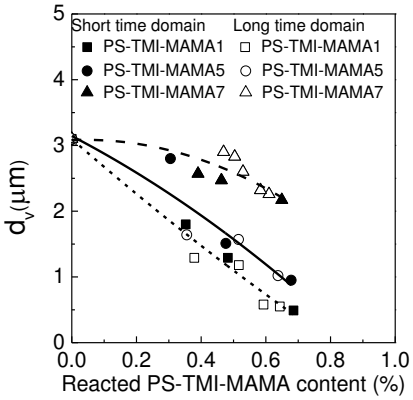

（c）

Figure 6.4 Effect of the TMI content of the reactive compatibilizer-tracer on the emulsification

curve (a), RCC-CC curve, (b) and the effective emulsification curve (c) of PS/PA6 (80/20) system. Feed rate: 13 kg/h; screw speed: 100 rpm; amount of tracer-compatibilizer: 3.2 g; reactive compatibilizer-tracer injection location: port 2.

6.3.3 Graft reactive compatibilizer-tracer vs. block reactive compatibilizer-tracer

Figure 6.5 shows the RTD curves of the graft reactive compatibilizer-tracer PS-TMI-MAMA5 (M_n=38.9 kg/mol) and block reactive compatibilizer-tracer Anhy-PS-Anth (M_n=32.9 kg/mol). It can be seen that these two RTD curves almost superimpose.

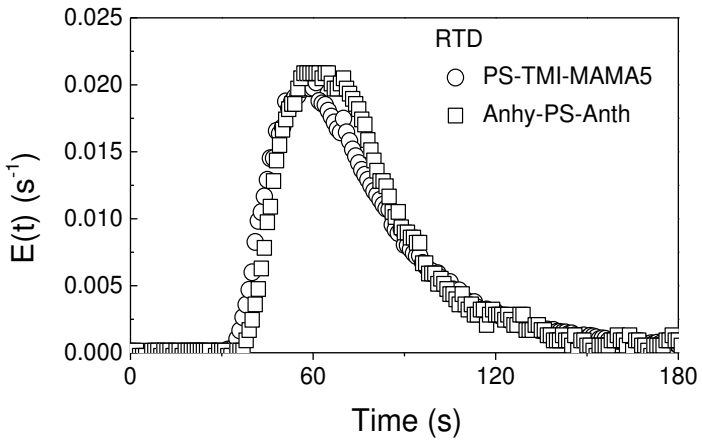

Figure 6.5 Effect of type of the reactive compatibilizer-tracer on the RTD curve for the PS/PA6 (95/5) blend. Feed rate: 13 kg/h; screw speed: 100 rpm; amount of reactive compatibilizer-tracer: 3.2g; reactive compatibilizer-tracer injection location: port 2.

Figure 6.6 shows the emulsification curve (a), RCC-CC curve (b) and effective emulsification curve (c) of PS-TMI-MAMA5 and Anhy-PS-Anth. It can see from Figure 6.6 (a) that the emulsification curve of PS-TMI-MAMA5 is below that of Anhy-PS-Anth, especially for the long time domain. This indicates that the dispersed phase domain size of PS-TMI-MAMA5 is smaller than that of Anhy-PS-Anth. On the other hand, it can be seen from Figure 6.6 (b) that the amount of the in-situ formed copolymer for these two systems is almost the same. It can also be seen from Figure 6.6c that the effective emulsification curve of PS-TMI-MAMA5 is below that of Anhy-PS-Anth, indicating that the compatibilizing efficiency of PS-TMI-MAMA5 is

higher than that of Anhy-PS-Anth. Joen[93] found similar result that the compatibilzing efficiency of block copolymer PS-b-PMMA is lower than that of graft copolymer PS-g-PMMA for the PS/PMMA blend.

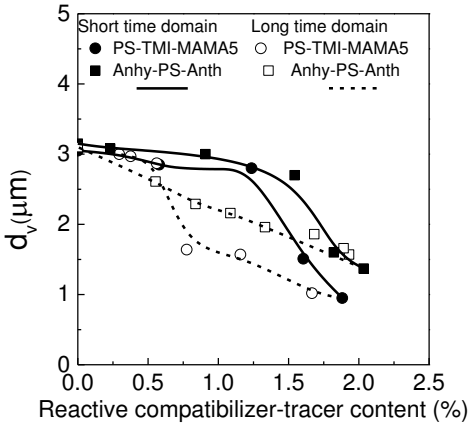

（a）

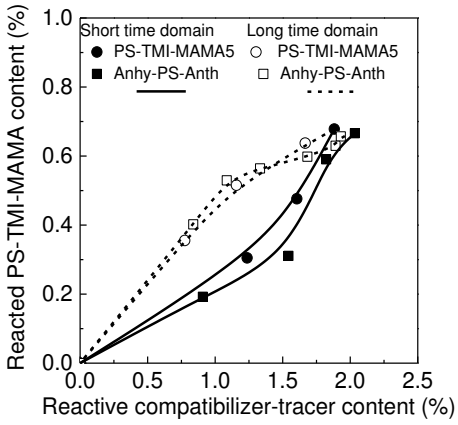

（b）

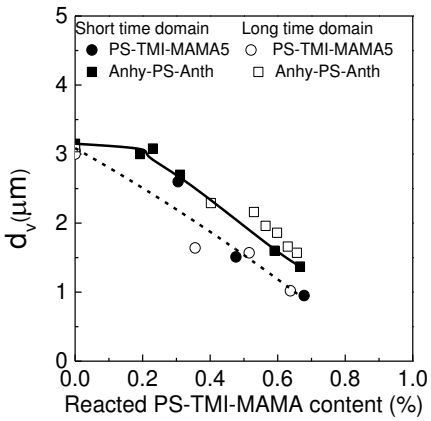

（c）

Figure 6.6 Effect of type of the reactive compatibilizer-tracer on the emulsification curve (a), RCC-CC curve (b) and the effective emulsification curve (c) of PS/PA6 (80/20) system. Feed rate: 13 kg/h; screw speed: 100 rpm; amount of tracer-compatibilizer: 3.2 g; reactive compatibilizer-tracer injection location: port 2.

6.4 Conclusion

The reactive compatibilizer-tracer is used together with RTD transient experiments to investigate the effect of the molecular architecture of reactive compatibilizer-tracer on the reactive polymer blending process.

When the TMI content in PS-TMI-MAMA is fixed and the molar mass increases from 17.0 kg/mol to 64.6 kg/mol, PS-TMI-MAMA diffuses to the interface slower, resulting in the decreases in the amount of the in-situ formed PS-g-PA6-MAMA and the increase in the dispersed phase domain size. However, when the amount of the in-situ formed PS-g-PA6-MAMA is fixed, the dispersed phase domain size obtained with PS-TMI-MAMA of different molar mass is almost the same. Therefore, the molar mass influences the interfacial reaction rate and then the dispersed phase domain size but not the effective compatibilizing efficiency.

When the molar mass of PS-TMI-MAMA is fixed, the amount of in-situ formed graft copolymer is almost the same but the dispersed phase domain size decreases with increasing TMI content. Therefore, the TMI content does not influence much the interfacial reaction but affects significantly the comaptibilizing efficiency. In the case of the graft reactive compatibilizer PS-TMI-MAMA5 and block reactive compatibilizer Anhy-PS-Anth, the compatibilizing efficiency of PS-TMI-MAMA5 is higher than that of Anhy-PS-Anth.

Chapter 7 Effect of the degree of fill on the PS/PA6/PS-TMI-MAMA reactive polymer

7.1 Introduction

A single screw extruder has only one operating parameter which is screw speed. The latter has to be increased to increase the throughput. By contrast, a twin screw extruder has two operating parameters which are screw speed, N, and throughput, Q. They may have significant influences on the morphology and interfacial reaction of reactive polymer blending processes. Most of the literature reported that screw speed and throughput could affect the residence time. In fact, they may also affect the degree of fill. When the Q/N ratio is fixed, the degree of fill is fixed, whatever the values of Q and N [155]. This chapter investigates the effect of the degree of fill on the reactive polymer blending process via the Q/N ratio.

7.2 Experimental

7.2.1 Materials

The characteristics of the PS and PA6 are shown in Table 3.2. The number-average molar mass, the TMI content and the MAMA content of PS-TMI-MAMA were 38.9 kg/mol, 5.1 wt% and 0.5 wt%, respectively.

7.2.2 Reactive blending

The composition of the PS/PA6 blend was 95/5. The reactive compatibilizer-tracer PS-TMI-MAMA was injected at port 2 which was far away from the die exit. The values of Q and N as well as the Q/N ratios are listed in Table 7.1. The volume throughput Q was the mass throughput divided by density. The densities of the PS and PA6 were 970 and 1130 kg/m^3, respectively. That of the PS/PA6 (95/5) blend was estimated to be 978 kg/m^3.

Table 7.1 Experiments carried out in this work and their operating conditions

Experiment No.	1	2	3	4	5	6	7	8	9	10	11
Screw Speed N（rpm）	80	100	120	200	80	100	120	50	80	100	120
Mass throughput（kg/h）	5.2	6.5	7.8	13	10.4	13	15.6	13	20.8	26	31.2
Volume throughput Q ($\times 10^{-3}$ l/min)	5.31	6.64	7.97	13.3	10.6	13.3	15.9	13.3	21.3	26.5	31.9
Specific throughput Q/N ($\times 10^{-3}$ l/rev.)	1.11	1.11	1.11	1.11	2.21	2.21	2.21	4.43	4.43	4.43	4.43

7.3 Result and discussion

7.3.1 Effect of screw speed

Figure 7.1 shows the effect of screw speed on the emulsification curve (a), RCC-CC curve (b) and effective emulsification curve (c) when the throughput is fixed at 13 kg/h. It can be seen from Figure 7.1 (a) and 7.1 (b) that as screw speed increases, the emulsification curve moves up and the RCC-CC curve moves down. It indicates that the dispersed phase domain size increases and the content of the in-situ formed graft copolymer decreases with increasing screw speed. Similar result was found by Li et al. [42] that the dispersed phase domain size reached a minimum at 400 rpm.

The shear stress could be calculated by shear rate and viscosity [42]:

$$\tau_m = \eta_m \dot{\gamma} = M\dot{\gamma}^n \tag{7-1}$$

τ_m is the shear stress of matrix, η_m is the matrix viscosity, $\dot{\gamma}$ is the shear rate, M is the coefficient of power function，n is the index of power function（0<n<1）. It could be deduced from equation (7-1) that the shear stress of matrix increases with increasing shear rate. As screw speed increases, the shear stress increases and then the dispersed phase domain size should decrease when the interface slip could be neglected. However, it is contradictory to the result of the emulsification curve.

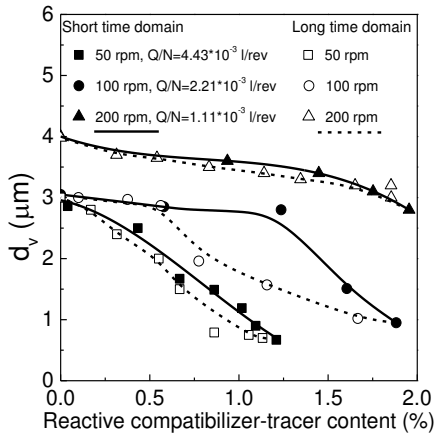

(a)

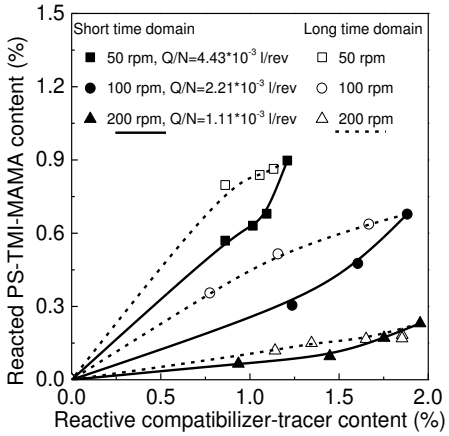

(b)

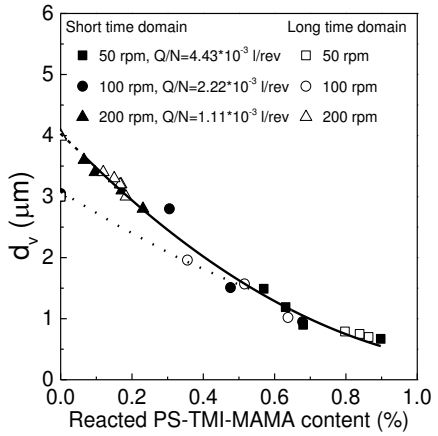

(c)

Figure 7.1 Effects of screw speed on the emulsification curve (a), RCC-CC curve (b) and effective emulsification curve (c).

Why does the dispersed phase domain size increase with increasing screw speed? It can be seen from the effect of screw speed on the RTD curve (Figure 7.2) that the

residence time decreases with increasing screw speed. There is no enough residence time for PS-TMI-MAMA to react with PA6 and the amount of the in-situ formed graft copolymer is not enough at higher screw speed (Figure 7.1b), leading to an increase in the dispersed phase domain size. On the other hand, it can be seen from the effective emulsification curve (Figure 7.1c) that the effective emulsification curves at 50, 100 and 200 rpm could be divided into two regimes. In the first regime, the content of the reacted PS-TMI-MAMA is zero or very low and the effective emulsification curve at 200 rpm is above those at 50 and 100 rpm. In this regime, since the content of the reacted PS-TMI-MAMA is low, mechanical conditions control the dispersed phase domain size. An increase in screw speed is expected to shorten the residence time and increase the mixing intensity. The former disfavor the emulsification process and the latter favors it. It will be shown later that it is the degree of fill and not the screw speed nor throughput that controls the mixing and therefore the emulsification process. In the second regime where the content of the reacted PS-TMI-MAMA is above some values, the effective emulsification curves at 50, 100 and 200 rpm almost superimpose, indicating that in this regime it is the content of the in-situ formed PS-g-PA6-MAMA that controls the dispersed phase domain size.

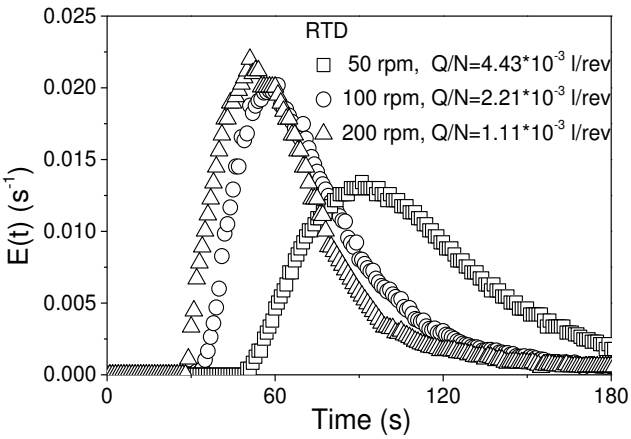

Figure 7.2 Effect of the screw speed on the RTD curves.

7.3.2 Effect of throughput

Figure 7.3 and 7.4 shows the effect of throughput on the residence time (Figure

7.3) and emulsification curve (Figure 7.4a), RCC-CC curve (Figure 7.4b) and effective emulsification curve (Figure 7.4c) when the screw speed is fixed at 100 rpm. It can be seen from Figure 7.3 that an increase in throughput decreases the residence time. However, it can be seen from Figure 7.4 (a) and 7.4 (b) that as throughput increases, the emulsification curve moves down and the RCC-CC curve moves up, indicating that the dispersed phase domain size decreases and the content of the in-situ formed graft copolymer increases. The above results seem to be contradictory and imply that for a given screw speed, the residence time is not the controlling parameter of the emulsification process. Rather, we speculate that it is the degree of fill that controls the mixing and consequently the emulsification process.

Degree of fill is one of the most important parameters which influence the reactive polymer blending process in a twin screw extruder [156]. As the throughput decreases, the degree of fill decreases too and then the shear applied to the polymer blend decreases. Therefore, even if the residence time is long enough, there is no enough in-situ formed graft copolymer at the interface to prevent the dispersed phase domains from coalescing and their size increases. Besides, it can be seen from Figure 7.4 (c) that there is a significant difference among the effective emulsification curves obtained at different throughputs when the content of the reacted PS-TMI-MAMA is low: the emulsification curve moves down as the throughput increases. The difference narrows with increasing content of the reacted PS-TMI-MAMA.

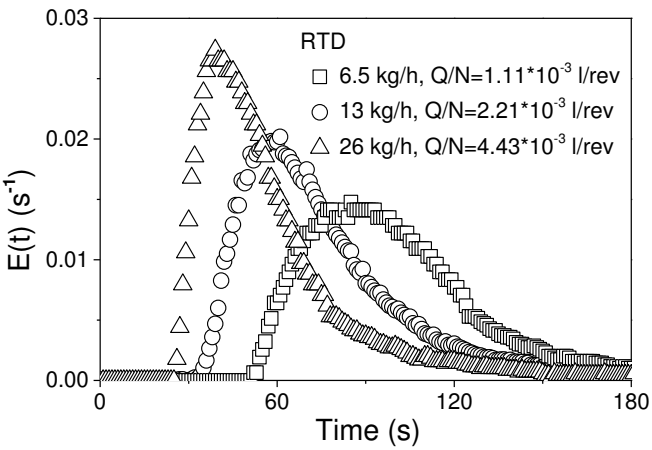

Figure 7.3 Effect of the throughput on the RTD curve. Screw speed = 100 rpm.

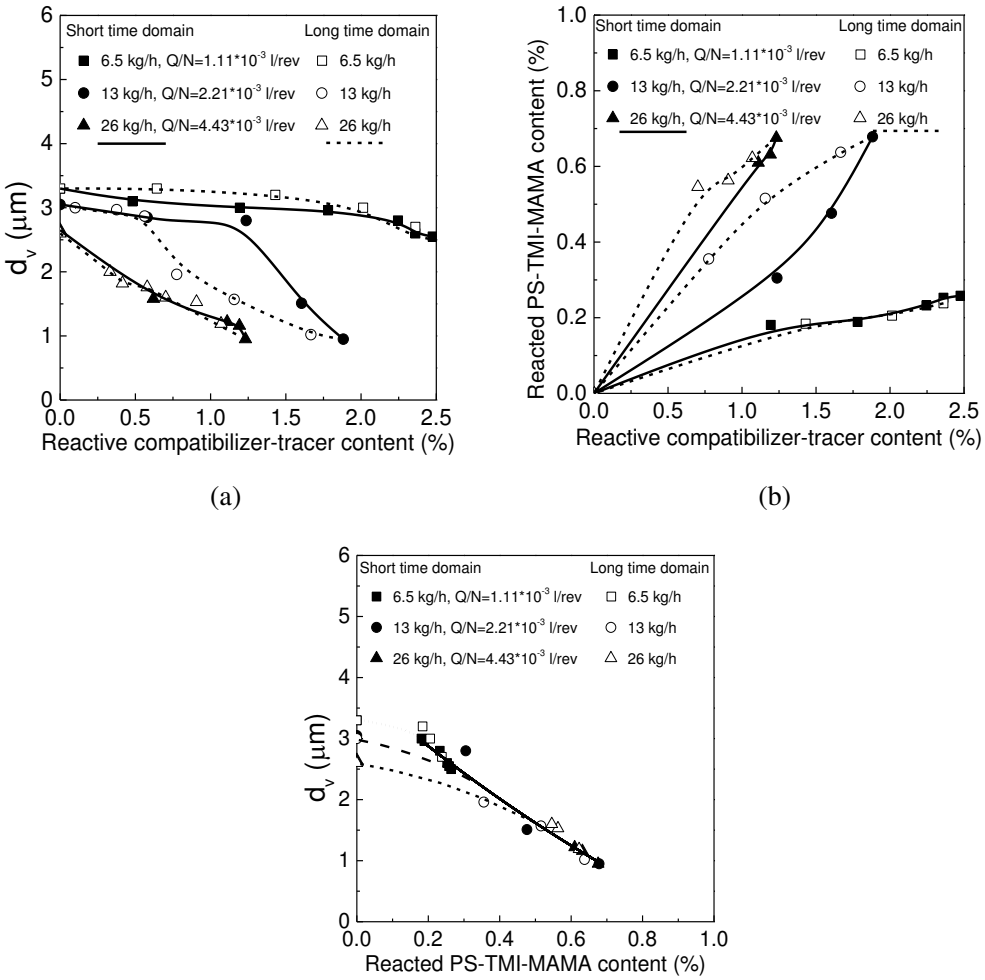

Figure 7.4 Effect of throughput on the emulsification curve (a), RCC-CC curve (b) and effective emulsification curves (c).

7.3.3 Effect of degree of fill

The experiments of different degree of fill were carried out to further confirm that the effect of the throughput on the interfacial reaction and morphology of the reactive polymer blending process is caused by the degree of fill. Firstly, define the degree of fill. Degree of fill (f) is the ratio of the effective volume (V_{eff}) which is the material volume in the twin screw extruder and the free volume (V) between the screw and the barrel. It can be calculated by following equation:

$$f = \frac{Q \times \bar{t}}{V} \tag{7-2}$$

where Q is the throughput and $\bar{t}$ is the mean residence time.

Dimensionless residence time (τ), revolution (n) and extrudate volume (v) are shown as follows:

$$\tau = t/\bar{t} \tag{7-3}$$

$$n = tN \tag{7-4}$$

$$v = tQ \tag{7-5}$$

where N is the screw speed and t is the residence time. Hence, there is the following equation:

$$\tau = \frac{t}{\bar{t}} = \frac{n}{\bar{t}N} = \frac{V}{\bar{t}Q} \tag{7-6}$$

where τ is the dimensionless residence time ($\tau = t/\bar{t}$)[118, 157].

When the ratio of Q and N is fixed, the E(τ)-τ curves of different screw speed and throughput superimpose (Figure 7.5), indicating that E(τ)-τ curve is independent on Q and N. According to the literature [157], residence revolution distribution (RRD-n) and residence volume distribution (RVD-v) is independent on the Q and N when Q/N is fixed. Hence, there is the following equation:

$$N\bar{t} = k_1 = constant1 \tag{7-7}$$

$$Q\bar{t} = k_2 = constant2 \tag{7-8}$$

where k_1 and k_2 are the fixed value and $k_2/k_1=Q/N$. Hence, $N\bar{t}$ and $Q\bar{t}$ is the fixed value when Q/N is fixed.

Taking equation (7-2) into the equation (7-7) and equation (7-8), there is the following equation:

$$f = \frac{k_1}{V} \times \frac{Q}{N} = constant3 \tag{7-9}$$

This equation implies that the degree of fill is the fixed value when Q/N is fixed.

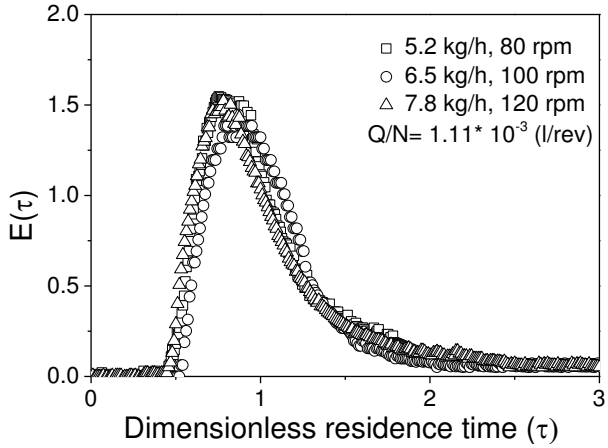

Figure 7.5 Effect of screw speed and throughput on the dimensionless residence time distribution curves for a Q/N of 1.11 $\times 10^{-3}$ liter/revolution.

The experiments with different degree of fill were carried out and the processing parameters are listed in Table 7.1. The value of $Q\bar{t}$ (Table 7.2) could represent for the degree of fill because the free volume of twin screw extruder is fixed. It can be confirmed again that the degree of fill is fixed when Q/N is fixed. When Q/N increases from 1.11×10^{-3} l/rev to 2.21×10^{-3} l/rev, the degree of fill increases by 1.5 folds; when Q/N further increases to 4.43×10^{-3} l/rev, the degree of fill is almost full ,which is 2 folds of that at 1.11×10^{-3} l/rev,

Table 7.2 The degree of fill of with different screw speed and throughput.

	Q (kg/h)	N (rpm)	$Q\bar{t}$ (l)	Q/N ($*10^{-3}$ l/rev)
1	5.2	80	0.18	1.11
2	6.5	100	0.18	
3	7.8	120	0.18	
4	13	200	0.19	
5	10.4	80	0.26	2.21
6	13	100	0.24	
7	15.6	120	0.26	
8	13	50	0.34	4.43
9	20.8	80	0.34	
10	26	100	0.38	
11	31.2	120	0.36	

The effect of screw speed and throughput on the emulsification curve when Q/N is fixed is shown in Figure 7.6. It can be seen from Figure 7.6 (a) that when the degree

of fill is low, the emulsification curves of different screw speed and throughput almost superimpose and the dispersed phase domain size just slightly decreases. When the degree of fill increases (Figure 7.6b and 7.6c), the dispersed phase domain size decreases significantly. Because when the degree of fill is low, the shear stress applied on the blend is weak, resulting in the low interfacial reaction between PS-TMI-MAMA and PA6. As the degree of fill increases, the shear stress increases and PS-TMI-MAMA has more opportunities to react with PA6. This could be confirmed by the RCC-CC curve that the amount of graft copolymer at the interface is few under low degree of fill (Figure 7.7a) and it increases significantly with increasing degree of fill (Figure 7.7b and 7.7c).

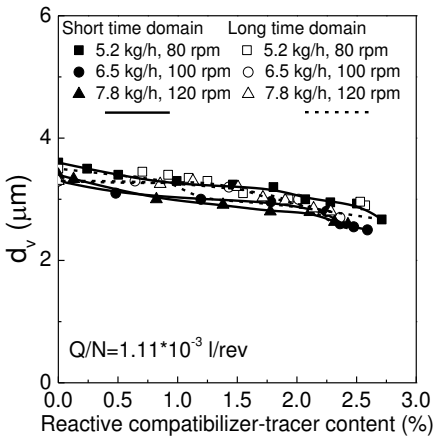

(a)

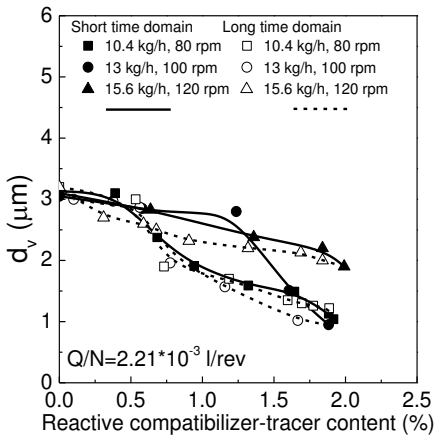

(b)

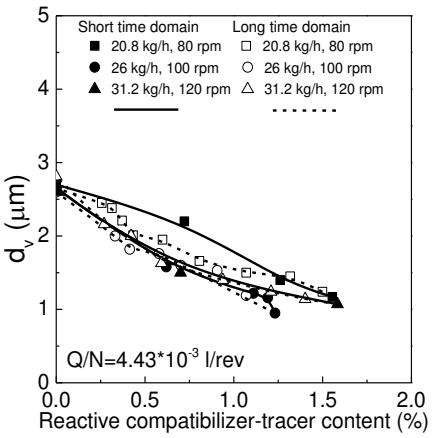

（c）

Figure 7.6 Effect of increasing screw speed and throughput on the emulsification curves based on the fixed value of Q/N. (a) low degree of fill: Q/N=1.11 $\times 10^{-3}$ l/rev; (b) medium degree of fill: Q/N=2.21 $\times 10^{-3}$ l/rev; (c) high degree of fill: Q/N=4.43 $\times 10^{-3}$ l/rev.

The kneading block only has transporting function and could not provide effective shear stress under low degree of fill. The interfacial generation is low and it is hard for PS-TMI-MAMA to diffuse to the interface to react with PA6. Under this condition, even if the residence time is long enough (decreasing throughput and screw speed), there is few copolymer in-situ formed at the interface. Therefore, the emulsification curves and RCC-CC curves of different screw speed and throughput almost superimpose and dispersed phase domain size hardly decreases. In other words, residence time has no influence on the content of reacted PS-TMI-MAMA and the dispersed phase domain size at low degree of fill. At medium degree of fill, the emulsification curves of different screw speed and throughput do not superimpose. The emulsification curve of the largest screw speed and throughput is at the top, indicating that the dispersed phase domain size is the largest. Because when the degree of fill increases from low to medium, the shear stress increase and the effect of the residence time appears. As the screw speed and throughput increases, the residence time decreases and the amount of the in-situ formed copolymer decreases, resulting in the increases in the dispersed phase domain size. Moreover, as the degree of fill further increases to fully occupied, the emulsification curves of different screw speed and throughput superimpose again. Because the shear stress is very strong, there is enough amount of the copolymer at the interface to decrease the dispersed phase domain size even if the residence time is short (increasing throughput and screw speed).

Figure 7.8 shows the effect of the screw speed and throughput on the effective emulsification curve when Q/N is fixed. It can be seen that the effective emulsification curves of different screw speed and throughput superimpose to one curve when the degree of fill is fixed. As the degree of fill increases, the effective emulsification curve decreases when the content of the reacted PS-TMI-MAMA is zero or very low. However, the difference among the effective emulsification curves obtained at various screw speeds and throughputs narrows or disappears when there is some graft copolymer formed at the interface.

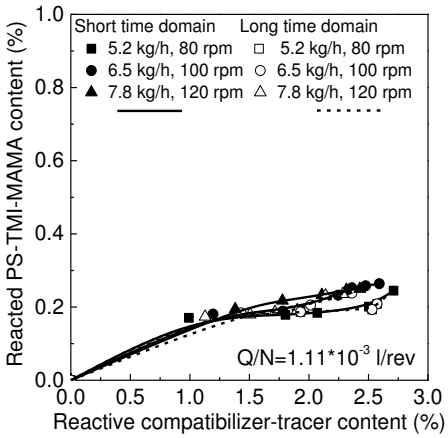
Short time domain
Long time domain
5.2 kg/h, 80 rpm
5.2 kg/h, 80 rpm
6.5 kg/h, 100 rpm
6.5 kg/h, 100 rpm
7.8 kg/h, 120 rpm
7.8 kg/h, 120 rpm
Q/N=1.11*10-3 l/rev
Reacted PS-TMI-MAMA content (%)
Reactive compatibilizer-tracer content (%)

（a）

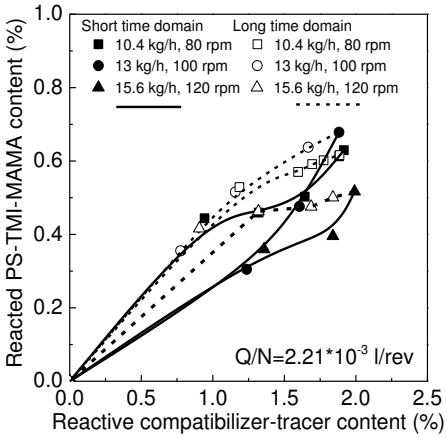
Short time domain
Long time domain
10.4 kg/h, 80 rpm
10.4 kg/h, 80 rpm
13 kg/h, 100 rpm
13 kg/h, 100 rpm
15.6 kg/h, 120 rpm
15.6 kg/h, 120 rpm
Q/N=2.21*10-3 l/rev
Reacted PS-TMI-MAMA content (%)
Reactive compatibilizer-tracer content (%)

（b）

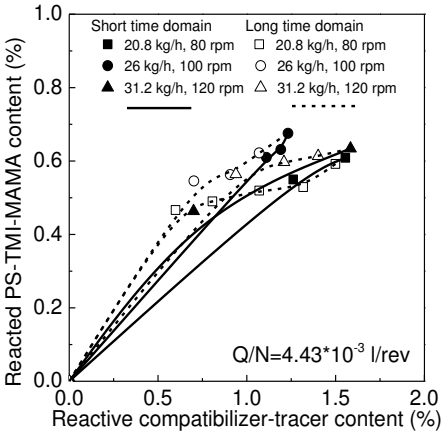
Short time domain
Long time domain
20.8 kg/h, 80 rpm
20.8 kg/h, 80 rpm
26 kg/h, 100 rpm
26 kg/h, 100 rpm
31.2 kg/h, 120 rpm
31.2 kg/h, 120 rpm
Q/N=4.43*10-3 l/rev
Reacted PS-TMI-MAMA content (%)
Reactive compatibilizer-tracer content (%)

（c）

Figure 7.7 Effect of increasing screw speed and throughput on the RCC-CC curves based on the fixed value of Q/N. (a) low degree of fill: Q/N=1.11 $\times 10^{-3}$ l/rev; (b) medium degree of fill: Q/N=2.21 $\times 10^{-3}$ l/rev; (c) high degree of fill: Q/N=4.43 $\times 10^{-3}$ l/rev.

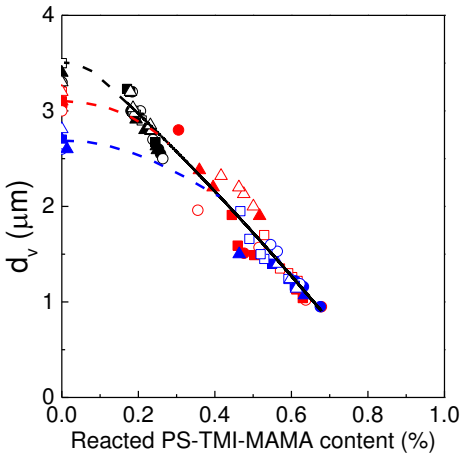

Figure 7.8 Effect of increasing screw speed and throughput on the RCC-CC curves based on the fixed value of Q/N. l:ow degree of fill-Q/N=1.11 ×10-3 l/rev: ■□: 5.2 kg/h, 80 rpm; ●○: 6.5 kg/h, 100 rpm; ▲△: 7.8 kg/h, 120 rpm; (b) medium degree of fill-Q/N=2.21 ×10-3 l/rev: ■□: 10.4 kg/h, 80 rpm; ●○: 13 kg/h, 100 rpm; ▲△: 15.6 kg/h, 120 rpm; (c) high degree of fill-Q/N=4.43 ×10-3 l/rev: ■□: 20.8 kg/h, 80 rpm; ●○: 26 kg/h, 100 rpm; ▲△: 31.2 kg/h, 120 rpm. Solid symbol: short time domain; open symbol: long time symbol.

The above results confirm that the effect of the throughput on the dispersed phase domain size is caused by the degrees of fill. When screw speed is fixed and throughput decreases, the residence time increases but the degree of fill deceases at the same time which leads to a decrease in the shear stress. The interfacial reaction between PS-TMI-MAMA and PA6 is difficult to occur and there is no enough amount of the copolymer formed at the interface to decrease the dispersed phase domain size. Hence, degree of fill has a more significant influence on the interfacial reaction and morphology of the reactive polymer blending process than residence time.

As screw speed changes, the Q/N changes and the degree of fill changes at the same time. Then the effect of screw speed can be discussed in terms of degree of fill. As the screw speed decreases, Q/N increases and degree of fill increases which leads to the increases in the shear stress. Strong shear stress improves the interfacial reaction and the amount of the in-situ formed copolymer increases, resulting in the

decrease in the dispersed phase domain size. Therefore as screw speed decreases, both the residence time and degree of fill increases which are beneficial to the interfacial reaction and reduction in the dispersed phase domain size.

7.4 Conclusion

The screw speed (N) and throughput (Q) have significant effects on the reactive polymer blending process in the twin screw extruder. When the ratio of throughput Q and screw speed N is fixed, RTD with different throughput and screw speed changes, however, the corresponding dimensionless residence time distribution superimpose to one curve and the degree of fill is fixed.

As screw speed increases, the mean residence time and degree of fill decreases at the same time. Then there is no enough graft copolymer in-situ formed at the interface, resulting in the increase in the dispersed phase domain size. As throughput increases, the residence time decreases, however, the degree of fill increases too which leads to the increase in the shear stress. Then the amount of the in-situ formed copolymer at the interface increases and the dispersed phase domain size decreases. The throughput and screw speed have significant influences on the reactive polymer blending processes through the degree of fill and residence time. The effect of degree of fill is more dominant than that of residence time. As the degree of fill increases, the interfacial reaction increases and the dispersed phase domain size decreases.

Chapter 8 Mixing efficiency of mixing elements in a twin screw extruder

8.1 Introduction

Screw elements in a twin screw extruder can be conveying elements and mixing elements. The mixing ability of the twin screw extruder depends on the screw configuration, especially the sequence of mixing elements, leading to different morphologies and performances of polymer blends. A mixing element provides both dispersive mixing and distributive mixing. [158-161] Dispersive mixing in polymer blending is related to the breakup and dispersion of the dispersed phase. Most researchers investigated the dispersive mixing based on the morphology of the polymer blends [162-165]. Distributive mixing is related to the stretch and deformation of the interface [166]. Most literature was focused on the simulation of distributive mixing because the latter is difficult to evaluate experimentally. Most importantly, dispersive mixing and distributive mixing are highly coupled so that it is challenging to study their efficiencies for individual mixing elements. This chapter uses the reactive compatibilizer-tracer together with RTD transient experiments to investigate the efficiency of mixing element of a twin screw extruder.

8.2 Experimental

8.2.1 Material

The characteristics of the PS and PA6 are shown in Table 3.2. The number-average molar mass, the TMI content and the MAMA content of PS-TMI-MAMA were 38.9 kg/mol, 5.1 wt% and 0.5 wt%, respectively.

8.2.2 Reactive blending

Reactive blending was carried out in a twin screw extruder and the screw configuration is shown in Figure 5.3. Figure 8.1 shows the mixing elements used in

this chapter. A kneading block (x/y/z) is composed of several kneading discs (number of kneading discs y) of 32 mm in total length (z) and the angle between two adjacent discs is x. For example, a kneading block 30/7/32 is composed of 7 kneading discs of 32 mm in total length and the angle between two adjacent kneading discs is 30°

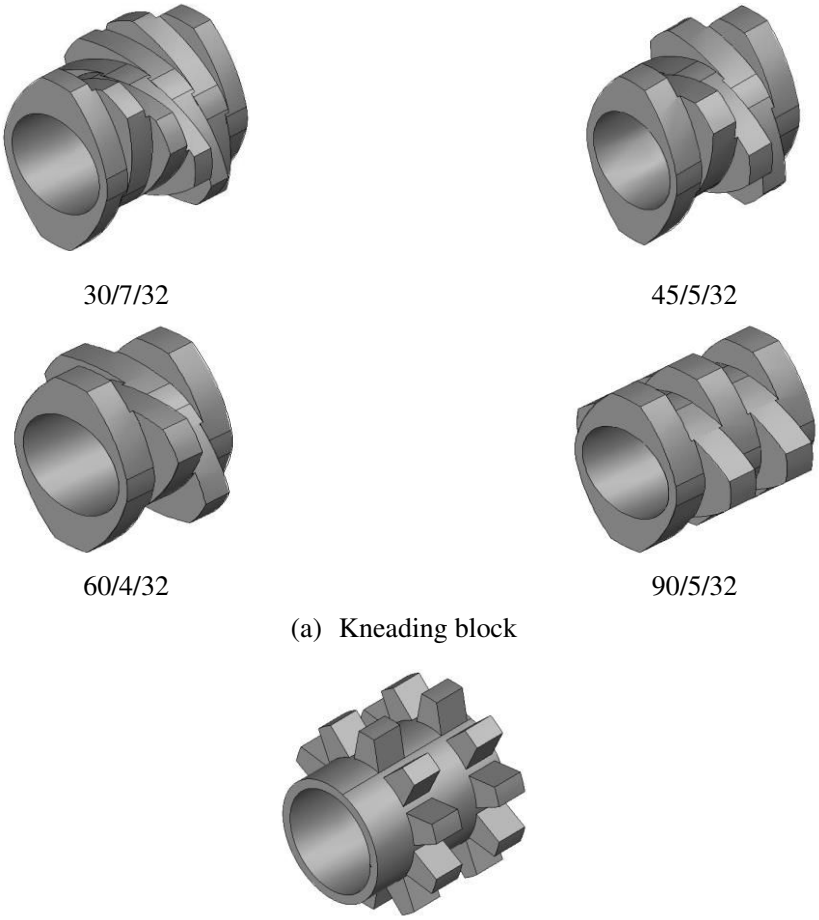

(a) Kneading block

(b) 90° Gear

Figure 8.1 Screw elements used in the experiments. (a) kneading blocks; (b) gear. Kneading block (x/y/z): x-kneading angle; y-number of kneading discs; z- length of kneading block. Kneading blocks can be forward and reverse kneading blocks. The kneading angle of the forward kneading blocks changes in clockwise direction, and that of reverse kneading blocks changes in counterclockwise direction. The 90° gear has 10 well-distributed gears and its length is the same as a kneading block (32 mm).

The reactive blending process is the same as in the Chapter 5. The blend composition of the PS and PA6 was 95/5. The throughput was 13 kg/h and screw speed was 100 rpm.

8.3 Results and discussion

8.3.1 Effect of kneading angle

Figure 8.2 shows the effect of the angle of mixing elements on the emulsification curves (a), RCC-CC curves (b) and effective emulsification curves (c) when the reactive compatibilizer-tracer is added in Tracer port 1. It can be seen from Figure 8.2 (a) that the emulsification curve of 30° kneading block is at the top, indicating that the dispersed phase domain size of 30° kneading block is the largest. As the kneading angle increases from 30° to 60°, the emulsification curve moves down, indicating the dispersed phase domain size decreases. A further increase in the kneading angle does not move the emulsification curve further down. In other words, the dispersed phase domain size of 60° kneading block, 90° kneading block and 90° gear is almost the same when the PS-TMI-MAMA content is fixed.

On the one hand, it can be seen from Figure 8.2 (b) that RCC-CC curve of 30° kneading block is at the top. As the kneading angle increases from 30° to 60°, the RCC-CC moves up. A further increase in the angle does not move the RCC-CC curve further down. This indicates that the content of the reacted PS-TMI-MAMA increases with increasing angle and remains unchanged after 60°. Distributive mixing is related to the interface stretch and deformation. As the distributive mixing increases, the interfacial generation increases and the interfacial reaction increases. Therefore the RCC-CC curve is used to evaluate the distributive mixing efficiency. The order of the distributive mixing efficiency of mixing element is as follows: 30°<45°<60° ≈ 90° ≈ 90°gear. As the angle of kneading block increases, the distributive mixing efficiency increases.

On the other hand, it can be seen from Figure 8.2 (c) that the order of the dispersed phase domain size is as follows when the content of the reacted PS-TMI-MAMA is fixed: 30° ≈ 45°>>60°≈90° ≈90°gear. The difference in the dispersed phase domain size of different mixing elements is related to the dispersive mixing efficiency. As the kneading angle increases from 45° to 60°, the dispersive mixing efficiency increases. It does not further increase with a further increase in the

angle of mixing elements.

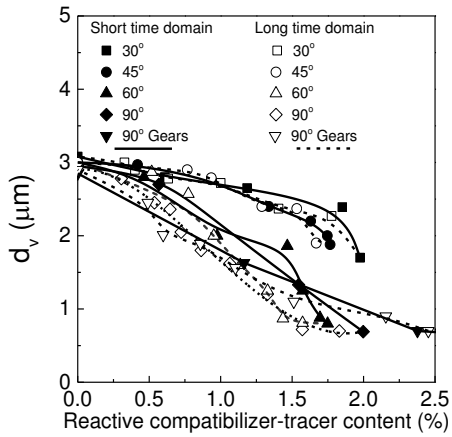

(a)

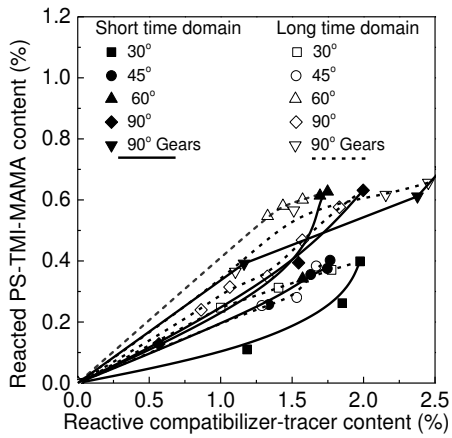

(b)

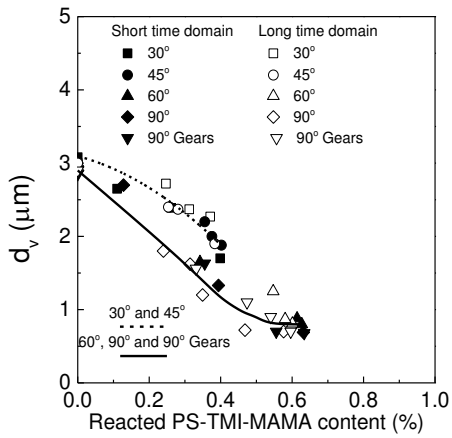

(c)

Figure 8.2 Effect of kneading angle on the emulsification curve (a), RCC-CC curve (b) and effective emulsification curves (c) when the reactive compatibilizer-tracer is added in the tracer

port 1.

The effect of the kneading angle on the residence time is shown in Figure 8.3. As the kneading angle increases, the RTD shifts to the long time domain. The residence time of the 90° gear is the longest. As the residence time increases, the interfacial reaction time increases and the content of the in-situ formed graft copolymer increases (Figure 8.2b), resulting in the decreases in the dispersed phase domain size. When the reactive compatibilizer-tracer is added from tracer port 2 or feeder, the residence time further increases. It can be seen from Figure 8.4 that the difference in the emulsification curve of different mixing elements decreases. Especially when the reactive compatibilizer-tracer is added from the feeder, the emulsification curve of 45°, 60°, 90°kneading block and 90°gear superimposes. This indicates that when residence time increases, the PS-TMI-MAMA has enough time to react with PA6 to form enough amount of the graft copolymer at the interface, resulting in a decreases in the difference of mixing elements.

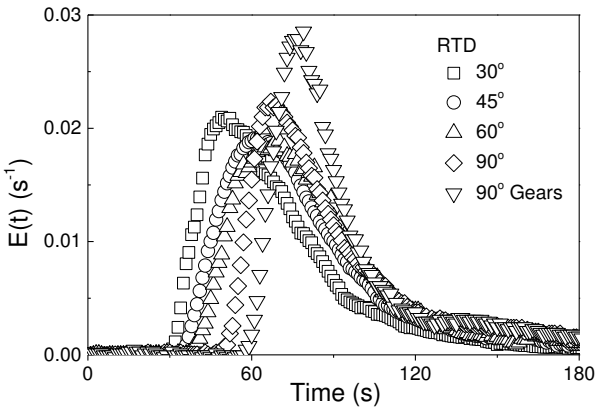

Figure 8.3 Effect of the kneading angle on the RTD curves when the reactive compatibilizer-tracer is added in tracer port 1.

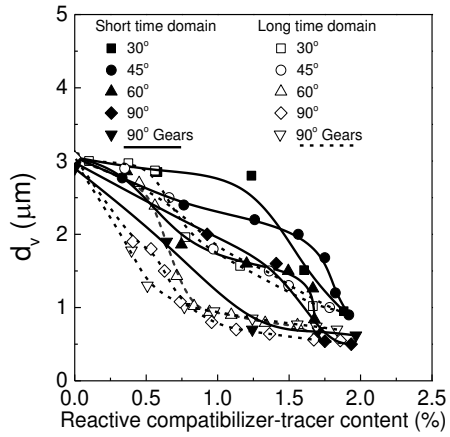

（a）

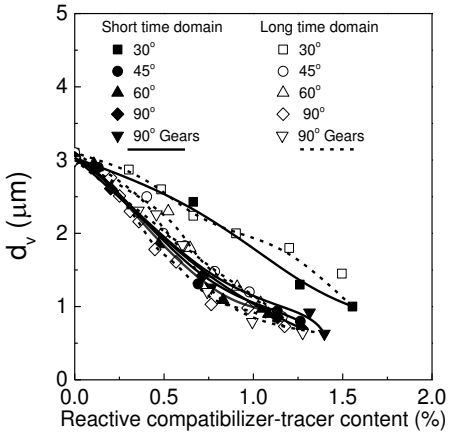

（b）

Figure 8.4 Effect of the kneading angle on the emulsification curves. (a) Tracer port: 2; (b) Tracer port: feeder.

Zhang et al. [167] used a three-dimensional finite element method to simulate the residence time and mixing condition of a kneading block section. The geometric configuration of the kneading block is the same as the one used in this chapter. Therefore its simulation result could provide a theoretical support. It shows that the residence time increases as the kneading angle increases which is the same as the result in Figure 8.3.

Ottino [168] evaluated the deformation of fluid unit and interface stretch ability which is distributive mixing ability based on the laminar flow model. In the initial fluid domain, when an infinitesimal material area |dA| with normal direction $\hat{N}$ is transformed into an area |da| with normal direction $\hat{n}$ at time *t*, the area stretch ratio

of material surface η is defined as follows:

$$\eta = \frac{|da|}{|dA|} \qquad (8\text{-}1)$$

Figure 8.5 shows the arithmetic mean of log η from the entry to the exit. It can be seen that the mean log of the area stretch η increases linearly with increasing axial distance Z, indicating that η increases exponentially with Z. As the kneading angle increases, the area stretch ratio increases, indicating the distributive mixing efficiency increases with increasing kneading angle which is in agreement with the experimental result in this chapter.

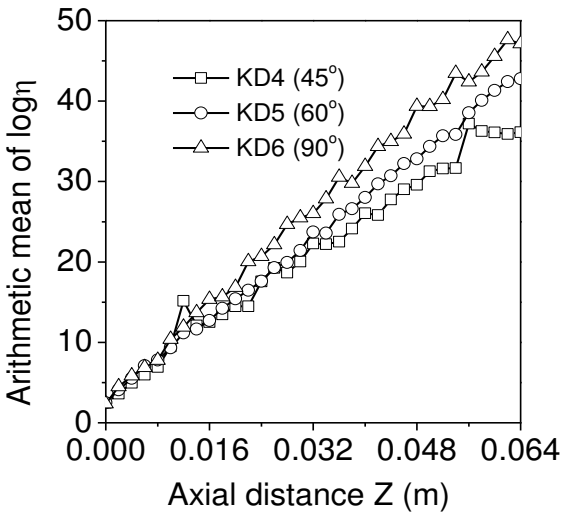

Figure 8.5 Axial evolution of mean log of the area stretch η; Screw speed: 150 rpm, feed rate: 17.8 kg/h. [167]

8.3.2 Effect of kneading block width

The above section discussed the effect of the angle of mixing elements on the reactive polymer blending process when the kneading block length is fixed at 32 mm. Then this section discusses the effect of the kneading block width of a 60° kneading block (22 mm and 32 mm) on the reactive polymer blending process.

Figure 8.6 shows the effect of block width on the emulsification curve (a), RCC-CC curve (b) and effective emulsification curve (c) when the reactive compatibilizer-tracer is added in the tracer port 1. It can be seen from Figure 8.6 (a) that the emulsification curve of 60° kneading block with 22 mm in width is below that

of 60° kneading block with 32 mm in width. This indicates that the dispersed phase domain size of 60° kneading block with 22 mm in width is smaller than that of 60° kneading block with 32 mm in width. The RTD curves of these two kneading blocks superimpose (Figure 8.7), indicating that block width has little influence on the residence time. In other words, the difference in the dispersed phase domain size is not caused by the residence time.

It can be seen from Figure 8.6 (c) that the effective emulsification curves of these two kneading blocks superimpose, indicating that the dispersed phase domain size of 60° kneading block with 22 mm and 32 mm in length is almost the same. In other words, the block width has little influence on the dispersive mixing efficiency. On the other hand, it can be seen from Figure 8.6 (b) that RCC-CC curve of 60° kneading block with 22 mm in length is above that of 60° kneading block with 32 mm in length, indicating the content of the in-situ formed PS-g-PA6-MAMA of 60° kneading block with 22 mm in width is larger than that of 60° kneading block with 32 mm in width. When the kneading block width is decreased from 32 to 22 mm, the number of kneading blocks is increased from 6 to 8.7 at the same time. An increase in distributive mixing efficiency increases the interfacial reaction between PS-TMI-MAMA and PA6, resulting in a decreases in the dispersed phase domain size.

Takeshi [169] investigated the dispersive and distributive mixing efficiency of kneading blocks with different block widths via an infinite element method. In terms of dispersive mixing, the number of particles through the high-shear section and low-shear section increases with increasing block width, indicating that the dispersive mixing efficiency does not increase with decreasing block width. In terms of distributive mixing, as the block width decreases, the area stretch increases, indicating that the distributive mixing efficiency increases.

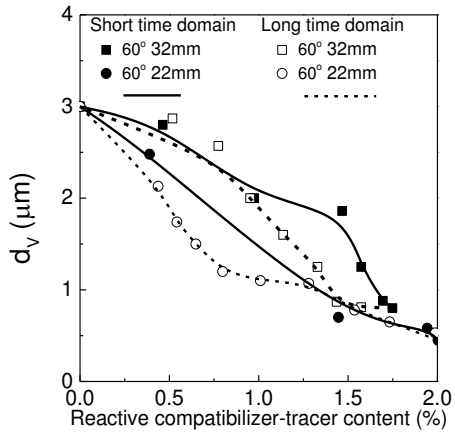

(a)

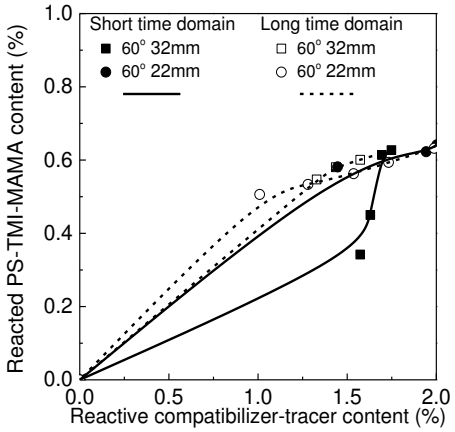

(b)

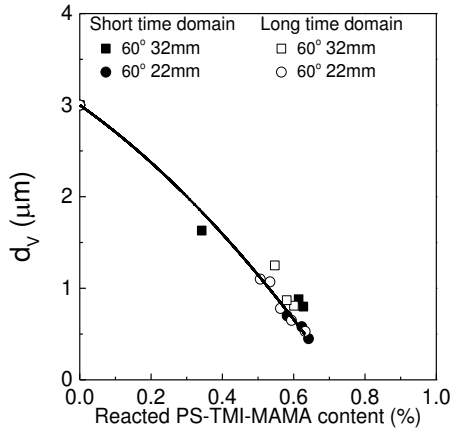

(c)

Figure 8.6 Effect of the kneading block width on the emulsification curve (a), RCC-CC curve (b) and effective emulsification curve (c) when the reactive compatibilizer-tracer is added in tracer port 1.

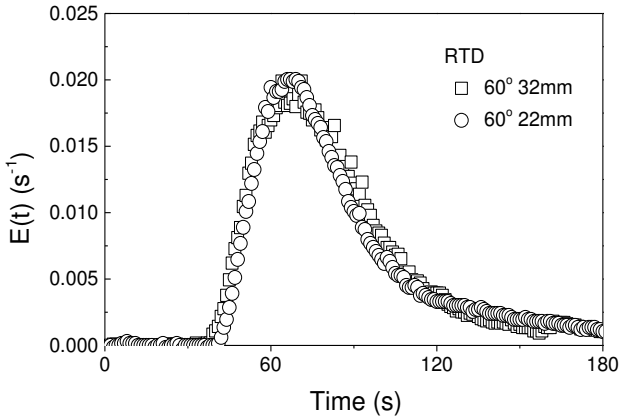

Figure 8.7 Effect of the kneading block width on the RTD curve when the reactive compatibilizer-tracer is added in tracer port 1.

8.3.3 Effect of combined mixing elements

If two 30° kneading blocks of the kneading zone whose mixing efficiency is the lowest are substituted by two 90° gear or reverse 30° kneading blocks, how does the interfacial reaction and morphology evolve? Table 8.1 shows four screw configurations of the kneading zone.

Table 8.1 Four screw configurations of the kneading zone.

	Sequence of mixing elements (From Tracer Port 1 to die exit)
Configutation 1	6×30° Kneading blocks
Configuration 2	1×90° Gear, 2×30° Kneading blocks, 1×90° Gear, 2×30° Kneading blocks
Configuration 3	1×Reverse 30° Kneading block, 2×30° Kneading blocks, 1×Reverse 30° Kneading block, 2×30° Kneading blocks
Configuration 4	6×90° Gears

Figure 8.8 shows the effect of the screw configuration of the kneading zone on the emulsification curve when the reactive compatibilizer-tracer is added in tracer port 1. The order of the dispersed phase domain size vs. reactive compatibilizer-tracer content (Figure 8.8a) follows: configuration 1 > configuration 2 >> configuration 3 ~

configuration 4. Figure 8.8 (b) shows that the content of the reacted PS-TMI-MAMA follows the order: configuration 1 ~ configuration 2 < configuration 3 ~ configuration 4. This order corresponds to that of the distributive mixing efficiency of these screw configurations. Figure 8.8c shows that for a given content of the reacted PS-TMI-MAMA, the dispersed phase domain size follows the order: configuration 1 > configuration 2 > configuration 3 ~ configuration 4. The order of the dispersive mixing efficiency of these screw configurations is exactly the opposite of this order. The above results indicate that an increase in the angle of the mixing element from 30 to 90° has a positive effect on its distributive and dispersive mixing efficiencies. Moreover, a negative angle has a very significant and positive effect on the distributive and dispersive mixing efficiencies of a mixing element. The distributive and dispersive mixing efficiencies of the gears are among the highest.

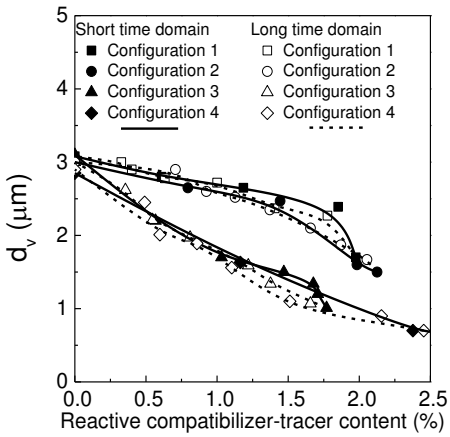

(a)

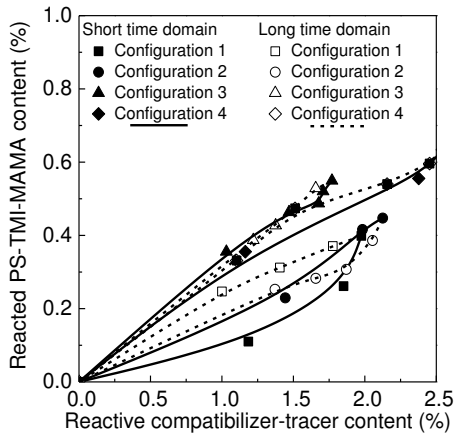

(b)

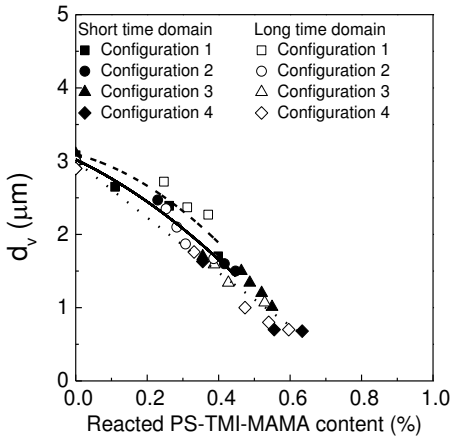

(c)

Figure 8.8 Effect of the sequence of mixing elements on the emulsification curve when the reactive compatibilizer-tracer is added in tracer port 1.

Kalyon and Sangani[170] found similar results based on a thermoplastic elastomer blend. Takeshi[169] also showed that the addition of reverse 60° kneading blocks could increase the dispersive and distributive mixing efficiencies.

Figure 8.9 shows the RTDs of the four screw configurations. The shift of the RTD curve the longer time domain follows the order: configuration 1 > configuration 2 > configuration 3 ~ configuration 4.

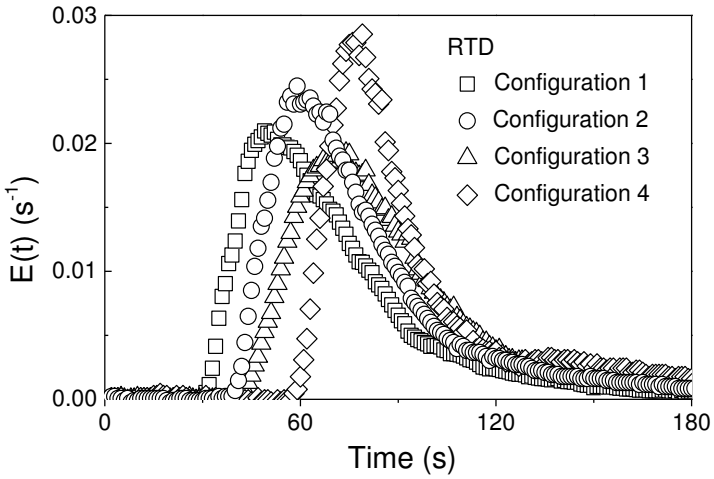

Figure 8.9 Effect of the sequence of mixing elements on the RTD curve when the reactive compatibilizer-tracer is added in tracer port 1.

8.4 Conclusion

This chapter investigates the distributive and dispersive efficiencies of different mixing elements. They are evaluated via RCC-CC (the content of PS-g-PA6-MAMA formed at the interface as a function of the reactive compatibilizer-tracer content) and effective emulsification curve (the dispersed phase domain diameter as a function of the content of PS-g-PA6-MAMA). It indicates that when the angle of mixing elements increases, the distributive and dispersive mixing efficiencies increase, resulting in an increase of interfacial generation and decrease in the dispersed phase domain diameter based on the same amount of PS-g-PA6-MAMA. The distributive mixing efficiency decreases with increasing width of the kneading block while the dispersive mixing

efficiency remains unchanged. When two 30° kneading blocks of a kneading zone are replaced by two 90° gears, the distributive mixing efficiency remains unchanged and the dispersive mixing efficiency increases. When they are replaced by two reverse 30° kneading blocks, the dispersive and distributive mixing efficiencies increase significantly.

Chapter 9 General conclusion and future work

9.1 General conclusion

Reactive polymer blend has become the most common and convenient method to prepare polymer materials with high performance. The interfacial reaction of a reactive polymer blending process has great influence on the morphology of the resulting blend which determines its performance. This thesis aims at addressing how to control the interfacial reaction and morphology of reactive polymer blends.

The first part of the thesis develops the concept of reactive compatibilizer-tracer and applies it to a reactive polymer blending process in a batch mixer. It allows studying the effects of mixing and reactive compatibilizer-tracer structure on the interfacial reaction and morphology.

9-(methylaminomethyl)anthracene (MAMA), a molecule which contains a fluorescent group, is incorporated into a random copolymer of styrene (St) and 3-isopropenyl-α, α'-dimethylbenzene isocyanate (TMI), denoted as PS-TMI, to form a reactive compatibilizer-tracer, denoted as PS-TMI-MAMA. The latter is used both as a reactive compatibilizer and tracer for polystyrene (PS)/polyamide 6 (PA6) blends. The NCO group of PS-TMI-MAMA could react with the terminal amine group of the PA6 to in-situ form a graft copolymer denoted as PS-g-PA6-MAMA which acts as a compatibilizer. On the other hand, MAMA in PS-TMI-MAMA has fluorescent property which allows detecting the amount of the reacted PS-TMI-MAMA via size exclusion chromatography (SEC) with a UV detector.

PS-TMI-MAMA is used as a reactive compatibilizer-tracer for the PS/PA6 (80/20) blend which is processed in a batch mizer. In the initial stage of mixing, the amount of the in-situ formed graft copolymer PS-g-PA6-MAMA rapidly increases and the dispersed phase domain size rapidly decreases. In a later stage of mixing, the amount of the PS-g-PA6-MAMA continues to increase in a lower pace whereas the dispersed phase domain size increases in an abrupt manner and reaches a value which

is close to that without compatibilizer. This is because that in the later stage of mixing, the number of PA6 grafts of the PS-g-PA6-MAMA increases and its thermodynamic stability at the PS/PA6 interfaces deteriorates accordingly. Under mixing, PS-g-PA6-MAMA could be pulled out of the interface to the PA6 phase and form micelles in the PA6 phase. Consequently it loses completely its compatibilizing role, resulting in an abrupt increase in the dispersed phase domain size.

A decrease in the number of PA6 grafts per PS-g-PA6-MAMA increases its interfacial thermodynamic stability. When the reactive copolymer-tracer bears only one terminal reactive group (reactive block compatibilizer-tracer Anhy-PS-Anth), the in-situ formed block copolymer could be thermodynamically more stable at the interface. Therefore the dispersed phase domain size always decreases and ultimately levels off with increasing mixing time, instead of an abrupt increase as it is the case for PS-TMI-MAMA, a multi-functional reactive compatibilizer-tracer.

Mixing has a dual effect on the reactive polymer blending processes. On the one hand, a higher mixing speed promotes the interfacial reaction between PS-TMI-MAMA and PA6 by generating more interfacial area. On the other hand, it helps the reaction between the NCO groups of PS-g-PA6-MAMA and PA6 leading to the increase in the number of PA6 grafts. Therefore the PS-g-PA6-MAMA graft copolymer could be more prone to be pulled out of the interface to the PA6 phase. During annealing, no additional PS-TMI-MAMA participates in the interfacial reaction. However, the NCO groups of the PS-g-PA6-MAMA could continue to react with the PA6. As the annealing time increases, the number of PA6 graft in PS-g-PA6-MAMA increases. Therefore annealing deteriorates the interfacial thermodynamic stability. This is why once mixing is resumed, a sharp increase in the dispersed phase domain size is observed.

When the PS/PA6 composition is 20/80, in the presence of PS-TMI-MAMA the dispersed phase domain size decreases with mixing time and then levels off, which is very different from the PS/PA6 (80/20) blend described above. This is because PS-g-PA6-MAMA could still be pulled out of the interface to the PA6 phase and form micelles in the later stage of mixing. However, the PA6 phase is now the matrix not

the dispersed phase. These micelles in the matrix could prevent the dispersed phase domains from coalescing.

The second part of this thesis deals with the reactive blending process in a twin screw extruder. More specifically, the use of the concept of reactive compatibilizer-tracer together with the concept of residence time distribution allows detecting the evolution of the interfacial reaction and morphology of PS/PA6/PS-TMI-MAMA reactive blend in the twin screw extruder with a small amount of reactive compatibilizer-tracer. It provides a powerful tool to assess the evolutions of the reactive compatibilizer-tracer content, the dispersed phase domain diameter, and the amount of the in situ formed graft copolymer, respectively, as a function of the residence time in a twin-screw extruder. Based on that the emulsification curve, the RCC-CC curve (the content of the in situ formed graft copolymer as a function of compatibilizer-tracer concentration) and effective emulsification curve (the dispersed phase domain size as a function of the content of the in situ formed graft copolymer) could also be obtained. Then the relationship between molecular architecture of reactive compatibilizer-tracer and compatibilizing efficiency, the effects of the processing parameters on the interfacial reaction and morphology and the dispersive and distributive mixing efficiency of mixing elements are investigated. The main results are summarized below:

(1) When the molar mass of reactive compatibilizer is fixed, increasing reactive group content has no influence on the interfacial reaction but decreases the dispersed phase domain size. When the reactive group content is fixed, increasing molar mass decreases the interfacial reaction rate, resulting in the decrease in the amount of the in-situ formed graft copolymer and increases in the dispersed phase domain size. However, when the amount in-situ formed graft copolymer is the same, the dispersed phase domain size of the blend system with PS-TMI-MAMA of different molar mass is the same. The molar mass influences the interfacial reaction rate but not affect the compatibilizing efficiency. The compatibilzing efficiency of graft reactive compatibilizer-tracer PS-TMI-MAMA5 is higher than block reactive compatibilizer-tracer Anhy-PS-Anth.

(2) When throughput (Q) and screw speed (N) is fixed, the RTD curves of different Q and N are different, however, the dimensionless residence time distribution curves superimpose to one curve and the degree of fill is the same. As the screw speed increases, the residence time and the degree of fill decrease, leading to the decrease in the amount of in-situ formed graft copolymer PS-g-PA6-MAMA and then the increase in the dispersed phase domain size. As the throughput decreases, the residence time increases but the degree of fill decreases which leads to the shear force applied on the polymer blend decreases. Then the amount of PS-g-PA6-MAMA decreases and the dispersed phase domain size increases. The throughput and screw speed have an influence on the reactive polymer blending processes through the degree of fill and residence time. The effect of degree of fill is more dominant than that of residence time. When the degree of fill is low, the shear intensity is weak leading to the low interfacial reaction and compatibilizing efficiency even though there is enough residence time.

(3) RCC-CC curve and effective emulsification curve are used to evaluate the distributive and dispersive mixing efficiency. It indicates that when the kneading angle of kneading blocks increases, the distributive and dispersive mixing efficiencies increase, resulting in an increase in the interfacial generation and a decrease in the dispersed phase domain size based on the same amount of in-situ formed PS-g-PA6-MAMA. As the width of kneading block decreases, the distributive mixing efficiency increases and the dispersive mixing efficiency remains unchanged. When two 30° kneading blocks are replaced by two reverse 30° kneading blocks, the dispersive and distributive mixing efficiencies increase significantly.

9.2 Future work

The thesis uses the reactive compatibilizer-tracer together with concept of residence time distribution to establish the measurement method of interfacial reaction and morphology of reactive polymer blending process. Based on that, the effect of molecular architecture, processing parameters and flow field are investigated. There are many research aspects could continue and develop:

(1) It is very difficult to investigate the interfacial reaction kinetics because the flow fields in a batch mixer and in twin screw extruder are very complex. It would be interesting to use a rheometer to investigate the interfacial reaction kinetics under a well-defined flow field.

(2) In this thesis work, the residence time distribution of the reactive compatibilizer-tracer in the twin screw extruder was measured by an in-line fluorescent measurement device. In-line small angle scattering and near infrared devices could also be installed on the twin screw extruder to monitor the morphology and interfacial reaction in real time.

(3) In this thesis work, the dispersive and distributive mixing efficiencies of different mixing elements were characterized experimentally. It would be interesting to develop mathematical models and validate them with the experimental data.

References

[1] Edgecombe, B. D., Stein, J. A., Fréchet, J. M., Xu, Z., Kramer, E. J. The role of polymer architecture in strengthening polymer-polymer interfaces: a comparison of graft, block, and random copolymers containing hydrogen-bonding moieties. Macromolecules, 1998. 31(4): 1292-1304.

[2] Hong, B. K., Jo, W. H. Effects of molar mass of SEBS triblock copolymer on the morphology, impact strength, and rheological property of syndiotactic polystyrene/ethylene-propylene rubber blends. Polymer, 2000. 41(6): 2069-2079.

[3] Feng, H., Ye, C., Tian, J., Feng, Z., Huang, B. Compatibilization effect of graft copolymer on immiscible polymer blends: 1. LLDPE/SBS/LLDPE-g-PS systems. Polymer, 1998. 39(10): 1787-1792.

[4] Baker, W. E., Scott, C. E., Hu, G. H. Reactive polymer blending. Hanser Verlag, 2001.

[5] Xanthos, M., Dagli, S. S. Compatibilization of polymer blends by reactive processing. Polymer Engineering & Science, 1991. 31(13): 929-935.

[6] Triacca, V. J., Ziaee, S., Barlow, J. W., Keskkula, H., Paul, D. R. Reactive compatibilization of blends of nylon 6 and ABS materials. Polymer, 1991. 32(8): 1401-1413.

[7] Kim, S., Shin, B., Hong, J., Cho, W., Ha, C. Reactive compatibilization of the PBT/EVA blend by maleic anhydride. Polymer, 2001. 42(9): 4073-4080.

[8] Koulouri, E. G., Georgaki, A. X., Kallitsis, J. K. Reactive compatibilization of aliphatic polyamides with functionalized polyethylenes. Polymer, 1997. 38(16): 4185-4192.

[9] Park, I., Barlow, J. W., Paul, D. R. The in situ reactive compatibilization of nylon−6/polystyrene blends using anhydride functionalized polystyrenes. Journal of Polymer Science Part B: Polymer Physics, 1992. 30(9): 1021-1033.

[10] Manas-Zloczower, I. Mixing and compounding of polymers: theory and practice. Hanser Verlag, 2009.

[11] Utracki, L. A., Favis, B. D. Polymer alloys and blends. Marcel Dekker: New York, 1989.

[12] Lepers, J. C., Favis, B. D. Interfacial tension reduction and coalescence suppression in compatibilized polymer blends. AIChE Journal, 1999. 45(4): 887-895.

[13] Li, H., Hu, G. H. The early stage of the morphology development of immiscible polymer blends during melt blending: compatibilized vs. uncompatibilized blends. Journal of Polymer Science Part B: Polymer Physics, 2001. 39(5): 601-610.

[14] Lin, B., Sundararai, U., Mighri, F., Huneault, M. A. Effect of pre-made compatibilizer and reactive polymers on polymer drop breakup. Society of Plastics Engineers, 2004. 1: 350-354.

[15] Gao, C., Zhang, S., Li, X., Zhu, S., Jiang, Z. Synthesis of poly (ether ether ketone)-block-polyimide copolymer and its compatibilization for poly (ether ether ketone)/thermoplastic polyimide blends. Polymer, 2014. 55(1): 119-125.

[16] Xu, Y., Thurber, C. M., Lodge, T. P., Hillmyer, M. A. Synthesis and remarkable efficacy of model polyethylene-graft-poly (methyl methacrylate) copolymers as compatibilizers in polyethylene/poly (methyl methacrylate) blends. Macromolecules, 2012. 45(24): 9604-9610.

[17] Xu, Y., Thurber, C. M., Macosko, C. W., Lodge, T. P., Hillmyer, M. A. Poly (methyl methacrylate)-block-polyethylene-block-poly (methyl methacrylate) triblock copolymers as compatibilizers for polyethylene/poly (methyl methacrylate) blends. Industrial & Engineering Chemistry Research, 2014. 53(12): 4718-4725.

[18] López-Barrón, C. R., Macosko, C. W. Rheology of compatibilized immiscible blends with droplet-matrix and cocontinuous morphologies during coarsening. Journal of Rheology, 2014. 58(6): 1935-1953.

[19] Matos, M., Favis, B. D., Lomellini, P. Interfacial modification of polymer blends-the emulsification curve: 1. Influence of molar mass and chemical composition of the interfacial modifier. Polymer, 1995. 36(20): 3899-3907.

[20] Cigana, P., Favis, B. D., Jérôme, R. Diblock copolymers as emulsifying agents in polymer blends: influence of molar mass, architecture, and chemical composition. Journal of Polymer Science Part B: Polymer Physics, 1996. 34(9): 1691-1700.

[21] Modesti, M., Lorenzetti, A., Bon, D., Besco, S. Effect of processing conditions on morphology and mechanical properties of compatibilized polypropylene nanocomposites. Polymer, 2005. 46(23): 10237-10245.

[22] Gadekar, R., Kulkarni, A., Jog, J. P. Blends of nylon with polyethylene: effect of compatibilization on mechanical and dynamic mechanical properties. Journal of Applied Polymer Science, 1998. 69(1): 161-168.

[23] Chen, C. C., White, J. L. Compatibilizing agents in polymer blends: interfacial tension, phase morphology, and mechanical properties. Polymer Engineering &

Science, 1993. 33(14): 923-930.
[24] Sathe, S. N., Devi, S., Rao, G. S., Rao, K. V. Relationship between morphology and mechanical properties of binary and compatibilized ternary blends of polypropylene and nylon 6. Journal of Applied Polymer Science, 1996. 61(1): 97-107.
[25] Palabiyik, M., Bahadur, S. Mechanical and tribological properties of polyamide 6 and high density polyethylene polyblends with and without compatibilizer. Wear, 2000. 246(1): 149-158.
[26] Huneault, M. A., Li, H. Morphology and properties of compatibilized polylactide/thermoplastic starch blends. Polymer, 2007. 48(1): 270-280.
[27] Liang, Z., Williams, H. L. Dynamic mechanical properties of polypropylene-polyamide blends: effect of compatibilization. Journal of Applied Polymer Science, 1992. 44(4): 699-717.
[28] Jang, S. P., Kim, D. Thermal, mechanical, and diffusional properties of nylon 6/ABS polymer blends: compatibilizer effect. Polymer Engineering & Science, 2000. 40(7): 1635-1642.
[29] Holsti Miettinen, R., Seppälä, J., Ikkala, O. T. Effects of compatibilizers on the properties of polyamide/polypropylene blends. Polymer Engineering & Science, 1992. 32(13): 868-877.
[30] Kim, J. K., Kim, S., Park, C. E. Compatibilization mechanism of polymer blends with an in-situ compatibilizer. Polymer, 1997. 38(9): 2155-2164.
[31] Kim, K. J., Cho, H. W., Yoon, K. J. Effect of P(MMA-co-MAA) compatibilizer on the miscibility of nylon 6/PVDF blends. European Polymer Journal, 2003. 39(6): 1249-1265.
[32] Argoud, A., Trouillet-Fonti, L., Ceccia, S., Sotta, P. Morphologies in polyamide 6/high density polyethylene blends with high amounts of reactive compatibilizer. European Polymer Journal, 2014. 50: 177-189.
[33] Entezam, M., Khonakdar, H. A., Yousefi, A. A., Jafari, S. H., Wagenknecht, U., Heinrich, G., Kretzschmar, B. Influence of interfacial activity and micelle formation on rheological behavior and microstructure of reactively compatibilized PP/PET blends. Macromolecular Materials and Engineering, 2012. 297(4): 312-328.
[34] Thurber, C. M., Xu, Y., Myers, J. C., Lodge, T. P., Macosko, C. W. Accelerating reactive compatibilization of PE/PLA blends by an interfacially localized catalyst. ACS Macro Letters, 2014. 4(1): 30-33.
[35] Xu, Y., Loi, J., Delgado, P., Topolkaraev, V., Mceneany, R. J., Macosko, C. W.,

Hillmyer, M. A. Reactive compatibilization of polylactide/polypropylene blends. Industrial & Engineering Chemistry Research, 2015. 54(23): 6108-6114.

[36] Fleischer, C. A., Morales, A. R., Koberstein, J. T. Interfacial modification through end group complexation in polymer blends. Macromolecules, 1994. 27(2): 379-385.

[37] Yu, Q. Y., Zhang, C. L., Gu, X. P., Wang, J. J., Feng, L. F. Compatibilizing efficiency of copolymer precursors for immiscible polymer blends. Journal of Applied Polymer Science, 2012. 124(4): 3392-3398.

[38] 俞奇勇.嵌段反应聚合物Anhy-PS-Br/Anhy-PS-Anth的合成与相容特性.浙江大学. 2011.

[39] Dagli, S. S., Xanthos, M., Biesenberger, J. A. Kinetic studies and process analysis of the reactive compatibilization of nylon 6/polypropylene blends. Polymer Engineering & Science, 1994. 34(23): 1720-1730.

[40] Tsou, A. H., Favis, B. D., Hara, Y., Bhadane, P. A., Kirino, Y. Reactive compatibilization in brominated poly (isobutylene-co-p-methylstyrene) and polyamide blends. Macromolecular Chemistry and Physics, 2009. 210(5): 340-348.

[41] Sundararaj, U., Macosko, C. W., Nakayama, A., Inoue, T. Milligrams to kilograms: an evaluation of mixers for reactive polymer blending. Polymer Engineering & Science, 1995. 35(1): 100-114.

[42] Li, H., Sundararaj, U. Morphology development of polymer blends in extruder: the effects of compatibilization and rotation rate. Macromolecular Chemistry and Physics, 2009. 210(10): 852-863.

[43] Huang, C., Yu, W. Role of block copolymer on the coarsening of morphology in polymer blend: effect of micelles. AIChE Journal, 2015. 61(1): 285-295.

[44] Li, Y., Shimizu, H. Compatibilization by homopolymer: significant improvements in the modulus and tensile strength of PPC/PMMA blends by the addition of a small amount of pvac. ACS Applied Materials & Interfaces, 2009. 1(8): 1650-1655.

[45] Charoensirisomboon, P., Weber, M. Reactive PSU/PA blends: comparison of materials prepared by mini-twin screw extruder and batch mixer. Polymer, 2001. 42(16): 7009-7016.

[46] Charoensirisomboon, P., Chiba, T., Solomko, S. I., Inoue, T., Weber, M. Reactive blending of polysulfone with polyamide: a difference in interfacial behavior

between in situ formed block and graft copolymers. Polymer, 1999. 40(24): 6803-6810.

[47] Kitayama, N., Keskkula, H., Paul, D. R. Reactive compatibilization of nylon 6/styrene–acrylonitrile copolymer blends. Part 1. Phase inversion behavior. Polymer, 2000. 41(22): 8041-8052.

[48] Kitayama, N., Keskkula, H., Paul, D. R. Reactive compatibilization of nylon 6/styrene-acrylonitrile copolymer blends. Part 2. Dispersed phase particle size. Polymer, 2000. 41(22): 8053-8060.

[49] Liu, N. C., Xie, H. Q., Baker, W. E. Comparison of the effectiveness of different basic functional groups for the reactive compatibilization of polymer blends. Polymer, 1993. 34(22): 4680-4687.

[50] Majumdar, B., Paul, D. R., Oshinski, A. J. Evolution of morphology in compatibilized vs uncompatibilized polyamide blends. Polymer, 1997. 38(8): 1787-1808.

[51] Saleem, M., Baker, W. E. In situ reactive compatibilization in polymer blends: effects of functional group concentrations. Journal of Applied Polymer Science, 1990. 39(3): 655-678.

[52] Dedecker, K., Groeninckx, G. Reactive compatibilisation of A/(B/C) polymer blends. Part 1. Investigation of the phase morphology development and stabilisation. Polymer, 1998. 39(21): 4985-4992.

[53] Dedecker, K., Groeninckx, G. Reactive compatibilisation of A/(B/C) polymer blends. Part 2. Analysis of the phase inversion region and the co-continuous phase morphology. Polymer, 1998. 39(21): 4993-5000.

[54] Dedecker, K., Groeninckx, G., Inoue, T. Reactive compatibilization of A/(B/C) polymer blends. Part 3. Quantitative analysis of the interfacial thickness and the interfacial reaction. Polymer, 1998. 39(21): 5001-5010.

[55] Willemse, R. C., De Boer, A. P., Van Dam, J., Gotsis, A. D. Co-continuous morphologies in polymer blends: the influence of the interfacial tension. Polymer, 1999. 40(4): 827-834.

[56] Bhadane, P. A., Champagne, M. F., Huneault, M. A., Tofan, F., Favis, B. D. Erosion-dependant continuity development in high viscosity ratio blends of very low interfacial tension. Journal of Polymer Science Part B: Polymer Physics, 2006. 44(14): 1919-1929.

[57] Bhadane, P. A., Champagne, M. F., Huneault, M. A., Tofan, F., Favis, B. D.

Continuity development in polymer blends of very low interfacial tension. Polymer, 2006. 47(8): 2760-2771.

[58] Li, J., Ma, P. L., Favis, B. D. The role of the blend interface type on morphology in cocontinuous polymer blends. Macromolecules, 2002. 35(6): 2005-2016.

[59] Ottino, J. M., Deroussel, P., Hansen, S., Khakhar, D. V. Mixing and dispersion of viscous liquids and powdered solids. Advances in Chemical Engineering, 1999. 25: 105-205.

[60] Scott, C. E., Macosko, C. W. Morphology development during reactive and non-reactive blending of an ethylene-propylene rubber with two thermoplastic matrices. Polymer, 1994. 35(25): 5422-5433.

[61] Scott, C. E., Macosko, C. W. Morphology development during the initial stages of polymer-polymer blending. Polymer, 1995. 36(3): 461-470.

[62] Lee, J. K., Han, C. D. Evolution of polymer blend morphology during compounding in a twin-screw extruder. Polymer, 2000. 41(5): 1799-1815.

[63] Lindt, J. T., Ghosh, A. K. Fluid mechanics of the formation of polymer blends. Part I: formation of lamellar structures. Polymer Engineering & Science, 1992. 32(24): 1802-1813.

[64] Sundararaj, U., Dori, Y., Macosko, C. W. Sheet formation in immiscible polymer blends: model experiments on initial blend morphology. Polymer, 1995. 36(10): 1957-1968.

[65] Willemse, R. C., Ramaker, E., Van Dam, J., De Boer, A. P. Morphology development in immiscible polymer blends: initial blend morphology and phase dimensions. Polymer, 1999. 40(24): 6651-6659.

[66] Tomotika, S. On the instability of a cylindrical thread of a viscous liquid surrounded by another viscous fluid Proceedings of the Royal Society of London. Series A, Containing Papers of a Mathematical and Physical Character, 1935, 150(870): 322-337.

[67] Hu, G. H., Feng, L. F. Extruder processing for nanoblends and nanocomposites. Macromolecular Symposia, 2003. 195(1): 303-308.

[68] Taylor, G. I. The viscosity of a fluid containing small drops of another fluid. Proceedings of the Royal Society of London. Series A, Containing Papers of a Mathematical and Physical Character, 1932. 138(834): 41-48.

[69] Taylor, G. I. The formation of emulsions in definable fields of flow. Proceedings of the Royal Society of London. Series A, Containing Papers of a Mathematical and

Physical Character, 1934. 146(858): 501-523.
[70] Wu, S. Formation of dispersed phase in incompatible polymer blends: interfacial and rheological effects. Polymer Engineering & Science, 1987. 27(5): 335-343.
[71] Roland, C. M., Böuhm, G. Shear-induced coalescence in two-phase polymeric systems. I. Determination from small-angle neutron scattering measurements. Journal of Polymer Science: Polymer Physics Edition, 1984. 22(1): 79-93.
[72] Allan, R. S., Mason, S. G. Particle motions in sheared suspensions. XIV. Coalescence of liquid drops in electric and shear fields. Journal of Colloid Science, 1962. 17(4): 383-408.
[73] Sundararaj, U., Macosko, C. W. Drop breakup and coalescence in polymer blends: the effects of concentration and compatibilization. Macromolecules, 1995. 28(8): 2647-2657.
[74] Elmendorp, J. J., Van der Vegt, A. K. A study on polymer blending microrheology: Part IV. The influence of coalescence on blend morphology origination. Polymer Engineering & Science, 1986. 26(19): 1332-1338.
[75] Lu, Q. W., Macosko, C. W., Horrion, J. Compatibilized blends of thermoplastic polyurethane (TPU) and polypropylene. Macromolecular Symposia, 2003. 198(1): 221-232.
[76] Lu, Q., Macosko, C. W. Comparing the compatibility of various functionalized polypropylenes with thermoplastic polyurethane (TPU). Polymer, 2004. 45(6): 1981-1991.
[77] Liu, N. C., Baker, W. E. Basic functionalization of polypropylene and the role of interfacial chemical bonding in its toughening. Polymer, 1994. 35(5): 988-994.
[78] Leibler, L. Emulsifying effects of block copolymers in incompatible polymer blend. Macromolecular Symposia, 1988, 16(1): 1-17.
[79] Vilgis, T. A., Noolandi, J. Theory of homopolymer-block copolymer blends. The search for a universal compatibilizer. Macromolecules, 1990. 23(11): 2941-2947.
[80] Dan, N., Tirrell, M. Diblock copolymer microemulsions. A scaling model. Macromolecules, 1993. 26(4): 637-642.
[81] Anastasiadis, S. H., Gancarz, I., Koberstein, J. T. Compatibilizing effect of block copolymers added to the polymer/polymer interface. Macromolecules, 1989. 22(3): 1449-1453.
[82] Wagner, M., Wolf, B. A. Effect of block copolymers on the interfacial tension between two ‘immiscible’ homopolymers. Polymer, 1993. 34(7): 1460-1464.

[83] Lyu, S., Jones, T. D., Bates, F. S., Macosko, C. W. Role of block copolymers on suppression of droplet coalescence. Macromolecules, 2002. 35(20): 7845-7855.

[84] Milner, S. T., Xi, H. How copolymers promote mixing of immiscible homopolymers. Journal of Rheology, 1996. 40(4): 663-687.

[85] Meijer, H., Lemstra, P. J., Elemans, P. Structured polymer blends. Macromolecular Symposia, 1988. 16(1): 113-135.

[86] White, J. L., Min, K. Development of polymer blend phase morphology during processing. Macromolecular Symposia, 1988, 16(1): 19-39.

[87] Jeon, H. K., Kim, J. K. The effect of the amount of in situ formed copolymers on the final morphology of reactive polymer blends with an in situ compatibilizer. Macromolecules, 1998. 31(26): 9273-9280.

[88] Macosko, C. W., Jeon, H. K., Hoye, T. R. Reactions at polymer-polymer interfaces for blend compatibilization. Progress in Polymer Science, 2005. 30(8): 939-947.

[89] Orr, C. A., Cernohous, J. J., Guegan, P., Hirao, A., Jeon, H. K., Macosko, C. W. Homogeneous reactive coupling of terminally functional polymers. Polymer, 2001. 42(19): 8171-8178.

[90] Tan, N. B., Tai, S., Briber, R. M. Morphology control and interfacial reinforcement in reactive polystyrene/amorphous polyamide blends. Polymer, 1996. 37(16): 3509-3519.

[91] Dedecker, K., Groeninckx, G. Interfacial graft copolymer formation during reactive melt blending of polyamide 6 and styrene-maleic anhydride copolymers. Macromolecules, 1999. 32(8): 2472-2479.

[92] Jeon, H. K., Kim, J. K. Effect of reaction rate on morphological change of reactive blends. Macromolecules, 2000. 33(22): 8200-8210.

[93] Jeon, H. K., Zhang, J., Macosko, C. W. Premade vs. reactively formed compatibilizers for PMMA/PS melt blends. Polymer, 2005. 46(26): 12422-12429.

[94] Jeon, H. K., Feist, B. J., Koh, S. B., Chang, K., Macosko, C. W., Dion, R. P. Reactively formed block and graft copolymers as compatibilizers for polyamide 66/PS blends. Polymer, 2004. 45(1): 197-206.

[95] Yquel, V., Machado, A. V., Covas, J. A., Flat, J. J. Contribution of the melting stage to the evolution of the morphology and chemical conversion of immiscible polyamide/polyethylene blends in twin-screw extruders. Journal of Applied Polymer Science, 2009. 114(3): 1768-1776.

[96] Kim, H. Y., Ryu, D. Y., Jeong, U., Kho, D. H., Kim, J. K. The effect of chain architecture of in situ formed copolymers on interfacial morphology of reactive polymer blends. Macromolecular Rapid Communications, 2005. 26(17): 1428-1433.

[97] Canto, L. B., Hage, E., Pessan, L. A. Effects of the molecular architecture of impact modifier and compatibilizer on the toughening of PBT/SBS/PS-GMA blends. Journal of Applied Polymer Science, 2006. 102(6): 5795-5807.

[98] Kudva, R. A., Keskkula, H., Paul, D. R. Properties of compatibilized nylon 6/ABS blends: Part II. Effects of compatibilizer type and processing history. Polymer, 2000. 41(1): 239-258.

[99] Filippi, S., Chiono, V., Polacco, G., Paci, M., Minkova, L. I., Magagnini, P. Reactive compatibilizer precursors for LDPE/pa66 blends, 1. Ethylene/acrylic acid copolymers. Macromolecular Chemistry and Physics, 2002. 203(10-11): 1512-1525.

[100] Guégan, P., Macosko, C. W., Ishizone, T., Hirao, A., Nakahama, S. Kinetics of chain coupling at melt interfaces. Macromolecules, 1994. 27(18): 4993-4997.

[101] Kim, S., Kim, J. K., Park, C. E. Effect of molecular architecture of in situ reactive compatibilizer on the morphology and interfacial activity of an immiscible polyolefin/polystyrene blend. Polymer, 1997. 38(8): 1809-1815.

[102] Chen, L. F., Wong, B., Baker, W. E. Melt grafting of glycidyl methacrylate onto polypropylene and reactive compatibilization of rubber toughened polypropylene. Polymer Engineering & Science, 1996. 36(12): 1594-1607.

[103] Yin, Z., Koulic, C., Jeon, H. K., Pagnoulle, C., Macosko, C. W., Jérôme, R. Effect of molar mass of the reactive precursors in melt reactive blending. Macromolecules, 2002. 35(24): 8917-8919.

[104] Godshall, D., White, C., Wilkes, G. L. Effect of compatibilizer molar mass and maleic anhydride content on interfacial adhesion of polypropylene-PA6 bicomponent fibers. Journal of Applied Polymer Science, 2001. 80(2): 130-141.

[105] Broseta, D., Fredrickson, G. H., Helfand, E., Leibler, L. Molar mass and polydispersity effects at polymer-polymer interfaces. Macromolecules, 1990. 23(1): 132-139.

[106] Helfand, E. Theory of inhomogeneous polymers: fundamentals of the gaussian random-walk model. The Journal of Chemical Physics, 1975. 62(3): 999-1005.

[107] Helfand, E., Sapse, A. M. Theory of unsymmetric polymer-polymer interfaces. The Journal of Chemical Physics, 1975. 62(4): 1327-1331.

[108] Kressler, J., Higashida, N., Shimomai, K., Inoue, T., Ougizawa, T. Temperature

dependence of the interaction parameter between polystyrene and poly (methyl methacrylate). Macromolecules, 1994. 27(9): 2448-2453.

[109] Kumar, S. K. Chemical potentials of polymer blends from Monte Carlo simulations: consequences on SANS-determined. chi. Parameters. Macromolecules, 1994. 27(1): 260-271.

[110] Reiter, J., Zifferer, G., Olaj, O. F. Monte Carlo studies of the interface between two polymer melts. Macromolecules, 1990. 23(1): 224-228.

[111] Nakayama, A., Inoue, T., Guégan, P., Macosko, C. W. Compatibilizers for melt blending: Premade vs. reactively formed block copolymers. Polymer Preprints, 1993. 34(2): 840-841.

[112] Pagnoulle, C., Jérôme, R. Reactive compatibilization of SAN/EPR blends. 2. Effect of type and content of reactive groups randomly attached to SAN. Macromolecules, 2001. 34(4): 965-975.

[113] Martin, P., Gallez, C., Devaux, J., Legras, R., Leemans, L., van Gurp, M., van Duin, M. Reactive compatibilization of blends of polybutyleneterephthalate with epoxide-containing rubber. The effect of the concentrations in reactive functions. Polymer, 2003. 44(18): 5251-5262.

[114] Chang, H., Wu, J., Chang, F. Reactive compatibilization of ABS/nylon 6, 6 blends: effects of reactive group concentration and blending sequence. Journal of Polymer Research, 1994. 1(3): 235-245.

[115] Cigana, P., Favis, B. D. The relative efficacy of diblock and triblock copolymers for a polystyrene/ethylene-propylene rubber interface. Polymer, 1998. 39(15): 3373-3378.

[116] Zhang, C. L., Zhang, T., Feng, L. F. In situ control of co-continuous phase morphology for PS/PS-co-TMI/PA6 blend. Journal of Applied Polymer Science, 2014. 131(6): 39972(1-7).

[117] Hu, G. H., Sun, Y. J., Lambla, M. Effects of processing parameters on the in situ compatibilization of polypropylene and poly (butylene terephthalate) blends by one-step reactive extrusion. Journal of applied polymer science, 1996. 61(6): 1039-1047.

[118] Hu, G. H., Kadri, I. Modeling reactive blending: An experimental approach. Journal of Polymer Science Part B: Polymer Physics, 1998. 36(12): 2153-2163.

[119] Maréchal, P., Coppens, G., Legras, R., Dekoninck, J. M. Amine/anhydride reaction versus amide/anhydride reaction in polyamide/anhydride carriers. Journal of

Polymer Science Part A: Polymer Chemistry, 1995. 33(5): 757-766.

[120] Callis, J. B., Illman, D. L., Kowalski, B. R. Process analytical chemistry. Analytical Chemistry, 1987. 59(9): 624A-637A.

[121] Coates, P. D., Barnes, S. E., Sibley, M. G., Brown, E. C., Edwards, H. G., Scowen, I. J. In-process vibrational spectroscopy and ultrasound measurements in polymer melt extrusion. Polymer, 2003. 44(19): 5937-5949.

[122] Dumoulin, M. M., Gendron, R., Cole, K. C. Techniques for real-time monitoring of polymer processing. Trends in Polymer Science, 1996. 4(4): 109-114.

[123] Alig, I., Steinhoff, B., Lellinger, D. Monitoring of polymer melt processing. Measurement Science and Technology, 2010. 21(6): 62001.

[124] Barnes, S. E., Brown, E. C., Sibley, M. G., Edwards, H., Scowen, I. J., Coates, P. D. Vibrational spectroscopic and ultrasound analysis for in-process characterization of high-density polyethylene/polypropylene blends during melt extrusion. Applied Spectroscopy, 2005. 59(5): 611-619.

[125] Bridge, B., Cheng, K. H. On-line ultrasonic monitoring of the extrusion of $CaCO_3$-filled polypropylene. Journal of Materials Science Letters, 1987. 6(2): 219-222.

[126] Françla, D. R., Jen, C. K., Nguyen, K. T., Gendron, R. Ultrasonic in-line monitoring of polymer extrusion. Polymer Engineering & Science, 2000. 40(1): 82-94.

[127] Tatibouet, J., Huneault, M. A. In-line ultrasonic monitoring of filler dispersion during extrusion. International Polymer Processing, 2002. 17(1): 49-52.

[128] Wang, D., Min, K. In-line monitoring and analysis of polymer melting behavior in an intermeshing counter-rotating twin-screw extruder by ultrasound waves. Polymer Engineering & Science, 2005. 45(7): 998-1010.

[129] Alig, I., Lellinger, D., Engel, M., Skipa, T., Pötschke, P. Destruction and formation of a conductive carbon nanotube network in polymer melts: In-line experiments. Polymer, 2008. 49(7): 1902-1909.

[130] Alig, I., Lellinger, D., Dudkin, S. M., Pötschke, P. Conductivity spectroscopy on melt processed polypropylene-multiwalled carbon nanotube composites: Recovery after shear and crystallization. Polymer, 2007. 48(4): 1020-1029.

[131] Hansen, M. G., Khettry, A. In-line monitoring of molten polymers: near infrared spectroscopy, robust probes, and rapid data analysis. Polymer Engineering & Science, 1994. 34(23): 1758-1766.

[132] Khettry, A., Hansen, M. G. Real-time analysis of ethylene vinyl acetate random copolymers using near infrared spectroscopy during extrusion. Polymer Engineering & Science, 1996. 36(9): 1232-1243.

[133] Reshadat, R., Desa, S., Joseph, S., Mehra, M., Stoev, N., Balke, S. T. In-line near-infrared monitoring of polymer processing. Part I: Process/monitor interface development. Applied Spectroscopy, 1999. 53(11): 1412-1418.

[134] Rohe, T., Becker, W., Krey, A., Nägele, H., Kölle, S., Eisenreich, N. In-line monitoring of polymer extrusion processes by NIR spectroscopy. Journal of Near Infrared Spectroscopy, 1998. 6(1): 325-332.

[135] Deshpande, B. J., Dhamdhere, M. S., Li, J., Hansen, M. G. In-line fiber-optic Raman spectroscopy: Simultaneous monitoring of composition and rheological properties in poly (ethylene vinyl acetate) copolymers. Technical Papers of The Annual Technical Conference-Society of Plastics Engineers Incorporated. 1998, 2: 1672-1675.

[136] Tumuluri, V. S., Kemper, M. S., Lewis, I. R., Prodduturi, S., Majumdar, S., Avery, B. A., & Repka, M. A. Off-line and on-line measurements of drug-loaded hot-melt extruded films using Raman spectroscopy. International Journal of Pharmaceutics, 2008. 357(1): 77-84.

[137] Melo, T. J. A., Canevarolo, S. V. In-line optical detection in the transient state of extrusion polymer blending and reactive processing. Polymer Engineering & Science, 2005. 45(1): 11-19.

[138] Barnes, S. E., Sibley, M. G., Edwards, H., Coates, P. D. Process monitoring of polymer melts using in-line spectroscopy. Transactions of the Institute of Measurement and Control, 2007. 29(5): 453-465.

[139] Wang, Y., Steinhoff, B., Brinkmann, C., Alig, I. In-line monitoring of the thermal degradation of poly (l-lactic acid) during melt extrusion by UV-vis spectroscopy. Polymer, 2008. 49(5): 1257-1265.

[140] Bur, A. J., Roth, S. C., Thomas, C. L. Fluorescence anisotropy sensor and its application to polymer processing and characterization. Review of Scientific Instruments, 2000. 71(3): 1516-1523.

[141] Cherdhirankorn, T., Harmandaris, V., Juhari, A., Voudouris, P., Fytas, G., Kremer, K., Koynov, K. Fluorescence correlation spectroscopy study of molecular probe diffusion in polymer melts. Macromolecules, 2009. 42(13): 4858-4866.

[142] Bur, A. J., Gallant, F. M. Fluorescence monitoring of twin screw extrusion.

Polymer Engineering & Science, 1991. 31(19): 1365-1371.
[143] Alig, I., Fischer, D., Lellinger, D., Steinhoff, B. Combination of NIR, Raman, ultrasonic and dielectric spectroscopy for in-line monitoring of the extrusion process. Macromolecular symposia, 2005. 230(1): 51-58.
[144] Alig, I., Lellinger, D. Ultrasonic spectroscopy for measurement of phase velocity and attenuation at high frequencies in polymer systems. Acta Acustica united with Acustica, 1992. 76(6): 273-282.
[145] Zhang, C. L., Feng, L. F., Gu, X. P., Hoppe, S., Hu, G. H. Tracer-compatibilizer: synthesis and applications in polymer blending processes. Polymer Engineering & Science, 2012. 52(2): 300-308.
[146] Zhang, C. L., Feng, L. F., Gu, X. P., Hoppe, S., Hu, G. H. Kinetics of the anionic polymerization of ε-caprolactam from an isocyanate bearing polystyrene. Polymer Engineering & Science, 2011. 51(11): 2261-2272.
[147] Zhang, C. L., Feng, L. F., Hoppe, S., Hu, G. H. Grafting of polyamide 6 by the anionic polymerization of ε-caprolactam from an isocyanate bearing polystyrene backbone. Journal of Polymer Science Part A: Polymer Chemistry, 2008. 46(14): 4766-4776.
[148] Koulic, C., Yin, Z., Pagnoulle, C., Gilbert, B., Jérôme, R. Premade versus in situ formed compatibilizer at the ps/pmma interface: contribution of the raman confocal microscopy to the fracture analysis. Polymer, 2001. 42(7): 2947-2957.
[149] Zhang, C., Feng, L., Gu, X., Hoppe, S., Hu, G. Determination of the molar mass of polyamide block/graft copolymers by size-exclusion chromatography at room temperature. Polymer Testing, 2007. 26(6): 793-802.
[150] Mohammed, S., Daniels, E. S., Klein, A., El Aasser, M. S. Bulk copolymerization of dimethyl meta-isopropenyl benzyl isocyanate (TMI): determination of reactivity ratios. Journal of Applied Polymer Science, 1998. 67(3): 559-568.
[151] Anastasiadis, S. H., Russell, T. P., Satija, S. K., Majkrzak, C. F. The morphology of symmetric diblock copolymers as revealed by neutron reflectivity. The Journal of Chemical Physics, 1990. 92(9): 5677-5691.
[152] Charoensirisomboon, P., Inoue, T., Weber, M. Pull-out of copolymer in situ-formed during reactive blending: Effect of the copolymer architecture. Polymer, 2000. 41(18): 6907-6912.
[153] Koning, C., Ikker, A., Borggreve, R., Leemans, L., Möller, M. Reactive

blending of poly (styrene-co-maleic anhydride) with poly (phenylene oxide) by addition of α-amino-polystyrene. Polymer, 1993. 34(21): 4410-4416.

[154] De Roover, B., Devaux, J., Legras, R. Pamxd, 6/PP-g-MA blends. I. Compatibilization. Journal of Polymer Science Part A: Polymer Chemistry, 1997. 35(5): 901-915.

[155] Zhang, X. M., Feng, L. F., Hoppe, S., Hu, G. H. Local residence time, residence revolution, and residence volume distributions in twin-screw extruders. Polymer Engineering & Science, 2008. 48(1): 19-28.

[156] Martelli, F. G. Twin screw extruders: a basic understanding. Van Nostrand Reinhold Company, 1983.

[157] Hu, G. H., Kadri, I. Preparation of macromolecular tracers and their use for studying the residence time distribution of polymeric systems. Polymer Engineering & Science, 1999. 39(2): 299-311.

[158] Kajiwara, T., Nakayama, Y. Capturing the efficiency of a melt-mixing process for polymer processing. Journal of Chemical Engineering of Japan, 2011. 44(11): 831-839.

[159] Cheng, H., Manas Zloczower, I. Study of mixing efficiency in kneading discs of co‐rotating twin‐screw extruders. Polymer Engineering & Science, 1997. 37(6): 1082-1090.

[160] Lawal, A., Kalyon, D. M. Mechanisms of mixing in single and co‐rotating twin screw extruders. Polymer Engineering & Science, 1995. 35(17): 1325-1338.

[161] Lawal, A., Kalyon, D. M. Simulation of intensity of segregation distributions using three-dimensional fem analysis: Application to corotating twin screw extrusion processing. Journal of Applied Polymer Science, 1995. 58(9): 1501-1507.

[162] Lee, S., White, J. L. Continuous mixing of low viscosity and high viscosity polymer melts in a modular co-rotating twin screw extruder. International Polymer Processing, 1997. 12(4): 316-322.

[163] Franzheim, O., Stephan, M., Rische, T., Heidemeyer, P., Burkhardt, U., Kiani, A. Analysis of morphology development of immiscible blends in a twin screw extruder. Advances in Polymer Technology, 1997. 16(1): 1-10.

[164] Gogos, C. G., Esseghir, M., Todd, D. B., Yu, D. W. Dispersive mixing in immiscible polymer blends. Macromolecular Symposia, 1996. 101(1):185-198.

[165] Bourry, D., Favis, B. D. Morphology development in a

polyethylene/polystyrene binary blend during twin-screw extrusion. Polymer, 1998. 39(10): 1851-1856.

[166] Bigio, D., Erwin, L. The effect of axial pressure gradient on extruder mixing characteristics. Polymer Engineering & Science, 1992. 32(11): 760-765.

[167] 张先明. 挤出过程停留时间分布的实验研究和数值模拟. 浙江大学. 2008.

[168] Ottino, J. M. The kinematics of mixing: stretching, chaos, and transport. Cambridge University Press, 1989.

[169] Ishikawa, T., Kihara, S. I., Funatsu, K. 3-D non-isothermal flow field analysis and mixing performance evaluation of kneading blocks in a co-rotating twin srew extruder. Polymer Engineering & Science, 2001. 41(5): 840-849.

[170] Kalyon, D. M., Sangani, H. N. An experimental study of distributive mixing in fully intermeshing, co-rotating twin screw extruders. Polymer Engineering & Science, 1989. 29(15): 1018-1026.

Titre de Thèse

Développement d'un concept d'agent compatibilisant-traceur réactif visant à étudier l'évolution de la réaction interfaciale et de la morphologie de mélanges de polymères réactifs

Résumé

Le mélange de polymères est une méthode répandue pour élaborer des matériaux polymères. Cependant, la plupart des polymères sont thermodynamiquement immiscibles entre eux, engendrant une séparation de phase des mélanges et une détérioration de leurs propriétés. Afin de palier ces problèmes, la méthode dite compatibilisation réactive est souvent employée. Elle est basée sur la formation in-situ de copolymères à bloc ou greffés par l'intermédiaire de réactions interfaciales entre polymères réactifs. Cette thèse a pour objet de développer un concept dit agent compatibilisant-traceur réactif qui permettra d'utiliser de faibles quantités d'agents compatibilisants réactifs pour évaluer leurs efficacités de compatibilisation directement sur des extrudeuses bi-vis industrielles, d'une part ; et de caractériser la performance du mélange d'une extrudeuse bi-vis en fonction des conditions opératoires et/ou du profil de vis employé.

Mots-clés : Mélange de polymères réactifs ; agent compatibilisant-traceur réactif ; mélange ; extrudeuse bi-vis ; réaction interfaciale.

Thesis Title

Development of a concept of reactive compatibilizer-tracer for studying the evolution of the interfacial reaction and morphology of reactive polymer blends

Abstract

Polymer blending is a common method to prepare high-performance polymer materials. However, most polymer pairs are thermodynamically immiscible, leading to phase separation and deterioration in material properties. To overcome such problems, the most common method is reactive compatibilization which is based on the in-situ formation of a graft or block copolymer by interfacial reaction between reactive polymers. This thesis aims at developing a concept of reactive compatibilizer-tracer which will allow using small amounts of reactive compatibilizers to evaluate their compatibilizing efficiency in industrial scale twin screw extruders, on the one hand; and to characterize the mixing performance of a twin screw extruder as a function of process conditions and/or screw profile.

Keywords: reactive polymer blending; reactive compatibilizer-tracer; mixing; twin screw extruder; interfacial reaction.